BIOCHEMICAL CHARACTERIZATION OF THE *Mycobacterium tuberculosis* Ni(II) SENSOR NmtR AND *Streptococcus pneumoniae* Zn(II) SENSOR AdcR

A Dissertation

by

HERMES REYES CABALLERO

Submitted to the Office of Graduate Studies of
Texas A&M University
in partial fulfillment of the requirements for the degree of

DOCTOR OF PHILOSOPHY

August 2011

Major Subject: Biochemistry

BIOCHEMICAL CHARACTERIZATION OF THE *Mycobacterium tuberculosis* Ni(II) SENSOR NmtR AND *Streptococcus pneumoniae* Zn(II) SENSOR AdcR

A Dissertation

by

HERMES REYES CABALLERO

Submitted to the Office of Graduate Studies of
Texas A&M University
in partial fulfillment of the requirements for the degree of

DOCTOR OF PHILOSOPHY

Approved by:

Co-Chairs of Committee,	David P. Giedroc
	James C. Sacchettini
Committee Members,	Geoffrey M. Kapler
	Paul A. Lindahl
Head of Department,	Gregory D. Reinhart

August 2011

Major Subject: Biochemistry

ABSTRACT

Biochemical Characterization of the *Mycobacterium tuberculosis* Ni(II) Sensor NmtR and *Streptococcus pneumoniae* Zn(II) Sensor AdcR.

(August 2011)

Hermes Reyes Caballero, B.A., Instituto Tecnologico y de Estudios Superiores de Monterrey;

M.S., Centro de Investigacion y Estudios Avanzados del Instituto Politecnico Nacional

Co-Chairs of Advisory Committee: Dr. David P. Giedroc
Dr. James C. Sacchettini

NmtR and AdcR belong to two structural and functional classes of transcriptional metalloregulators. The present study shows that AdcR is a novel Zn(II) dependent repressor and the first ever metalloregulator of the MarR family. In contrast, NmtR is a repressor that is inactivated by Ni(II) binding.

NmtR is a member of the extensively characterized ArsR/SmtB family. Two Ni(II) ions bind to the NmtR dimer in an octahedral coordination complex with stepwise binding affinities of K_{Ni1} = 1.2 (±0.1) x 10^{10} and K_{Ni2} = 0.7 (±0.4) x 10^{10} M^{-1} (pH 7.0). A glutamine scanning mutagenesis approach reveals that Asp 91, His 93, His 104 and His 107 in the α5 helix and His 3 at the extreme N-terminal contribute to K_{Ni}. In contrast residues from the C-terminal tail (H109, D114 and H116), previously implicated in NmtR binding, are characterized by near wild-type K_{Me} and allosteric coupling free energies. However, deletion of most of the C-terminal tail to create Δ111 NmtR reduce

Ni(II) binding stoichiometry to one per dimer and greatly reduced Ni(II) responsiveness. H3Q and Δ111 NmtR also show important perturbations in the rank order of metal responsiveness, with both different from wild-type NmtR. The use of both presumably unstructured N- and C- terminal extensions is a unique property relative to other members of the ArsR/SmtB family previously characterized and provides a distinct metal specificities profile.

AdcR binds two regulatory Zn(II) ions per dimer in an unusual five coordinate geometry as determined by X-ray and electronic absorption spectroscopy. Functional characterization of single residue substitution mutants identified His 108 and His 112 in α5 helix and His 42 in α2 helix, as residues essential for allosteric activation of DNA operator binding by AdcR as revealed by fluorescence anisotropy experiments. The stability constant for the regulatory site, K_{Zn}, is sensitive to pH and range from ~10^{10} M^{-1} at pH 6.0 to ~10^{12} M^{-1} at pH 8.0. Zn(II) binds to an additional one to two pairs of ancillary sites per dimer depending on the pH. A novel feature not shared by other Zn(II) regulators is an apparent reduced metal specificity, since non-cognate metals Mn(II) and Co(II) activate AdcR to the same extent than Zn(II) does. However, each non-cognate metal binds with very low affinity (≤ 10^6 M^{-1} at pH 8.0) and are not inducers *in vivo*.

DEDICATION

I dedicate this work to my parents Lidia and Marco, to whom I would be forever in debt for bringing me into this life; to my sister for her unconditional love; to my wife for bringing me happiness; to my friends, since they encourage me to keep carrying on with a smile; and to the mystery that is beyond the limits of the known for showing me the excitement of discovery.

ACKNOWLEDGMENTS

I want to thank my advisor, Prof. David. P. Giedroc, for his guidance throughout the realization of this work and my committee for their helpful comments on the manuscript. I owe my laboratory skills to senior graduate students in the Giedroc Lab and in many other laboratories.

Special thanks to Karin J. Ekholm, for her kind revisions made to this document.

I also want to thank Pat Swigart, Sherry Coronado, and Juanita Withem at the Biochemistry and Biophysics Department office for all their help.

NOMENCLATURE

Bs	*Bascilus subtillis*
CDF	Cation difusion facilitator
EGTA	Ethylene glycol tetraacetic acid
Me	Metal
Mf2	Mag-fura-2
Mtb	*Mycobacterium tuberculosis*
MW	Molecular weight
NTA	Nitriloacetic acid
PEI	Polyethylenimine
Spn	*Streptococcus pneumoniae*
XAS	X-ray absorption spectroscopy

TABLE OF CONTENTS

Page

ABSTRACT iii

DEDICATION v

ACKNOWLEDGMENTS vi

NOMENCLATURE vii

TABLE OF CONTENTS viii

LIST OF FIGURES x

LIST OF TABLES xiii

CHAPTER

I INTRODUCTION 1

Metal Homeostasis in Prokaryotes 4
Metal Selectivity, Ligand Donor Sets and Coordination Geometry 14
Allosteric Signal Propagation 22
Thermodynamics of Allosteric Regulation by Metals 27
Conformational Dynamics in Allosteric Regulation by Metals 33
Scope of this Dissertation 36

II BIOCHEMICAL STUDIES OF *Mycobacterium tuberculosis* NmtR 39

Introduction 39
Materials and Methods 43
Results 46
Discussion 74

III BIOCHEMICAL STUDIES OF *Streptococcus pneumoniae* AdcR 82

CHAPTER Page

Introduction 82
Materials and Methods 86
Results 93
Discussion 118

IV SUMMARY AND PERSPECTIVES 124

Summary 124
Perspectives 126

REFERENCES 132

APPENDIX A 164

APPENDIX B 165

APPENDIX C 166

APPENDIX D 167

APPENDIX E 168

APPENDIX F 169

APPENDIX G 170

VITA 171

LIST OF FIGURES

FIGURE		Page
1.1	Zn(II) and Ni(II) homeostasis in *E. coli*	9
1.2	Native metal coordination geometries for selected bacterial metalloregulatory proteins	21
1.3	Proposed allosteric communication pathway in *Synechococcus* SmtB	24
1.4	Histidine as allosteric trigger as illustrated from the (a) "closed'' PerRMnZn and (b) "open" PerR apoZn structures.	26
1.5	Ligand binding coupled equilibrium reactions of metallosensors	29
1.6	Thermodynamics parameters of Zn(II), apo and DNA CzrA complexes.	30
1.7	Schematization of NmtR and AdcR operon .	38
2.1	Multiple sequence alignment of SmtB/ArsR family members that were obtained with NmtR as a query	47
2.2	Ni(II) binding to (a) wild-type and (b) H3Q NmtRs at 5.0 μM protein monomer	48
2.3	Metal-chelator competition experiments with wild-type and H3Q NmtRs	50
2.4	Allosteric regulation of DNA binding by wild-type and H3Q NmtR variants	54
2.5	Calibration of mag-fura-2 binding affinity for Ni(II)	59
2.6	Ni(II) binding to α5-site in Gln substitution mutant NmtRs variants	60

FIGURE Page

2.7 Lack of allosteric regulation of α5 missense mutant NmtRs 64

2.8 Distinct allosteric regulation of H104Q Ni(II)NmtR 65

2.9 Ni(II) binding stoichiometry and affinity for different metals of Δ111 NmtR. 66

2.10 Binding of Ni(II) to C-terminal NmtR variants 68

2.11 NTA and EGTA metal competition experiments with C-terminal missense mutant NmtRs. 69

2.12 Ni(II) dependent allosteric regulation of NmtR C-terminal variants. 70

2.13 Δ111 NmtR is nearly refractive to Ni(II)-dependent regulation but not to Co(II) regulation 71

2.14 Co(II) electronic absorption spectra of H3Q and C-terminal variant NmtRs 75

3.1 Sephadex G75 gel filtration chromatography of apo-AdcR 95

3.2 A small fraction of apo-AdcR forms a covalent dimer by denaturing SDS-PAGE analysis 97

3.3 Zn(II) binding to AdcR in the presence of competitor chelators 101

3.4 Zn(II) binding to AdcR variants in the presence of competitor chelators 104

3.5 Mn(II) binding to C30A AdcR 105

3.6 The binding of Mn(II) and Co(II) to AdcR as monitored by isothermal titration calorimetry 107

3.7 Co(II) electronic absorption spectra of AdcR 108

FIGURE Page

3.8 X-ray absorption spectroscopy of Zn(II)-bound AdcR. 109

3.9 X-ray absorption spectroscopy of Zn(II) bound C30A and wild-type AdcRs 110

3.10 DNA binding by wild-type and mutant AdcRs 113

LIST OF TABLES

TABLE		Page
1.1	Metal binding affinities for selected bacterial transition metal sensor proteins	7
1.2	Known ligand sets and coordination numbers for bacterial metalloregulator proteins	16
2.1	Putative and known metal ion transporters in *M. tb.* with known transcriptional regulators	41
2.2	Ni(II) binding affinities of NmtR wild-type and mutant variants	51
2.3	NmtR wild-type DNA binding affinities for different metal complexes	53
2.4	DNA binding affinities of H3Q NmtR with different metal complexes	57
2.5	DNA binding affinities of α5 missense mutant NmtRs in presence of Ni(II)	61
2.6	Metal induced DNA binding by H104Q NmtR	63
2.7	DNA binding affinities of C-terminal NmtR variants	72
2.8	DNA binding affinities of Δ111 NmtR in complex with various metals ions	73
3.1	Hydrodynamic parameters of wild-type AdcR obtained from sedimentation velocity experiments	98
3.2	Electrospray ionization-mass spectrometry of apo-wild-type and C30A AdcR	99
3.3	Binding affinities of Zn(II) and other metal ions for wild-type and selected mutant AdcR homodimers	102

TABLE Page

3.4 Curve fitting results for Zn K EXAFS 112

3.5 Equilibrium binding affinities resolved from fluorescein anisotropy-based AdcR operator binding isotherms for individual AdcR derivatives in the presence and absence of Zn(II)..... 115

CHAPTER I

INTRODUCTION*

Transition metals are essential to many biological processes in the cell. The wide range of functions in which metals participate are determined by their intrinsic properties. These range from roles as essential cofactors for oxidation-reduction and acid-base chemistry, to structural centers that stabilize the fold of a domain or protein. Zn(II) is relative unique among first row transition metals in that it poses a dual role in the cell, as both a structural element and catalytic cofactor. In eukaryotic cells, Zn(II) stabilize an α helical conformation that is required for "zinc-finger" domains to bind to DNA and RNA (*1, 2*). On the other hand, Zn(II) is an essential co-factor of many hydrolytic enzymes, including proteases, phosphatases, esterases and deacetylases, where it function as a Lewis acid to activate a water molecule for catalysis (*3*). An important catalytic function of transition metals is that they are essential to cope with oxidative stress in the form of catalases and superoxide dismutases (SOD). SODs are ubiquitous enzymes found in virtually all cells and oxygen-tolerant organisms that employ distinct metal cofactor ranging from Ni to Cu to Cu/Zn to Mn and Fe SOD, to catalyze the same reaction, sometimes in the same cell (*4*). Nickel, with no agreement in its nutrimental or carcinogenic importance for humans (*5-7*), is a cofactor for urease,

---

This dissertation follows the style of *Biochemistry*.

*This chapter is reproduced with permission from "The Metalloregulatory Proteins: Metal Selectivity and Allosteric Switching" Reyes-Caballero, H., Campanello, G.C.,Giedroc, D.P. (2011), *Biophysical Chemistry,* in press. doi:10.1016/j.bpc.2011.03.010.

an essential enzyme of *H. pylori* that allows this organism to colonize the acidic gastric lumen (*8*).

On the other hand, essential metal ions, notably iron and copper, can access oxidized or reduced forms and as a result, can catalyzed the production of highly toxic reactive oxygen species by Fenton or Haber-Weiss-like chemistry from partially reduced forms of oxygen that form as by-products of aerobic respiration (*9, 10*). In addition non-essential heavy metals and metalloids that play no biological role, like mercury, cadmium, arsenic, lead and tin, are extremely toxic often as a result of forming irreversible binding to sulfhydryl groups of metalloproteins that change their function or stability (*11, 12*).

An organism that requires transition metal ions has evolved mechanisms to regulate the metal quota (total metal concentration) in the cellular compartment in which the toxicity or essentiality of the metal is manifest. This is the cytoplasm in Gram-positive bacteria or the cytoplasm and periplasm in Gram-negative bacteria. This regulation is termed metal homeostasis, in which a variety of proteins maintain metal concentration at normal levels, this set include metallochaperones, metal importers and metal efflux transporters. The expression of genes encoding these proteins is controlled by a panel of specialized transcriptional regulators, known as metalloregulatory proteins, or "metal sensor" proteins. These transcriptional regulators specifically sense one or a small number of metal ions and are classified on the basis of structural homology in ten families (*13, 14*). Binding of the cognate metal to the metalloregulator activates or inhibits protein-DNA operon binding to regulate genes that in most cases codify for

proteins of metal homeostasis (*15, 16*). In many other instances the regulon also includes genes with functionalities beyond metal homeostasis, an may include virulence determinants (in *Streptococcus pneumoniae* AdcR regulon (*17*)), oxidative stress response (in *Deinococcus sp*. DtxR/IdeR regulon (*18*)) and precursors of enzymatic pathways (in *H. pylori* NikR regulon (*19*)) for example. Indeed, these operons are often vital for the survival of pathogenic bacteria in humans.

An increased level of complexity introduced when metalloregulatory networks specific for one metal ion intersect with one another in the cell. Structurally unrelated metallosensors with distinct metal specificities may interact in the same cytoplasm. For example Ni(II) and Fe(II) metalloregulators NikR and FurR in *H. pylori* have overlapping DNA binding sites in the promoter regions of their regulons (*20, 21*), a finding consistent with numerous examples of Ni-Fe cross-talk in cells (*22, 23*). Metals homeostasis of ions of similar radii size and coordination preferences can be interacting (Appendix G). In *B. japonicum* the Fur-family regulator Irr appears to be targeted for proteolytic degradation upon heme binding. Under conditions of low iron, heme is scarce and not sufficient to signal Irr for degradation; in addition, Mn(II) binds to Irr and further stabilizes it against denaturation. Therefore, when *B. japonicum* is grown under Mn(II) depleted conditions, Irr senses heme-Fe(II) at correspondingly lower concentrations, consistent with the hypothesis that Mn(II) and Fe(II) homeostasis are interconnected (*24*). Non-cognate metal binding affects transition metal homeostasis as well. For example, in the human pathogen *S. pneumoniae*, Zn(II) stress induces a strong Mn(II) deprivation phenotype, thought to be caused by competition between Zn(II) and

Mn(II) at the high affinity Mn(II) uptake system and possibly in the cytoplasmic Mn(II) sensor PsaR (*25, 26*).

Emerging evidence clearly reveals that transition metal homeostasis impact many fundamental aspects of cell biology and bacterial pathogenesis (*27, 28*) and is therefore essential to understand the mechanisms of metalloregulation operative within the cell (*13*). Important insights into what governs these processes in the cell come from biophysical and structural studies of purified metalloregulatory proteins. In this introductory chapter, we focus on two main aspects of metal homeostasis regulation at the physicochemistry level, the coordination chemistry of metal coordination that governs the specificity of the response, and structural, thermodynamic and dynamical mechanisms of allosteric regulation of operator-promoter binding by cognate vs. non-cognate metal ions.

METAL HOMEOSTASIS IN PROKARYOTES

Transition metal homeostasis refers to a series of processes that actively maintain the intracellular metal quota (total metal concentration) among the boundaries beyond which metal is in excess or deprivation. It is well established that all cells concentrate cell-associated transition metals to approximately the same degree irrespective of the organism, with total measurable zinc and iron buffered at 10^{-4}-10^{-3} M, manganese and copper approximately 10-fold lower, with nickel and cobalt another 10-fold lower (*25, 29*). In prokaryotes, the cellular response to perturbations in metal homeostasis is nearly exclusively transcriptional. In most of the cases, a classical repressor model(*30-32*) is

operative where a metal sensor binds to a specific DNA operator that overlaps the promoter sequence in order to sterically block the binding of the RNA polymerase (*33-35*). A significant departure from this model is transcriptional activation by MerR-family regulators, where the metal-bound or otherwise "activated" form of the repressor allosterically changes the structure of the promoter from a poor promoter to a strong promoter, without protein dissociation (*36-38*). This reduces or eliminates the cytoplasm content of mRNA that codify for proteins that are relevant for transition metal homeostasis processes.

The simplest mechanism of allosteric regulation of operator binding, from which MerR family members are excluded, requires that a metalloregulator (*P*) has at least one DNA binding domain (*D*) and one metal (*M*) regulatory site, typically but not always located in structurally separated domains within a homooligomer (dimer or tetramer). The "ligand" binding sites can interact with each other in two ways: If the binding of *M* stimulates binding of *D* then this is termed positive allosteric regulation, and occurs most often in metal-mediated repression of uptake genes. On the contrary, if the binding of *M* antagonizes the binding of *D*, this manifest as negative heterotropic allosteric regulation and it is this process that occurs most often in metal-mediated transcriptional derepression (*14*).

In the case of the cytoplasm experiencing metal excess, for example, gene transcription derepression of proteins for metal efflux or detoxification, and concomitant repression of genes encoding systems for metal uptake, restores the cytoplasm to homeostasis. Thus, a long-standing hypothesis (*39*) is that the intracellular metal

activity or free metal concentration at which a metalloregulator is inhibited or activated to bind to its operator (or allosterically change the promoter structure) may establish the threshold or sensitivity of the transcriptional response (*29, 40, 41*). This hypothesis holds that the reciprocal of the metal association constant K_{Me} ($1/K_{Me}$) defines the buffered or labile pool of metal at half-maximal activation or inhibition of the transcriptional response.

For example in *E. coli* the Zn(II) specific homeostasis system is under control of two metalloregulators, Zur and ZntR (Figure 1.1). The Zn(II) sensor Zur is a member of the Fur family (*42*) that represses the expression of *znuABC*, which encodes a Zn(II) uptake ABC transporter in the presence of Zn(II). Conversely, ZntR is a MerR regulator that activates the transcription of *zntA*, a gene that encodes a cation P-type ATPase that efflux zinc from the cytoplasm to the periplasm (*43, 44*). *In vitro* transcription experiments reveal that each metalloregulator competes for Zn(II) with an affinity constant ($1/K_{Me}$) offset by approximately one log unit, resulting in an activation threshold positioned at femtomolar (10^{-15} M) Zn(II) (*29*). As shown in Table 1.1, other Zn(II) metalloregulator proteins bind Zn(II) with log K_{Me} of ≈12-13 at or above neutral pH; if this hypothesis is correct then Zn(II) may well be buffered at high concentration, 10^{-12} -10^{-13} M in the other microorganisms. In the eukaryotic cell, cytosolic Zn(II) is

Table 1.1 Metal binding affinities (K_{Me}) for selected bacterial transition metal sensor proteins

Reg.	Biol. Proc.[a]	Cognate metal	Fam.	Species	Metal	log K_{Me}	pH	Ref.
Zur	uptake	Zn	Fur	*E. coli*	**Zn(II)**	**15.7**	7.6	(*29*)
ZntR	efflux	Zn	MerR	*E. coli*	**Zn(II)**	**15.0**	7.6	(*29*)
CzrA	efflux	Zn	ArsR	*S. aureus*	**Zn(II)**	**12.4**[b]	7.0	(*45*)
					Co(II)	9.0	7.0	
SmtB	efflux/ seq'n	Zn	ArsR	*Synechococcus*	**Zn(II)**	**11.3**[c]	7.4	(*46*)
					Co(II)	9.7	7.4	
AztR	efflux/ seq'n	Zn/Cd	ArsR	*Anabaena PCC7120*	**Zn(II)**	**>10**	7.0	(*47*)
					Co(II)	≥7.3	7.0	
					Cd(II)	7.3	7.0	
					Pb(II)	6.2	7.0	
BxmR	efflux/ seq'n	Zn/Cd/Cu/ Ag	ArsR	*O. brevis*	**Zn(II)**	**13.0**[d]	6.3	(*48*)
					Cu(I)	**7.6**[e]	6.3	
AdcR	uptake	Zn	MarR	*S. pneumoniae*	**Zn(II)**	**12.1**[f]	8.0	(*17*)
						10.0[f]	6.0	
					Co(II)	6.8	8.0	
						5.4	6.0	
					Mn(II)	5.1	8.0	
CueR	efflux	Cu	MerR	*E. coli*	**Cu(I)**	**20.7**	8.0	(*49, 50*)
					Au(I)	34.7	7.7	
$CsoR_{BS}$	efflux	Cu	CsoR	*B. subtilis*	Zn(II)	8.2	6.5	(*51*)
					Cu(I)	**≥19.0**	6.5	
					Ni(II)	9.5	6.5	
					Co(II)	≤5.0	6.5	
$CsoR_{MT}$	efflux	Cu		*M. tuberculosis*	**Cu(I)**	**18.0**	7.0	(*52*)
$CsoR_{SA}$	efflux	Cu		*S. aureus*	**Cu(I)**	**18.1**	7.0	(*53*)
CupR	efflux	Au	MerR	*R. metallidurans*	**Au(I)**	**34.1**	7.7	(*50*)
					Cu(I)	16.1, 18.2	7.7	
$NikR_{EC}$	uptake	Ni	NikR	*E. coli*	Zn(II)	>12.0	7.6	(*54*)
					Cu(II)	16.9	7.6	
					Ni(II)	**12.0**	7.6	
					Co(II)	8.7	7.6	
					Cd(II)	>9.0	7.6	
$NikR_{HP}$	uptake	Ni	NikR	*H. pylori*	**Ni(II)**	**11.5**	7.6	(*55*)
						8.8	5.8	

Table 1.1 Continued

Reg.	Biol. Proc.[a]	Cognate metal	Fam.	Species	Metal	log K_{Me}	pH	Ref.
NmtR	efflux	Ni/Co	ArsR	*M. tuberculosis*	Zn(II)	≥9.0	7.0	(*33*)
					Ni(II)	**10.0**	7.0	*g*
					Co(II)	**5.9**	7.0	(*33*)
RcnR	efflux	Ni/Co	CsoR	*E. coli*	**Ni(II)**	**>7.6**	7.0	(*56*)
					Co(II)	**>8.3**	7.0	
Fur	uptake	Fe	Fur	*E. coli*	Zn(II)	5.9	7.0	(*57*)
					Co(II)	6.8	7.0	
					Fe(II)	**5.9**	7.0	
					Mn(II)	4.6	7.0	
MntR	uptake	Mn	DtxR	*B. subtilis*	Zn(II)	7.9	7.2	(*58*)
					Ni(II)	5.7	7.2	
					Co(II)	5.3	7.2	
					Mn(II)	**3.8[h]**	7.2	
					Cd(II)	**7.0**	7.2	

[a]Indicated regulator controls the transcription of genes encoding proteins involved in metal uptake into the cytoplasm (uptake), extrusion from the cytoplasm (efflux), and of intracellular sequestration by metallothioneins (seq'n). [b]First of two binding sites (K_{Zn1}) on the dimer (see text for details). [c]α5 site affinity. [d]α3 site affinity. [e]α3N site average affinity for each of two bound Cu(I) ions bound in a Cu_2 cluster. [f]Highest affinity regulatory site; lower affinity sites not shown. [g]H. Reyes-Caballero, D. Giedroc, manuscript in preparation. [h]Determined by EPR spectroscopy. *B. anthracis* AntR (an MntR homolog), log K_{Mn}=4.2 determined using EPR spectroscopy(*59*).

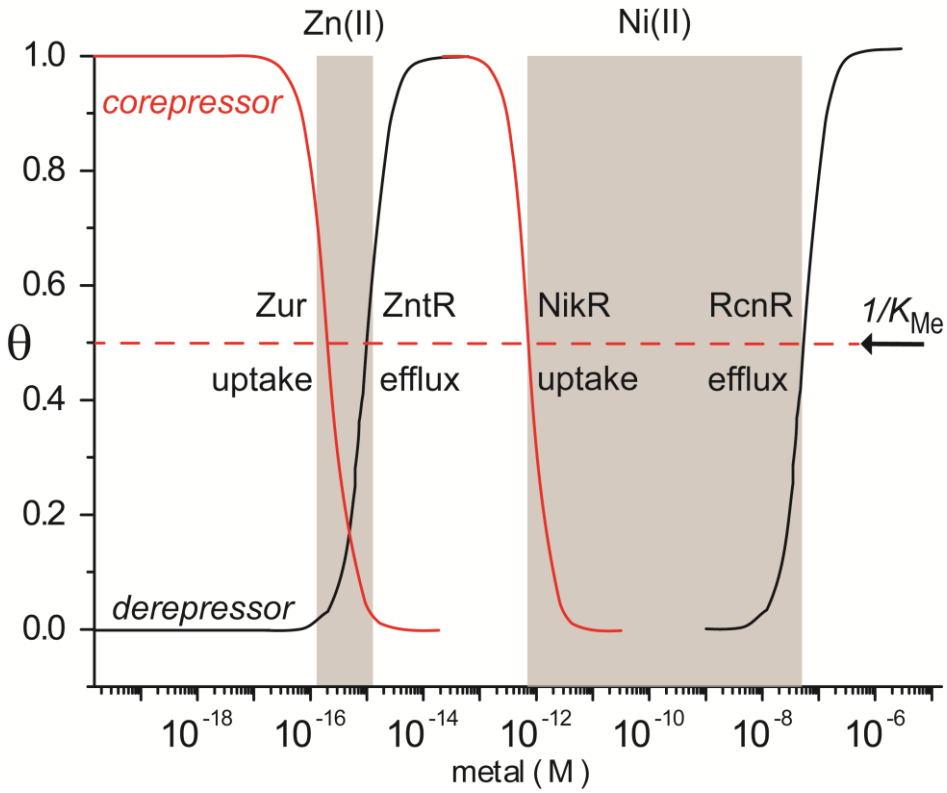

Figure1.1 Zn(II) and Ni(II) homeostasis in *E. coli*. The threshold of free metal is show in gray. Below or above this level the cell senses metal stress. The metal uptake systems will be de-activated as the optimal concentration is reach (red), while the detoxification systems are activated (black) as the metal concentration passes the boundary of homeostasis. The Zn(II) regulon in *E.coli* is shown in contraposition of the Ni(II) regulon. See Table 1.1 for references.

buffered at $\approx 10^{-9}$ M, with a labile pool of 0.2 μM in the mitochondrial matrix(*60*). This suggests that the bacterial cytoplasm and mammalian cytosol possess different buffering capacities for zinc.

The affinities of metalloregulatory proteins for transition metal ions essentially follow the Irving-Williams series of divalent metals binding to model chelates, with Zn(II) and Cu(II) binding with the highest affinity, while Mn(II) and Fe(II) binding with the lowest affinity ($Zn^{2+} \leq Cu^{2+} >> Ni^{2+} \geq Co^{2+} \geq Fe^{2+} \geq Mn^{2+}$) (*61*). Metalloregulatory proteins that have been extensively characterized largely follow this expected trend, although there are also some outliers (Table 1.1.). The Irving-Williams series classifies Zn(II) as a highly "competitive" metal, *i.e.,* Zn may be capable of binding as a non-cognate metal far more tightly than the corresponding cognate metal ($K_{Zn} >> K_{Mn}$ for *B. subtilis* MntR, for example) (Table 1.1). As a result, the cytoplasm employs an overcapacity to chelate Zn(II), and it has been postulated that ribosomal proteins play an important role in this process (*62-64*). The obligatory participation of specific metallochaperones that traffic Cu(I) to target proteins with $K_{Cu(I)} \geq 10^{18}$ M^{-1} also likely reflects the need to maintain the bioavailable concentration of this metal under very tight control as well (*65, 66*). As a consequence, *E. coli* CueR, a copper-selective member of the MerR family, is activated by Cu(I) *in vivo* and binds Cu(I) with an affinity of $10^{20.7}$ M^{-1} (Table 1.1) (*49*). Other copper sensors, *e.g.* CsoR, are characterized by a log $K_{Cu(I)}$ of 18-19, in range of that of CueR (*51-53*). Thus, this hypothesis (*39*) suggests that in *E. coli*, the buffered range of free bioavailable Zn(II) and Cu(I), is kept very low at picomolar-femtomolar and attomolar-zeptomolar range, respectively. In constrast *E.*

coli Fur, an Fe(II)-dependent transcriptional repressor, appear to be activated in response to low micromolar range of iron (Table 1.1) (*57*), with binding affinities for Mn(II) regulators in the 10^3-10^5 M^{-1} range of K_{Me} (Table 1.1). The low affinity constants suggest that at least part of the Mn(II) and Fe(II) concentrations in the cell is expected to be weakly bound or highly mobile with rapid off-rates (*15*). Thus, inherent to the efficient regulation of the availability of free metal in the cell is that metal selectivity of proteins is attained at least in the context of the right *vs*. left hand sides of the Irving-Williams series. This argument is supported from recent *in vivo* experiments that show how the cellular stress response to excess of metal ions that are highly competitive to bind is associated to depravation responses (uptake) of metals that are loosely bound. For example, *in vivo* Ni(II) stress activates an Fe(II) deficiency response in *E.coli* (*22*) and Zn(II) stress activates a Mn(II) deficiency response in *S. pneumoniae* (*25*).

The degree to which pairs of metalloregulators possess relatively well-matched metal affinities and specificities, is not yet known. For example, a Cu(I) uptake regulator or an Fe or Mn efflux regulator have not yet been identified which suggests that "one-armed" transcriptional control may be sufficient to maintain intracellular homeostasis of Cu(I) and Fe/Mn. The case of Ni(II) homeostasis in *E. coli* provides an interesting contrast to these systems (Figure 1.1). Like Zn(II), Ni(II) homeostasis in *E.coli* is controlled by a pair of regulators, in this case NikR and RcnR. NikR is a Ni(II) specific repressor, a four symmetry related tetramer in solution (*67, 68*), that controls the transcription of *nikABCD*, a high affinity Ni(II) uptake transporter (*69, 70*). The Ni(II) ion binds with an affinity of 10^{12} M^{-1} to the each C-terminal regulatory site at the

tetrameric interface, flanked by the ribbon-helix-helix (RHH) DNA binding domains (*54, 68*). RcnR is a Ni(II) specific efflux regulator from the CsoR family that dissociates from the DNA operator sequence when Ni(II) binds, allowing the expression of *rcnA,* a gene that encodes for a Ni(II)/Co(II) transporter (*71*). Ni(II) binds to RcnR with an affinity of $10^{7.6}$ M^{-1} or approximately 5 orders of magnitude weaker than NikR at similar pH (Table 1.1); this would thus appear to be inconsistent with the simple Zn(II) homeostasis model (*56*). However, NikR has in addition to the high affinity site mention above, an additional pair of low affinity Ni(II) regulatory sites (log K_{Ni} = 9) that are required for full NikR activation *in vitro* (*72, 73*). This might suggest an ordered or step-wise regulatory response in the cell where uptake is first partially repressed, and then fully repressed, prior to Ni(II) efflux re-establishing Ni(II) homeostasis. However, in *E.coli in vivo* experiments it was shown that NikR mediated inhibition of the expression of the Ni(II) uptake system and the RcnR mediated activation of the Ni(II) efflux pump, occurs at an external concentration of 0.1 and 0.5 μM Ni(II) respectively, a < 1 log concentration range (*56, 71, 74*). Interestingly, two paralogous efflux regulators from the ArsR family (*75*) NmtR and KmtR present in the actinomycete *M. tuberculosis,* may well collaborate to establish a similar two-step or graded repression response to Ni(II) toxicity as well, given log K_{Ni} values of 12 and 10, respectively (*33, 76*) (H. Reyes-Caballero and D. Giedroc, manuscript in preparation). The physiological importance of a potentially graded response to nickel in *E. coli* and *M. tuberculosis* has not yet been firmly established, but it may be suggested that Nature fine tuned the affinity of these metal sensors to monitored Ni(II)/Co(II) at a broad concentration range

and to mount a stress response at two different scales. The activity of a second metal ion efflux pump may increase the efficiency of the adaptation to environments with high Ni(II) concentration. This idea is supported by results of *in vivo* experiments that show a serial activation of both metal sensors as the Ni(II) concentration increases from nM to μM (*76*). Whatsoever the physiological importance of a potentially graded response to nickel in *E. coli* and *M. tuberculosis* has not yet been firmly established. The recent discovery in other actinomycete, *S. coelicolor*, of a two pairs of metalloregulatory sites within homodimeric Zur (*77*) which appear to influence zinc-mediated repression at different promoters to different degrees, is also consistent with a graded response to zinc stress in that organism as well (*78*). The sensitivity of the zinc efflux regulator has not yet been established in *S. coelicolor*.

A similar case that is currently investigated is Zn(II) homeostasis in *S. pneumoniae*, where two metalloregulators, AdcR and SczA control the expression of genes that codify for Zn(II) acquisition and detoxification proteins, respectively. AdcR is the first known metal-sensing MarR family member (*79*), and binds Zn(II) with an affinity of 10^{12} M^{-1} at pH 8.0 (*17*) as would be anticipated on the basis of K_{Zn} found for other Zn(II) metallosensors (Table 1.1). However, preliminary data on SczA, a novel Zn(II) sensing TetR family member (*80*) reveals $K_{Zn} \approx 10^{8}$ M^{-1} under the same conditions (K. R. Geiger and D.P. Giedroc unpublished results), or about two orders of magnitude weaker than K_{Zn} for AdcR. This is consistent with expression analysis which suggests that under all conditions containing ≥20 μM total zinc on liquid media, the AdcR

regulon is fully repressed and the cellular response to perturbation of zinc homeostasis is governed exclusively by SczA and metal efflux (*17, 25*).

METAL SELECTIVITY, LIGAND DONOR SETS AND COORDINATION GEOMETRY

A large number of metal sensor proteins have now been structurally characterized by x-ray crystallography, NMR spectroscopy and other spectroscopic methods. As a result, it is now possible to identify common features of metal sensing sites specific for a particular metal ion. The metal ligand donor set in the regulatory site often satisfies metal preferences to bind to a particular kind of ligand residue anticipated on the basis of fundamental inorganic chemistry. Transition metal ions become more polarizable or "soft" as the number of electrons in the *d* orbital increases. Although the first row transition metal ions Fe(II), Co(II), Ni(II), Cu(II) and Zn(II) are considered as a group to be borderline hard/soft (*81*), subtle ligand preferences are apparent as Mn(II) is *d*5 and is considered "hard" relative to *d*10 Zn(II) which is correspondingly "soft". Likewise, Cu(I) is "softer" that Cu(II) since a decrease in valence means an additional *d*-electron has been added (*81, 82*). "Soft" metals prefer "soft" ligands with the trend in polarizability decreasing from Cys to His/Met to Asp/Glu.

These trends in metal-ligand polarizabilities from small molecule coordination chemistry are largely capitulated in metal ligand donor sets in metal sensor proteins. This has been most extensively established in the ArsR/SmtB (or ArsR) family of metalloregulatory proteins, widely represented across bacterial species (*76*). ArsR

family proteins regulate the expression of genes that encode for proteins responsible for metal ion detoxification, sequestration and cytoplasmic efflux, as well as many other processes not yet discovered (*16*). The metalloregulators of this family have collectively evolved an impressive range of regulatory metal binding sites on a relatively unchanging protein scaffold with clearly distinct metal specificities (*14*). Soft metal ions sensors from the ArsR family, such as Cd(II)/Pb(II) sensor of *S. aureus* CadC, the Cd(II)/Pb(II) sensor of *M. tuberculosis* CmtR, As(III)/Sb(III) sensor *E. coli* ArsR and the cyanobacterium Cu(I) sensor *O. brevis* BxmR, all harbor metal regulatory sites that are rich in cysteine residues (Table 1.2). In contrast, the Zn(II)/Co(II) sensor *S. aureus* CzrA (*45*) and the Ni(II)/Co(II) *M. tuberuclosis* sensor NmtR bind the metal with more electronegative and less polarizable "hard" donor ligands including glutamate and aspartate aminoacid residues (Table 1.2).

B. subtillis MntR, is a Mn(II)-dependent repressor of the transcription of *mntABCD*, which encodes a high affinity Mn(II) importer. MntR binds Mn(II) weakly with K_{Me} in the order of 10^5 M^{-1} (*58*), yet is Mn(II)-specific among first-row transition metal ions *in vivo* (*83*). Structurally MntR is similar to the Fe(II) sensor DtxR/IdeR (*84, 85*), but is a stable dimer that binds one to two metal ions per subunit depending in solution conditions (*86*). Among non-cognate metals, Cd(II) activates MntR *in vitro* to the same or greater degree while Zn(II), Ni(II), Fe(II), and Cu(II), activate DNA binding with low efficacy (*87*). A similar metal specificity profile characterizes DtxR-like family repressors PsaR and ScaR from *Streptococcus spp* (*25, 88*). Selective allosteric

Table 1.2 Known ligand sets and coordination numbers for bacterial metalloregulator proteins.

Regulator	Ligands	Activator	Geometry	Ref.
CzrA	D_{84}*H_{86}*H_{97},*H_{100}*,[a]	Zn(II)	Tetrahedral	(*45*)
SmtB	D_{104},H_{106},$H_{117'}$,$C_{121'}$	Zn(II)	Tetrahedral	(*46, 89*)
AdcR[b]	$H_{42}H_{108}H_{112}$ + $(N/O)_2$	Zn(II)	N_3 + $(N/O)_2$	(*17*)
AztR	$C_{21}C_{72}C_{74}$ + N	Zn(II)	Dist. tetrahedral	(*47*)
ZntR[c]	$C_{114}C_{124}$ -$C_{79'}$ -$C_{115}C_{119}$+ PO_4^{3-}	Zn(II)	Tetrahedral	(*49*)
BxmR[c]	C_{23},C_{31},C_{75},C_{77}	Cu(I)	Binuclear S_4	(*48*)
		Ag(I)	Trigonal planar	
		Cd(II)	Tetrahedral	
	D_{119},H_{121},$H_{132'}$,$E_{135'}$	Zn(II)	Tetrahedral	
$CsoR_{BS}$	$C_{45}H_{70}C_{74}$	Cu(I)	Trigonal	(*51, 52*)
$CsoR_{MT}$	$C_{36}H_{61}C_{65}$	Cu(I)	Trigonal	(*90*)
CueR	$C_{112}C_{120}$	Cu(I)	Linear	(*49, 91*)
NmtR	$H_3D_{91}H_{93}H_{104}H_{107}$	Ni(II)	Octahedral	b
RcnR	αNH_2-H_3NH-$C_{35}H'_{60}H_{64}$	Ni(II)	Octahedral	(*56*)
Nur	$H_{70}H_{72}H_{126}$ $2H_2O$	Ni(II)	Octahedral or Sq. bipyramid	(*92*)
NikR	$H_{87}H_{89}C_{95}H'_{76}$	Ni(II)	Sq. planar, SN_3	(*54, 68, 93*)
MntR	E_{99},E_{102},$H_{103}D_8$	Mn(II)	Octahedral	(*58, 86, 87*)
CadC	C_7,C_{11},$C_{58}C_{60}$	Cd(II)	Dist. tetrahedral	(*94*)
	C_7,$C_{58}C_{60}$	Pb(II)	Trigonal	
CmtR	$C_{57}C_{61}C'_{102}$+ O	Cd(II)	S_3 or S_3O	(*95*)
CupR	$C_{112}C_{120}$ + S	Au(I)	S_3	(*50*)

[a] Variable residues are italicized
[b] In this work
[c] binuclear
[d] Ni(II) second regulatory site

switching by Mn(II) over Fe(II) appears to be based on ligand preferences of Mn(II) vs. Fe(II) (*96*). The metal regulatory sites in MntR and DtxR/IdeR are structurally equivalent, yet differ in the nature of the coordinating ligands. Here the thioether sulfur of Met10 in the α1 helix and thiolate sulfur Cys102 in the regulatory domain found in the Fe(II) selective repressor DtxR/IdeR are replaced by Asp8 and Glu99, respectively, in Mn(II)-specific MntR (*96*).

Inspection of the structural database confirms that Nature selects against coordination of Mn(II) by cysteine, which is a "hard" metal ion (*81*) that prefer N/O ligand donors, in contrast to the well known propensity of Fe(II) to form iron-sulfur clusters of varying nuclearities (*96*). On the other hand, Mn(II) selects against Zn(II), on the basis of distinct coordination geometries of each, since the tetrahedral coordination of Zn(II) differs from the native more highly coordinated hexa- or heptavalent coordination geometry observed for Mn(II) and Cd(II), respectively (*58, 97*).

The *S. aureus* Zn(II) metalloregulator CzrA of the ArsR/SmtB family represses the transcription of the cation diffusion facilitator (CDF) CzrB in the absence of metal stress (*16*). CzrA is denoted "α5" ArsR family sensor as it binds Zn(II) with negative homotropic cooperativity at two regulatory sites positioned between the pair of α5 helices at the dimer interface with step-wise binding affinities K_{Zn1} and K_{Zn2} of $\approx 10^{12}$ M^{-1} and 10^{10} M^{-1}, respectively, at pH 7.0 (Table 1.1) (*98*). Functional characterization of metal ligands in the α5 helix shows a tolerance for variation at some liganding positions, while other metal ligands are absolutely essential for allosteric regulation of DNA binding (*45*). In contrast, the mutagenesis of any of the α5 ligands in the homologous

Ni(II)/Co(II) sensor *M. tuberculosis* NmtR abrogates allosteric inhibition of DNA binding (H. Reyes-Caballero and D. Giedroc, manuscript in preparation). NmtR binds Ni(II) in an octahedral coordination geometry, but shares an analogous core of four α5 ligands with CzrA (*99*).

Comparative structural and spectroscopic studies of CzrA and the related zinc sensor, *Synechococcus* SmtB with NmtR reveals a key aspect of regulation by "α5" ArsR sensors. These studies establish that Zn(II) binds in a tetrahedral or distorted tetrahedral coordination geometry to CzrA and SmtB (*45, 89*), while Ni(II) binds to NmtR in an octahedral coordination geometry (*99*). These coordination geometries parallel the natural preferences of each metal (*100-103*). However, a non-cognate metal ion will often bind to the same site in such a way to force a new non-native coordination geometry, consistent with intrinsic preferences of the non-cognate metal (*99*). However, formation of a non-native coordination geometry always results in a weaker or abrogated allosteric response, relative to the cognate metal, and thus a poorer ability to sense these metals in the cell. For example, in the functional analysis of the α5 metal ligand chelate of CzrA, only those substitutions that preserved a native tetrahedral Zn(II) coordination geometry were capable of allosteric regulation of DNA binding *in vitro* and could adopt an allosterically inhibited conformational state, irrespective of K_{Zn} (*45*). These findings on CzrA support the hypothesis that a major determinant of biological specificity depends on the structure of the first coordination shell that has evolved around the cognate metal (*45*).

Detailed studies with other regulators are largely consistent with this hypothesis. The *M. tuberculosis* Cu(I) dependent repressor, $CsoR_{MT}$ is a founding member of a widespread family of bacterial metal regulatory proteins (*51, 56, 90*). *M. tuberculosis* CsoR controls the expression of *ctpV,* a gene that encodes a copper ATPase that effluxes Cu(I) from the cytoplasm (*27, 90*). CsoR binds to Cu(I) with an association equilibrium constant in the order of 10^{18} M^{-1} (*51, 52*). CsoR from *Bacillus subtillis* ($CsoR_{BS}$),and *S. aureus* ($CsoR_{SA}$) are homologus to $CsoR_{MT}$ and each adopt a S_2N coordination complex that is structurally identical to that of $CsoR_{MT}$ (*51, 53*). The tetrahedral and square planar coordination geometry of Zn(II) and Ni(II) respectively, despite tight binding, are quantitatively less capable than the trigonal Cu(I) of driving dissociation of $CsoR_{BS}$ from the DNA operator (*51*). In contrast, the CsoR-family Ni(II) efflux regulator *E.coli* RcnR, adopts an octahedral coordination geometry upon binding cognate metals Ni(II) and Co(II) by recruiting additional metal ligands from the N-terminal region that are not found in the copper sensor CsoR; this results in an $S(N/O)_5$ coordination sphere (*56*). The nature of the high specificity center for Cu(I) or Ni(II) is therefore dictated by the coordination geometry which may or may not track with metal affinity (*74*), analogous to the conclusions reached with the ArsR/SmtB family of regulators.

Full repression by the Ni(II) sensor *E.coli* NikR is observed *in vivo* only when cognate metal Ni(II) binds in a square planar coordination geometry to the C-terminal regulatory sites. Cu(II) forms a complex that is iso-structural with that of Ni(II), but will not be regulatory *in vivo* due to the vanishingly small concentrations of Cu(II) expected to be present in the reducing bacterial cytoplasm. However, a non-native coordination

geometry is adopted by all other non-cognate metals; Zn(II) adopts a tetrahedral coordination geometry and Co(II) and octahedral complex. As expected, both metals activate DNA operator binding by NikR poorly (*69, 72, 104, 105*).

This close correspondence of functional metal selectivity and coordination geometry also characterizes other classes of metalloregulatory proteins, including the transcriptional activators of the MerR family from E.coli, CueR and ZntR. In MerR family proteins, metal ions typically bind to a C-terminal loop which is packed against the N-terminal DNA binding domain. CueR binds Cu(I) in a characteristic linear Cu(I) bis-thiolato coordination geometry (*91*), a coordination structure also observed for CueR in complex with other abiological monovalent metals *e.g.* Ag(I) and Au(I) (*49*). In contrast, Zn(II) binds to ZntR to form a phosphate-bridged binuclear Zn(II) center, with each Zn(II) ion adopting a tetrahedral coordination geometry (Figure 1.2(d)) (*49*). Finally, the Fur family Ni(II) sensor Nur (*92*) (Table 1.2), has been proposed to discriminate against other metals by harboring an octahedral coordination site not found in other Fur family repressors, with an additional site analogous to the regulatory Fe(II) binding sites in the Fe(II)-specific regulator, Fur (*106*).

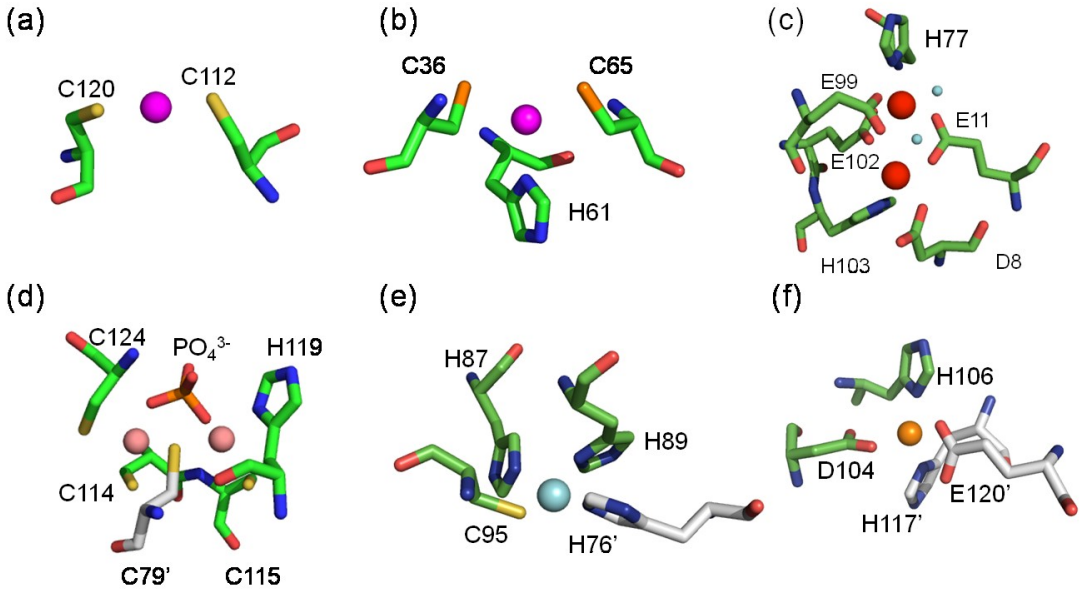

Figure 1.2 Native metal coordination geometries for selected bacterial metalloregulatory proteins. A colored sphere represent the metal ion unless is otherwise indicated. (a) *E. coli* CueR, Cu(I) linear (PDB ID:1Q05), (b) M. tuberculosis CsoR, trigonal Cu(I) (PDB ID: 2HH7), (c) *B. subtilis* MntR, penta-coordinate di-nuclear Mn(II), H_2O molecules are represented as cyan spheres (PDB ID: 1ON1), (d) *E. coli* ZntR, tetrahedral di-nuclear Zn(II) (PDB ID: 1Q08), (e) *E. coli* NikR, square planar Ni(II) (PDB ID: 2HZV), (f) *S. elongatus* PC7942 SmtB, Zn(II) tetrahedral (PDB ID: 1R22). Graphical representation was created using PyMol freeware (*107*).

In contrast, the regulatory site(s) in the Zn(II)-specific Fur family regulator, Zur, clearly adopt four-coordinate tetrahedral complexes (*78, 108*), fully consistent with nearly all other Zn(II) regulators, with the exception of AdcR (*17*). In no case, however, have systematic quantitative studies been carried out to assess the degree to which the coordination geometry of the cognate or regulatory metal differs from that of a non-cognate metal in allosteric activation of DNA binding.

ALLOSTERIC SIGNAL PROPAGATION

Recent structural studies are beginning to reveal how formation of a native coordination geometry is tied to structural changes in a repressor (*109, 110*). The crystallographic structures of the metal free apo and Zn(II) forms of *Synechoccocus* SmtB and *S. aureus* CzrA provided the first insights into a possible structural coupling mechanism (*111*). Two hydrogen bonds appeared to form a pathway that connected the α5 metal center and α4 DNA recognition helix on the αR-β1 loop upon metal atom binding (Figure 1.3). The non-chelating nitrogen (Nε2) of the essential ligand His 117 (H97 in CzrA) forms a key second coordination shell hydrogen bond and is therefore predicted to be responsible for triggering the allosteric response upon Zn(II) binding (*111*). Support for this model came from the observation of an intense Nε2-Hε2 correlation from H117 in the ^{1}H-^{15}N HSQC spectrum, which is lost upon metal dissociation (*111*). Analogous observations are found for H97 in the related Zn(II) sensor CzrA (*111, 112*).

Semisynthetic native chemical ligation is currently being used to directly test this allosteric coupling model in CzrA by site-specifically incorporating unnatural His97 analogs designed to maintain an Nδ1-Zn(II) coordination bond, but lack the ability to donate a hydrogen bond on the other side of the imidazole ring (Z. Ma., Y. Fu and D. Giedroc, manuscript in preparation). Such an approach was recently employed on the Cu(I) sensor *M. tuberculosis* CsoR in which it was established that the nonliganding Nε2 face of His61 mediates a hydrogen bonding network to Tyr35' and Glu81 across the subunit interface to stabilize the low DNA binding affinity of the tetramer (*52*). Although the precise structural mechanism of Cu(I) regulation in CsoR is not completely understood, these second coordination shell interactions seem to be required for allosterically coupling cognate metal binding and DNA binding sites. The neutral charge of the histidine at physiological pH and the frequency of events of this kind found in structural databases (*113, 114*) reveal that Nature exploits a recurring mechanism to propagate allosteric signal propagation in metal sensor proteins, probably due to the unique chemical bonding properties of histidine among any other amino acid (*115*).

The mechanism of activation of DNA binding by Fur family transcriptional repressor is based largely on studies of the hydrogen peroxide sensor PerR, which employs an iron chelate to sense oxidative stress in *B. subtillis*. Here, the metal ligand His37 from the N-terminal winged helix DNA binding domain effectively couples the N-terminal and C-terminal domain which stabilizes a "close" Fe(II)- bound

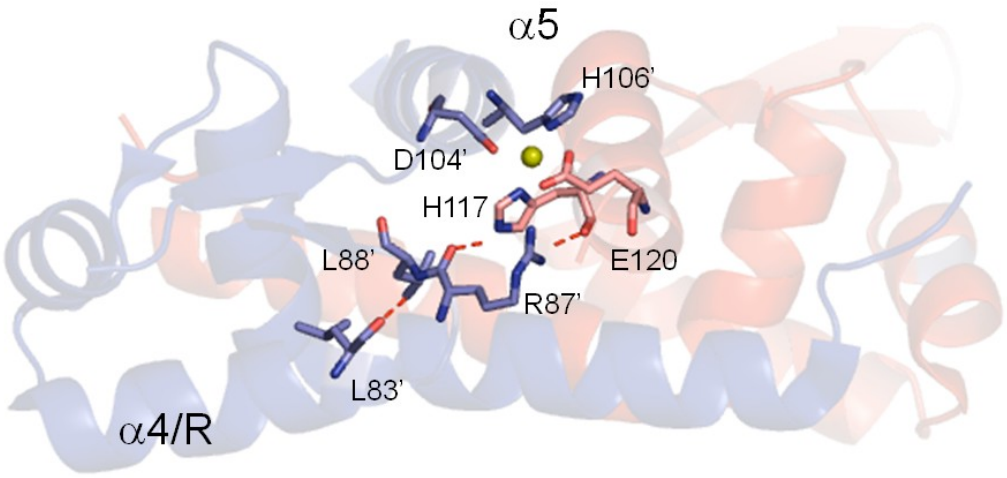

Figure 1.3 Proposed allosteric communication pathway in *Synechococcus* SmtB. The series of main chain-side chain, hydrogen bonds donor and acceptor implicated in the allosteric pathway are depicted. Upon Zn(II) binding the quaternary structure shift is described as a rotational movement on the plane of the dimer interface with the result of compacting the structure by 3 Å. In the SmtB-Zn(II) complex, His117 chelates Zn(II) trough Nδ1 and uses its non ligating Nε2 to form a hydrogen bond with the carbonyl group of R87' across the subunit interface, which positions the amide of the adjacent L88' (in the αR-β1 loop) in order to make a hydrogen bond to the carbonyl of L83' (in α4/R helix). The guanidino of R87' is involved in reciprocal hydrogen bonding interactions with H117 and E120 as shown. These later interactions are not conserved in CzrA or other Zn(II)-sensing α5 sites ArsR/SmtB sensors. Modified from Eicken *et al.* (*111*), PDB ID: 1R22. Graphical representation was created using PyMol freeware (*107*).

conformation that activates binding of PerR to operator sites upstream of oxidative stress sensing genes (Figure. 1.4) (*116*).

Mechanistically, $PerR_{BS}$ uses an open coordination site on Fe(II) to bind H_2O_2, which results in oxidation of Fe(II) to Fe(III) and creating OH• which in turn leads to oxidation of two metal liganding histidines, His37 and His91 to 2-oxo-histidine (*117*). This is thought to lower the affinity of $PerR_{BS}$ for Fe(III), allowing for metal dissociation, and triggering a quaternary structural change leading to an "open" apo-structure of lower DNA binding affinity, as predicted by the crystal structure of inactivated (apo) PerR (Figure. 1.4) (*116, 118, 119*). All the ligands in the regulatory site are essential for peroxide sensing *in vivo* but each plays a distinct function. His 37 appears to function in a key allosteric role, but this time via ligand oxidation and perturbation of the first coordination shell; this effectively uncouples the DNA binding domain from the regulatory domain. His 91, on the other hand, is predicted to play and important role in stabilizing the Fe(II) complex; oxidation therefore increases dissociation of the metal, which drives "open" the molecule (*120, 121*).

Other Fur family repressors bind metal to activate DNA binding to Fur-boxes upstream of genes that often encode for metal ion uptake systems (*122*). In the available structures of Fur homologs that are activated to bind DNA by divalent metal ions, *e.g.* Zn(II) sensing *M. tuberculosis* Zur (FurB) and *S. coelicolor* Zur (*78, 108, 123*), *P. aeuroginosa*, *V. colera* and *H. pylori* Fe(II) sensors Fur (*124-126*) and the Ni(II) sensor *Streptomyces coelicolor* Nur (*92*), all possess metal binding centers that are structurally analogous to the Fe(II) site in PerR. In most of the cases, it has been hypothesized that

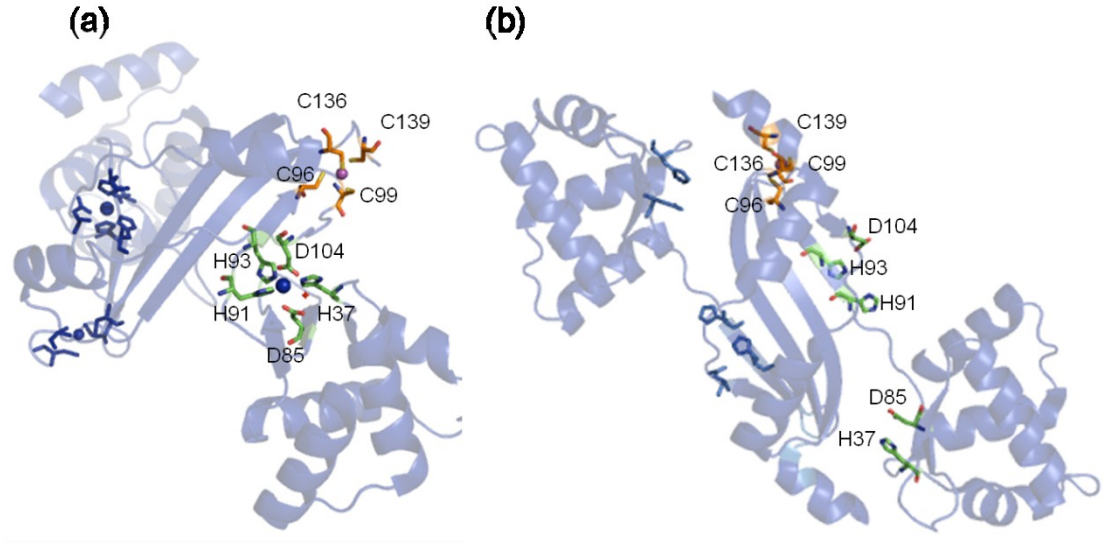

Figure 1.4 Histidine as allosteric trigger as illustrated from the (a) "closed'' PerR apoZn (2FE3) and (b) "open" PerRMnZn (3F89) structures. The structure shows two metal binding sites occupied by Mn(II) (blue) and Zn(II) (magenta). Mn(II) binds to the regulatory site in a distorted square pyramidal geometry involving ligands/substrate H37 and H91. In contrast, Zn(II) binds to a thiolate rich site that plays no role in the catalysis (*116, 117*), but is essential for structural integrity of the dimer (*120*).

coordination of metal ions by a conserved pair of His residues analogous to His37 and His91 in *B. subtilis* PerR stabilizes a "closed" conformation that is competent to bind operator DNA (*116, 126-129*).

THERMODYNAMICS OF ALLOSTERIC REGULATION BY METALS

An emerging topic in the study of allosteric regulation in metal sensor proteins is the measurement of the energetics and conformational dynamics that underlie the mechanism of metal activation or inhibition of DNA operator binding. These studies are motivated by the lack of dramatic structural change observed when comparing the metal-bound vs. metal free structures in crystal structures of ArsR/SmtB sensors, for example (*111*). This picture differs dramatically from the large conformational change in PerR and perhaps other Fur family regulators as well as in NikR (*110*) discussed above (Figure 1.4). In MerR family activators, there is little understanding of this process due to incomplete structural characterization of all relevant allosteric states, *e.g.,* apo-, ligand-bound, DNA-bound ligand activated, within a single MerR regulator (*38, 49*). Indeed, accumulating evidence suggests that allosteric proteins can clearly function in the absence of large structural changes, mediated instead by changes in conformational dynamics, *e.g.,* stiffening or enhanced mobility, that can be detected by residue-specific NMR methods or globally through thermodynamic methods (*130-132*).

Although biological systems are open systems that operate far from equilibrium (*133*), the study of metalloregulators in equilibrium with its two ligands, DNA operator and metal ion, represents a powerful tool that has enabled the discovery of many

fundamental aspects of metalloregulation (*15, 98*). This coupled equilibrium can be cast in terms of a simple thermodynamic cycle (Figure. 1.5) (*15*). The magnitude of the thermodynamic linkage, ΔG^{t}_{C}, defines the efficacy of the allosteric ligand (metal) to activate or inhibit DNA operator binding. Such a formalism facilitates quantitative comparisons of different metal sensors proteins with different metal ions, but more importantly provides a thermodynamic construct with which to identify key residues that are involved in the allosteric switching mechanism, independent of their effect on binding affinity for either ligand (*15, 52, 134*).

A complete set of thermodynamic parameters of the binding of Zn(II) to CzrA homodimer in the free form and in the protein DNA complex were obtained by isothermal titration calorimetry (ITC). This approach has allowed extraction of the homotropic coupling free energies within the two states and ultimately the step-wise heterotropic coupling free energies, ΔG_{c}^{i} (Figure. 1.6) (*98*). The Zn(II) binding isotherms were readily fit to two-step binding model where the energetics associated with formation of the Zn_1-CzrA and Zn_2-CzrA complexes could be measured in the free and the DNA bound complex (top, bottom horizontal equilibrium, Figure 1.6). The first Zn(II) binding event to the apoprotein is entropically driven ($-T\Delta S_1 = -16.6 \pm 0.8$ kcal mol^{-1}) with a small opposing enthalpy factor ($\Delta H_1 = 0.06 \pm 0.2$ kcal mol^{-1}) (*98*). Structurally, this Zn_1 state is characterized by loss of symmetry detectable in ^{1}H-^{15}N HSQC spectrum, representing a superposition of apo and metallated states, consistent with strong negative cooperativity of metal binding (*45, 135*). The magnitude of the heat capacity change ($\Delta C_p^{1} \approx -230$ cal mol K^{-1}) may be reporting on solvent

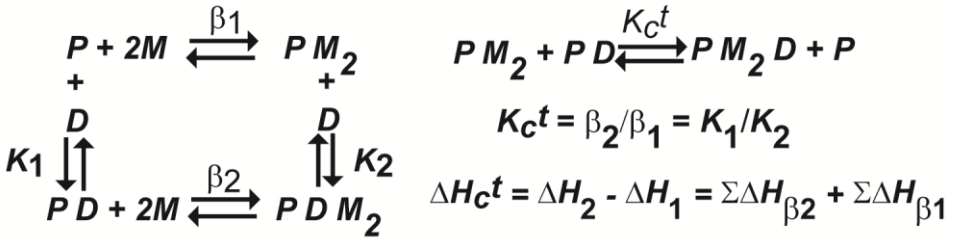

Figure.1.5 Ligand binding coupled equilibrium reactions of metallosensors. The affinity constant of each reaction *K* or β *(K1•K2)*, can be cast in energetic terms by the standard free energy $\Delta G^o = -RT \ln Ki = -RT \ln \beta i$, where *R* is the gas constant (1.98×10^{-3} kcal K^{-1} mol^{-1}) and *T* is temperature. If we measure that $\beta_1 > \beta_2$, then *D* is a negative allosteric ligand, and the standard free energy will be more favorable for *M* binding to *P* in absence ($\Delta G^o < 0$) than in presence ($\Delta G^o > 0$) of *D*. If for the contrary $K_1 < K_2$, then *D* is a positive allosteric ligand and will favor the binding of *M*. The allosteric effect is reciprocal, if $\beta 1 > \beta 2$ then $K_1 > K_2$, and *vice versa*. The total free energy (ΔG^t_C) between the free ligand and bound form is the subtraction of each reaction energetic components, $\Delta G^t_C = -RT \ln (\beta_2/ \beta_1)$ where the subscript in ΔG^tc denotes the *coupling* free energy. Because of the law of conservation of energy and since ΔG^tc is a state function independent of the path, then $\beta_2/ \beta_1 = K_2/ K_1$. Then the equation can be rewritten as $\Delta G^t_C = -RT \ln (K_2/ K_1)$ $\Delta G^t_C = -RT \ln Kc^t$ where Kc^t refers to the overall (t =total) equilibrium constant for the reaction shown, because Kc^t defines the equilibrium of the simultaneous reactions in the horizontal or vertical manifold after reordering the products and reactants. Hence, $\Delta G^t_C > 0$ characterizes negative allosteric regulation (inhibition) and $\Delta G^t_C < 0$ indicates positive allosteric regulation (activation). Another way of obtaining the energetic parameters of the coupled equilibrium is by direct measurement of the enthalpy (ΔH) of each of the ligand binding reactions by isothermal titration calorimetry (ITC). After subtracting the enthalpy of the reactions in presence and absence of the allosteric ligand, we cast the total enthalpy of the reaction, $\Delta H^t_C = \Delta H_2 - \Delta H_1 = \Sigma \Delta H_{\beta 2} - \Sigma \Delta H_{\beta 1}$. Then the entropy ($\Delta S^t_C$) of the binding reaction is given by $\Delta S^t_C = (\Delta H^t_C - \Delta G^t_C)/T$, where ΔG^t_C is calculated by the experimental value of the affinity constant (*K* or β *)*. Enthalpy changes refer to organization, if during a process structure is gained, the term would be negative. The entropy measures the degrees of freedom of the system relative to its surroundings (solvent). If the system gained freedom, the term $T\Delta S$ has a negative sign ($+\Delta S$).

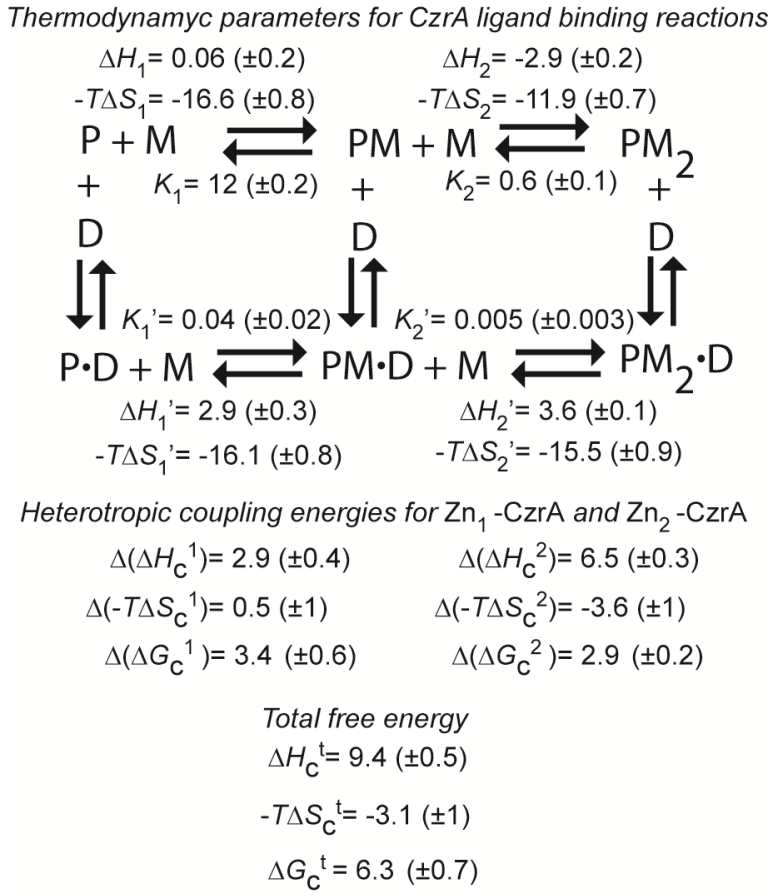

Figure 1.6 Thermodynamics parameters of Zn(II), apo and DNA CzrA complexes. The thermodynamic box represents two Zn(II) metal ions (M) step wise binding to apo CzrA (P) in the top horizontal equilibrium or to the CzrA-DNA complex (P•D) in the bottom horizontal equilibrium, with association constants K and K' ($x10^{11}$ M^{-1}) respectively. Stepwise Zn(II) CzrA binding energetic parameters enthalpy and entropy to apo (ΔH_i and $-T\Delta S_i$) and DNA complex ($\Delta H_i'$, $T\Delta S_i'$), is given in kcal mol^{-1}. In the same way, the heterotropic coupling energies for the first and second binding events (ΔG_c^i, ΔH_c^i and $-T\Delta S_c^i$) as well as the total free energy (ΔG_c^t, ΔH_c^t and $-T\Delta S_c^t$) is in kcal mol^{-1}. Thermodynamic parameters obtained by ITC (*98*).

reorganization as a result of restructuring the dimer interface (*98*). In striking contrast binding of the second Zn(II) to Zn_1-CzrA reveals an entropic penalty that is ≈ 5 kcal mol^{-1} smaller ($-T\Delta S_2 = -11.9 \pm 0.7$ kcal mol^{-1}) with respect to the first binding event. This is thought to be the energetic origin of negative homotropic cooperativity of Zn(II) binding, where the second site globally quenches the short timescale dynamics (*98*). Consistent with this hypothesis, the stabilization of the structure in the native Zn_2 state is more favorable on binding of the second metal ($\Delta\Delta H$=–2.9(±0.3) kcal mol^{-1}).

These thermodynamics of Zn(II) binding contrast sharply with those obtained with the repressing apo-CzrA-DNA complex. Here, the entropic penalty for the binding of the second Zn(II) relative to the first is far smaller ($\Delta(-T\Delta S') = 0.6$ kcal mol^{-1}) suggesting that the Zn_2-CzrA-DNA complex is far more dynamic than the unbound Zn_2-CzrA (*98*). Parallel differences are observed in the magnitude and sign of the enthalpy term, which while overall favorable in the free state, is unfavorable or near zero ($\Delta H_2' - \Delta H_1' \approx 0.7$ K cal mol^{-1}) in the DNA complex; this is consistent with the greatly reduced $\Delta(-T\Delta S')$. Thus, although metal binding to the protein-DNA complex is also negatively cooperative ($\Delta\Delta G$=1.3(±0.9) kcal mol^{-1}), the underlying energetics are completely different. This in turn drives strong negative heterotropic allosteric (heterotropic) cooperativity in this system, ΔG_c^t, which is sizable at 6.3 (±0.7) kcal mol^{-1}. In experiments that employed a covalently fused CzrA dimer, the intermediate Zn_1-CzrA state shows metal dependent inhibition of DNA binding *in vitro* to 70% that of the fully metallated Zn_2-state (*135*). In contrast, the wild-type system stepwise coupling free energies, ΔGc^1, ΔGc^2, were found to make approximately equal contributions to ΔG_c^t

(*135*). The origin of this discrepancy is unknown, but it may lie in the covalent coupling of the C-terminus of one protomer to the N-terminus of the other, since the linkage length was found to have a profound influence on the stoichiometry and cooperativity of Zn(II) binding to various fused CzrAs (*135*).

It is interesting to note that studies like these have the potential to systematically access all four allosteric "end-states," including the ternary CzrA-Zn_2-DNA complex (PM_2•D in Figure 1.6) (*136*). This complex is likely a transiently formed intermediate in the cell since Zn(II) binding by the repressing CzrA-DNA complex will quickly lead to disassembly of the complex. As might be expected, qualitative inspection of the ^{1}H-^{15}N TROSY spectrum of this intermediate reveals that CzrA adopts a "hybrid" conformation as it attempts to optimize interactions with both metal and DNA ligands(A. Arunkumar and D. Giedroc, unpublished results). There are a number of residues for which backbone amide and side chain methyl chemical shifts are distinguishable in the CzrA-Zn_2-DNA complex relative to the apo-CzrA-DNA and allosterically inhibited Zn_2 states. These residues are strong candidates for playing a key role in structural coupling between metal and DNA binding sites (*136*) which may buttress the hydrogen bonding pathway shown (Figure 1.3). In any case, when NMR studies like these are combined with a multiple sequence alignment of ArsR family regulators of known distinct metal binding sites(*16, 76*), this approach can be used to identify candidate residues for substitution and quantification of ΔG_c (*45, 98*).

CONFORMATIONAL DYNAMICS IN ALLOSTERIC REGULATION BY METALS

These global thermodynamics are in general consistent with insights gleaned from residue-specific conformational dynamics, readily measured by a variety of NMR approaches. For example, the fully metallated Zn_2 state of CzrA, relative to apo-CzrA, reveals that Zn(II) binding rigidifies the quaternary structure of the molecule (*109, 111*). The rate of hydrogen-deuterium solvent exchange of backbone amides is globally quenched (*111*) and investigation of the short timescale (ps-ns) dynamics and qualitative insights into intermediate (μs) timescale dynamics using the same methods are consistent with dynamical quenching of not only the α5 and α1 helical core that comprises much of the dimer interface, but also into the more peripheral α4 (DNA recognition) helices (Figure 1.3). The β-hairpin is structurally unaffected, which is conformationally dynamic in both apo and metallated states (*109*).

This picture of the allosterically inhibited Zn_2 state contrasts sharply with that of repressing apo-CzrA-DNA complex relative to same apo-CzrA reference state (*109*). Here, one observes the expected stabilization of the protein-DNA interfacial region; however, the metal binding sites in the α5 helix become highly mobile with very rapid H-D exchange rates coupled with increases in backbone dynamical disorder in the *ns* to *ps* time scale, which are small but extend into the core of the protein (*109*). These dynamical findings are consistent with the solution structure of the DNA-bound CzrA. This structure reveals that while the global fold of each protomer is unchanged relative to apo-CzrA, the quaternary structure differs dramatically, with the DNA recognition helices (α4) directed away from the core and pointing in a direction that allows for

favorable contacts with successive major grooves of the DNA operator. In order for this to occur, the α5 helices pull apart from one another, exposing the core of the dimer, and thus strongly enhancing conformational mobility in the allosteric sites. Enhanced dynamics in this region may well lower the barrier for Zn(II) binding, thus increasing the rate of metal association and subsequent dissociation of the Zn(II)-bound repressor from the DNA(*137*).

Although studies of the conformational dynamics have only been reported for a few other metal sensor proteins(*138, 139*), functionally important stabilization of the native structure by binding metals appears to be a recurring theme. This can result from metal binding to a structural site that plays no direct role in regulation or to the regulatory site(s) directly, similar to that which occurs in CzrA. For example in *H. pylori* Fur_{HP} (*21, 126, 140-144*), Zn(II) binds to a thiolate rich, distorted tetrahedral site found in a C-terminal regulatory domain involving two C-terminal Cys residues that are necessary to stabilize the dimer but play not direct role in metalloregulation (*145*). Hence, formation of this structural site is a necessary prerequisite of metal binding to the regulatory sites (*145*). This S_4 structural site This S_4 structural site is found in many, *e.g.,* Zur(*78, 108*), Nur (*92*)and PerR(*116*), but not all Fur family sensors. Some Fur family dimers contain a third pair of "secondary" metal binding sites, whose coordination structure and function seems to vary from the one to another regulator (*42, 78, 108, 125, 126, 146, 147*).

Similarly, DtxR/IdeR regulators often require metal occupancy of what is thought to be a secondary structural site that stabilizes the quaternary structure by

increasing the stability of the dimer (*148-150*). This may be a necessary prerequisite for a second metal to bind to the pair of regulatory sites in the dimer (*151*). In the ArsR/SmtB family, the α5 metal site that plays a regulatory role in CzrA (*45*) and in SmtB (*46*) is also present in many (but not all) Cd(II)/Pb(II) sensing CadCs but plays no role in regulation; it may stabilize the dimer and function as a necessary prerequisite for Cd(II) regulation in the more peripheral α3N sensing sites (*94, 152*). In *E. coli* NikR, the binding of cognate metal to the C-terminal domain nucleates a hydrogen bonding network that likely stabilizes the native structure against thermal denaturation; in contrast, non-cognate metals that adopt distinct coordination structures do not (*54, 68, 93, 104*). Structural stabilization of NikR allows formation of a pair of lower affinity Ni(II) sites that are essential for full activation of *nik* operator binding (*73, 153*).

The crystallographic structures of *C. diphtherium* DtxR, *M. tuberculosis* IdeR, *B. subtilis* and *E.coli* MntR in the metal-free and allosterically activated, metal-bound states reveal only small differences that bring the pair of DNA binding domains into a more "closed" conformation which is thought to directly stabilize protein-DNA interactions. (*87, 97, 151, 154, 155*). An alternative interpretation of these small structural changes is that the binding of activating metals functions largely to quench conformational dynamics which "locks in" or "freezes" a high DNA-binding affinity conformation. Hydrogen-deuterium exchange mass spectrometry carried out with Mn(II)-MntR (*139*) and EPR spectroscopy of the structural homolog *B. anthracis* AntR (*59, 138*) are generally consistent with this picture. In AntR, the DNA binding domain is characterized by an ensemble of different conformational states in rapid exchange on the

ns timescale that are narrowed by non-cognate Zn(II) binding (*59, 138*). The degree to which cognate metal Mn(II) narrows the distribution relative to Zn(II) is unknown but of interest since Zn(II) is a poor activator of operator binding by MntR and other MntR-like repressors including *S. pneumoniae* MntR and PsaR (*25, 26*) and *S. gordonii* ScaR (*88*). A subject of ongoing work in our laboratory is to determine the degree to which allosteric inhibition and activation may possess a common origin in "stiffening" or rigidifying the metal-bound conformation (*109*).

SCOPE OF DISSERTATION

In this dissertation, a systematic comparative study of the metal binding affinities and allosteric coupling free energies of metal dependent DNA binding of transcriptional repressors from two structural classes and of distinct biological functions are presented. These are the ArsR/SmtB family Ni(II) sensor, *M. tuberculosis* NmtR (Chapeter 2) and the Zn(II) sensor *S. pneumoniae* AdcR (Chapter 3). Ni(II) is an allosteric inhibitor of *nmt* operator binding by NmtR which results in to transcriptional derepression of the expression of NmtA, a Ni-Co P-type ATPase effluxer (Figure 1.7(a)) (*33*). In contrast Zn(II) is an allosteric activator of *adc* operator binding which represses transcription of a Zn(II) uptake transporter (Figure 1.7(b)) (*17*).

The genome of the human pathogen *M. tuberculosis* encodes twelve members of the ArsR/SmtB family, and includes the α5-site Zn(II) sensor $SmtB_{MT}$ (*156*) and Cd(II)-Pd(II) sensor CmtR (*95, 157*) and two characterized Ni(II) sensors, NmtR (*33*) and KmtR (*76*). Previous work supported that NmtR and KmtR have distinct sensitivities for

Ni(II) and in the present work we show that the affinity of NmtR for Ni(II) is 10^{10} M^{-1} (pH 7.0) which is 100 times lower than KmtR (*76*). This findings support the possibilities that two levels of Ni(II) sensing may exist in *M. tuberculosis*. Other SmtB/ArsR sensor, CmtR, and $SmtB_{MT}$ are not activated by Ni(II) (*156, 157*), which increases the diversity of metals that are sensed in the cytoplasm of this pathogen.

Allosteric Ni(II) site in NmtR was also studied trough the analysis of glutamine-missense mutations, which allow us to conclude that hisitidines in both N-terminal and C-terminal "tails" are required for high affinity Ni(II) binding while maintaining, the selectivity of the allosteric response Ni(II)>>Zn(II). These studies motivate ongoing NMR studies of NmtR.

In the second system, thorough examination of the mechanism of allosteric control of AdcR was carried out. This AdcR system is of intrinsic interest due to the fact that AdcR is the first metal sensor member of the MarR (multiple antibiotic repressor) family and any member that is characterized by allosteric activation of DNA binding by a metal. We show a strong pH dependence of Zn binding affinity (pH 6.0-8.0), consistent with a site rich in histidine residues.

Spectroscopic experiments reveal an unprecedented five-coordinate geometry for AdcR, unique among Zinc sensors. We established the structure of the first coordinate sphere, and show that the involvement of a key His (H42) from the N-terminal DNA binding domain, a feature reminiscent of the Fur-family members Fur, Zur, PerR (*108, 116, 126*). Important parallels between the two systems with respect to metal selectivity in their respective cytoplasm are discussed.

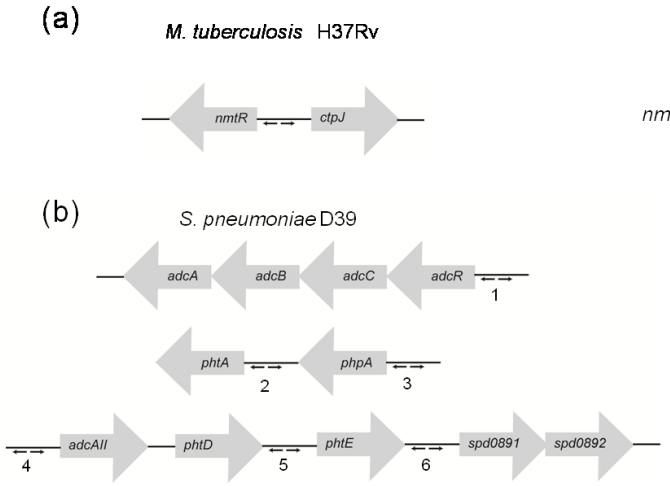

nmtR O.	Gen. coord.	Sequence
	4,195,497	TGAACA-TA-TGATCA

adcR O.	Gen. coord.	Sequence
1	1,977, 124	TTTA-CCA-GTTAA
2	1,064,359	TTAA-CTA-GTTAA
3	1,066,984	TTAA-CTG-GTTAA
4	898,953	TTAA-ATG-GTTAA
5	902,581	TTAA-ATG-GTTAA
6	905,941	TTAA-CTG-GTTAA

Figure 1.7 Schematization of NmtR and AdcR operon. Inverted repeat DNA sequences are indicated (opposing arrows) for (a) NmtR operon (*nmtR* O.): *nmtR* (Rv3744), *ctpJ* (Rv3743c) and (b) AdcR operon (*adcR* O.): *adcABCR* (SPD_1999, SPD_1998, SPD_1997, SPD_##), *phtA* (SPD_1037), *phpA* (SPD_1038), *adcAII* (SPD_0888), *phtD* (SPD_0889), *phtE* (SPD_0890), *spd0891*, *spd0892*. The positions in the genome map (genome coordinates), along with its DNA sequence (5'→3') are indicated.

CHAPTER II

BIOCHEMICAL STUDIES OF *Mycobacterium tuberculosis* NmtR

INTRODUCTION

The genome of the human *Mycobacterium tuberculosis* (*M tb.*) pathogen (*158*) encodes an impressive abundance and diversity of known and putative metal ion transporters including 12 putative P-ATPases and several ABC transporters and cation diffusion facilitators (CDF) (*159*). This diversity might have allowed a primordial soil-dwelling ancestor of *M tb*. to adapt to an environment of substrate complexity (*158*). At the present, this diversity might have enabled this obligate intracellular pathogen to efficiently respond to a range of host killing mechanisms (*160*), collectively known as nutritional immunity (*161, 162*).

A limited number of enzymes are known that require nickel as a cofactor (*163, 164*). *M tb*. encodes a urease gene (Rv1848), as well as a gene encoding a hypothetical Ni(II) enzyme (Rv0546c) glyoxylase, that metabolize the DNA abduct-forming methylglyoxal (*165*). In *M. bovis* BCG, thought to be a progenitor strain of *M tb.* (*166*), the catalytic product of urease, ammonia, is believed to be important in host survival as it neutralizes the pH of the phagosome, inhibits lysosomal-phagosomal fusion, attenuates the exposure of the major histocompatibility complex class II in the host cell surface, and is used for nitrogen biosynthesis (*167-169*). Since *M. tb.* does not compete against its host for nickel acquisition (*5, 170-172*), as is the case for other essential metals in humans including Fe (*173, 174*), this urease-dependent function may represent an

important pathogenesis determinant in *M tb*. As a result, *M tb.* is predicted to encode complete Ni-uptake and Ni-efflux systems. Nevertheless, the importance of Ni-homeostasis in *M tb*. pathogenesis remains poorly understood, although it is known that total nickel levels fall precipitously inside macrophages infected with *M tb*.(*175, 176*).

Nickel specific transcriptional regulation of genes encoding for uptake, efflux, detoxification, sequestration and regulatory proteins (*14, 177*) may well be central for adaptation and survival of *M tb.* in the human host (*70, 173, 178-180*). Some metalloregulators, transcriptional regulators that are activated or inhibited to bind DNA in respond to metal, that are encoded in the *M. tb.* genome had been characterized (Table 2.1). There are two Ni(II) specific regulators in mycobacteria and both are members of the ArsR/SmtB family of metal sensors (*14*). These are NmtR and KmtR, which regulate the expression of *ctpJ* and *cdf*, a cation P-type ATPase and a Cation Diffusion Facilitator pump respectively, each of which is predicted to mediate the export of Ni(II) and Co(II) from the cytoplasm (*76, 159*). In other organisms, complete Ni(II) homeostasis systems have been characterized. In E. coli, *rcnA* is Ni(II)/Co(II) efflux protein whose expression is controlled by RcnR (*56, 71*), a member of a newly discovery CsoR/RcnR family of regulators (*90*) while *nikABCDE*, is a high affinity ABC-type transporter that mediates acquisition of Ni(II), and is under the transcriptional control of NikR (*69, 181*). In the actomycete related to *M. tb*., *Streptomyces coelicolor* Nur, a Fur family member, coordinates the expression of Ni(II) *vs*. Fe(II) superoxide dismutase (*sodN* and *sodF*) and of *nikABCDE* (*23, 92*).

Table 2.1 Putative and known metal ion transporters in *M. tb.* with known transcriptional regulators

Family	Transporter	Regulator	Inducer	Family	Ref
P-ATPase (metal efflux)	*ctpG* (Rv1992c)	CmtR	Pb(II)/Cd(II)	ArsR/SmtB	(*95, 157*)
	ctpJ (Rv3743c)	NmtR	Ni(II)/Co(II)	ArsR/SmtB	(*157*)
	ctpV (Rv0969)	CsoR	Cu(I)	CsoR/RcnR	(*27, 90*)
Cation diffusion facilitator (metal efflux)	*cdf* (Rv2025c)	KmtR	Ni(II)/Co(II)	ArsR/SmtB	(*76*)
ABC transporters					
metal uptake	*irtAB*(Rv1348, 1349)	IdeR	Fe(II)	DtxR/IdeR	(*182-184*)
metal uptake	*znuAB* (Rv2059, 2060, 2061c)	FurB (Zur)	Zn(II)	Fur	(*108, 156*)

A few members of the ArsR family of metalloregulators have now been structurally characterized. The *S. aureus* Zn(II) sensor CzrA, is currently the best characterized family member as to its functional, structural and thermodynamic mechanism of allosteric regulation (*109, 111*). A current hypothesis is that transition metal selectivity in the cell is dictated primarily by coordination geometry and some of the support from this model come from comparative studies contrasting the metal center structures of two α5 site metalloregulators of the ArsR/SmtB, NmtR, a Ni(II)/Co(II) sensor and CzrA, a Zn(II)/Co(II) sensor (*14*). NmtR binds Ni(II) and Co(II) with a octahedral coordination while CzrA binds Zn(II) in a tetrahedral geometry (*99*). These metal coordination geometries correspond to the most common coordination geometries found for Ni(II) and Zn(II) in proteins (*103*). The binding of the non-cognate metal to NmtR or CzrA results in formation of a non-native coordination geometry that gives rise to a greatly reduced or elimination of metalloregulation of DNA binding (*99*). A residue substitution mutagenesis screen of CzrA revealed that two metal ligands were necessary to maintain the native coordination geometry and Zn(II)-mediated regulation, while two other ligands were necessary only for maintaining high metal stability with no or small effects on regulation, in what was called a "division of labor" organization (*45, 46*). As a result, it has been hypothesized (*15*) that the metal coordination geometry is a primary determinant of metal selectivity for metalloregulators (*40, 185*) and this hypothesis is well-supported by accumulating evidence from many families of metalloregulators, including CsoR and NikR (*72, 186*).

A previous *in vivo* study of NmtR identified functionally important metal ligands in the α5 helix, D91, H93, H104, H107 exactly coincident with the Zn(II) regulatory site of CzrA, as well as C-terminal residues H109 and H116 (*33*). In the present study, we further test this model by measuring the stability of the metal center and metal-mediated negative allosteric regulation of DNA binding of a panel of conserved glutamine substitution mutants (H to Q and D to Q) on NmtR. These studies provide a new insight into relative importance of the structural and functional relevance of the N- and C-terminal extensions in NmtR relative to CzrA in maintaining Ni(II) selectivity and Ni(II) mediated regulation in *M. tb*., and lay the ground work for ongoing structural studies of NmtR.

MATERIALS AND METHODS

Protein purification. Protein purification was essentially carried out as previously (*33, 99*), and briefly it consists of PEI precipitation of lysis supernatant, followed by two successive ammonium sulfate cuts (35 and 70%) and equilibration in 25 mM MES buffer pH 6.0, 0.1 M NaCl, 5 mM EDTA in preparation for a SP sulfopropyl column, followed by a Q column, in 25 mM Tris pH 8.0, 0.05 M NaCl. The final polishing step is a G75 preparative grade gel filtration run in 10 mM Hepes, pH 8.0, 0.2 M NaCl buffer. The G75 elution profile of all the NmtR mutants is consistent with a dimer assembly state in all cases. All mutant NmtR were shown by ESI-MS to give the expected molecular weight if one assumes that in all the proteins, Met1 is processed (Appendix F); to yield, a N-teminal Gly^2-His^3-Gly^4 sequence.

Anisotropy experiments. These binding experiments and the purification of DNA was done as previously described (*17*). The protein sample was diluted to a concentration of 10 μM and 2-4 μL of this stock solution was titrated into 1800 μL of 10 mM Hepes, pH 7.0, 25 ^{o}C and 10 nM dsDNA with 3-6 min equilibration time. The DNA sequence correspond to the wild type *nmt* operator containing the imperfect repeat known to be the binding site (underlined) (*33*) and is fluorescein labeled in the 3' (5'-GAAATAAA*TGAACA*TA*TGATCA*TATATTCT-3'-Fl). For non-specific DNA, 200 ng/ml of deoxyribonucleic acid (sodium salt) from salmon testes (SIGMA) was added to the buffer, diluted by stirring in a heating block at 60 ^{o}C for 6 hrs and autoclaved for preservation. Anisotropy measurements have an SD $\leq$ 0.001 with the slit set to 1.0 for experiments at 0.2 M NaCl and set to 2.0 for experiments at 0.4 M NaCl. The excitation monochrometer set to λ_{480}, instrument in L-format, longpass filter λ_{515} in the emission and '*G'* factor set to 1. All the data was fit to the model described in the text using DynaFit (*187*). The fit account for a dimerization constant of K_{apo}=1.9 x 10^5 M^{-1} or K_{Ni}=4.1 x 10^5 M^{-1} (*99*).

Tyrosine fluorescence experiments. Experiments were carried out as previously described (*33*). In 1800 μL of 10 mM Hepes buffer, pH 7.0, 25 ^{o}C and 0.2 M NaCl, wild-type NmtR and mutant variants were diluted to 5-10 μM and fluorescense measured every *i*th addition of 1-4 μL of 0.5-2 mM $NiCl_3$, waiting 3 minutes after each addition to allow for equilibration. The excitation monochrometer was set at λ_{260} and emission collected through monochrometer set at λ_{300}, and 2.0 slit, with a mesh used at the emission channel when the high protein concentration is used. The average of 100

iterations for each addition was recorded. The chelators nitriloacetic acid (NTA) or ethylene glycol tetraacetic acid (EGTA) was added to a concentration of 18-21 μM from a concentrated stock solution calibrated by metal addition monitored by ITC. Metal stocks were quantified by atomic absorption as described previously (*33, 99*).

Mag-fura 2 competition experiments. NmtR variants and competitor Mag-fura 2 (mf2) were diluted in 1800 μL of buffer (25 mM Hepes pH 7.0, 0.2 M NaCl and 25 °C) to the concentration indicated in the text. Aliquots of 2 μL from a 0.5 – 1 μM Ni(II) stock were added to the mixture, equilibrated for 3 minutes and the excitation spectra (λ_{ex} 377-383, slit 0.5) recorded (λ_{em} 497 , slit 1.0) using the monochrometer. The average of 30 iterations for every i*th* addition was recorded using an ISS PC1 instrument and software.

Co(II) electronic absorption spectroscopy. These experiments were carried out as previously described for wild-type NmtR (*99*). A sample of NmtR or NmtR variants was diluted in buffer (MES pH 6.0, 0.2 M NaCl, at room temperature) and titrated with 2-10 μL of 100 μM-2 mM Co(II) stock solution, and the U.V.-visible spectra recorded following every *i*th addition. The apo-protein spectra was subtracted and the resulting difference spectra corrected for dilution.

Calculation of NTA, EGTA and Mf2 Ni(II) affinity constants. EGTA-Ni(II) and NTA -Ni(II) affinity constants was calculated by the Schwarzenbach's α-coefficients method were;

$$\beta_n' = \beta_n / \alpha_M(\alpha_L)^n$$

$$\alpha_M = ([M] + [MOH] + [M(OH)2] + \ldots)/[M]$$

$$\alpha_L = ([L] + [HL] + [H2L] + \ldots)/[L]$$

and for the NTA-Ni(II) equilibria the NTA-Ω factor was also used:

$$\Omega = 1 + \beta\,[NTA] + \beta_2\,[NTA]^2$$

$$K' = \Omega \times K_{obs}$$

were K_{obs} is equal to the observed affinity while *K'* is the actual or corrected affinity of NmtR for Ni(II).

RESULTS

Wild-type NmtR metal binding affinity. The metal ligands were functionally characterized using intrinsic fluorescence as a reporter of metal binding. On a sequence alignment based on structural homologs, the three tyrosine residues are predicted to flank the metal binding domain (Figure 2.1) (*14*). As previous data indicates (*99*), NmtR binds Ni(II) or Zn(II) with an concomitant 30-35% increase in the intrinsic tyrosine fluorescence, with a stoichiometric of two metals per dimer or one per protomer (Figure. 2.2(a)). Since this binding curve is essentially stoichiometric, only a lower limit of the Ni(II) binding affinity of $\sim 10^8\ M^{-1}$ could be obtained. Thus, a competitor chelator was included in the binding experiments in order to extract quantitative metal stability constants. The carboxylate chelators EGTA (ethylene glycol tetraacetic acid) and NTA (nitrilotriacetic acid) were used for this purpose. EGTA competition were previously used to measure the Ni(II) binding affinity in the *E.coli* metalloregulator NikR, find to be in the order of $10^{10}\ M^{-1}$ (*54*). The apparent stability of EGTA for Ni(II) corrected for the experimental pH used here (pH 7.0, $K_{EGTA\text{-}Ni}$) $2.14 \times 10^9\ M^{-1}$, was calculated as

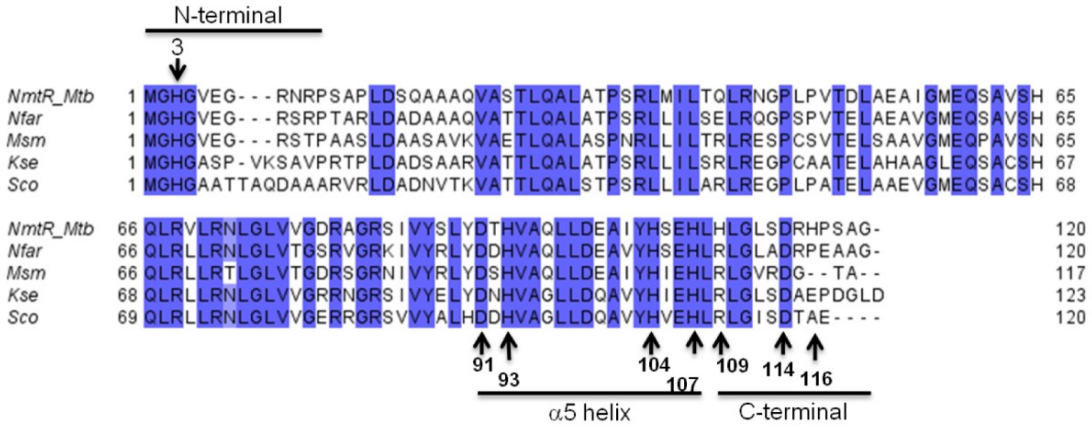

Figure 2.1 Multiple sequence alignment of SmtB/ArsR family members that were obtained with NmtR as a query. The results were filtered by selecting those sequences that posses a C-terminal extension that extent pass residue 114 of NmtR. Conserved residues are blue boxed. Arrows indicate residues that were substitute by glutamines at the present work, numeration as in NmtR. NCBI reference sequence: NmtR *M. tb*.:NP_218261.1, Nfar (*Nocardia farcinica*) YP_119316.1; Msm (*Mycobacterium smegmatis*) YP_889646.1; Kse (*Kitasataspora setae*) BAJ32877.1; Sco (*Streptomyces coelicolor*) NP_630544.1. All belong to phylum *Actinobacteria*.

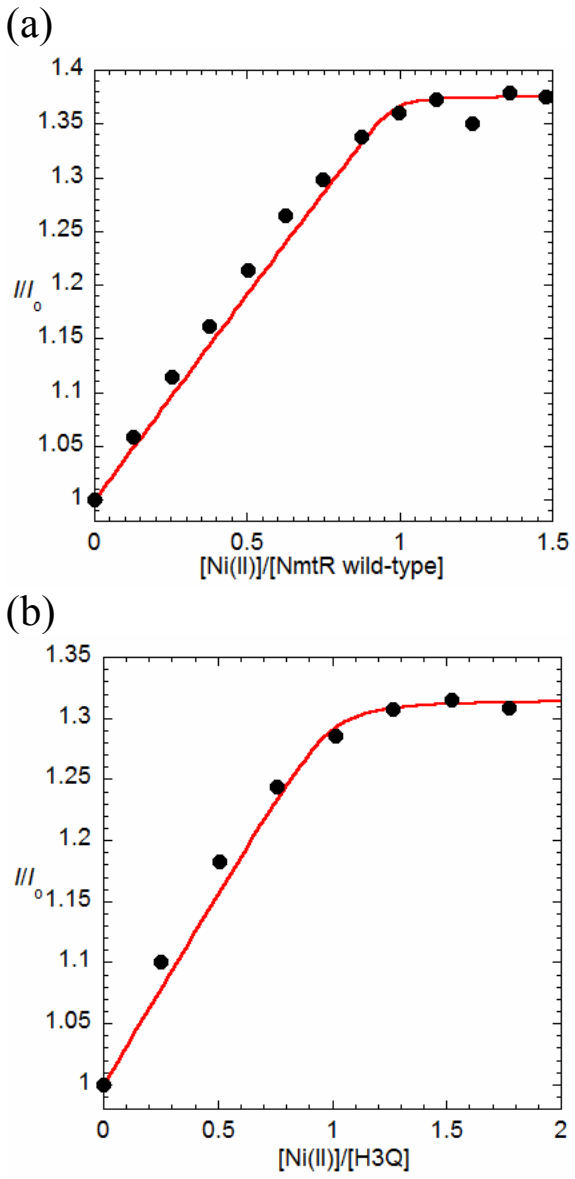

Figure 2.2 Ni(II) binding to (a) wild-type and (b) H3Q NmtRs at 5.0 μM protein monomer (2.5μM dimer). Ni(II) binding isotherm as monitored by a change in the intrinsic fluorescence intensity (I/I_o). The red line represents non-linear least-square fits to a 1:1 (Ni(II):monomer) binding model. (a) NmtR wild-type (K_{Ni}~ 8.94 x 10^8 M^{-1}), (b) H3Q NmtR (K_{Ni}~ 1.50 x 10^8 M^{-1}).

previously (*188*) using the Schwarzenbach's α-coefficient method (*189*) and the relevant pH-independent parameters taken from the published NIST values (*190*). Comparable binding affinities were obtained using NTA as the competitor. This chelator has also been used as a competitor for other metalloregulators (*98*). For this series of experiments, the affinities of Ni(II) for NTA were calculated (Materials and Methods) using the Ω-coefficient method (Ω=1.56 x 10^4, pH 7.0, 20 μM NTA), or the Schwarzenbach's α-coefficient (α_L= 4 x 10^2, $K_{NTA\text{-}Ni}$ = 6.01 x 10^8 M^{-1}, $\beta 2$ = 7.7 x 10^{13} M^{-2} at pH 7.0), with both methods giving similar results. The affinities calculated are consistent with previously tabulated results (*191*).

The binding isotherms measured in the presence of each competitor are very similar, and the shape indicates that NmtR affinity for Ni(II) is higher than that of NTA or EGTA for Ni(II) (Figure 2.3 (a) and (b)). Based on the binding stoichiometry of 1:1 (metal:monomer) and a dimeric assembly state from gel filtration in the μM range (Materials and Methods), we chose a Ni(II) binding model of two stepwise metal binding events (K_{Ni1} and K_{Ni2}) to a nondissociable dimer to analyze this data. The results show that wild-type NmtR binds Ni(II) with an affinity of $K_{Ni1} \sim K_{Ni2} \sim 10^{10}$ M^{-1} (Fig. 2.3(a), Table 2.2).

NmtR is allosterically regulated by Ni(II)>Co(II)>Zn(II). NmtR binds an inter-genomic operator/promoter region in the absence of Ni(II), and represses the expression of a reporter gene *in vivo* (Figure 1.7) (*33*). Transcription is de-repressed upon addition of Ni(II) or Co(II) to the growth medium, but not by the addition of Zn(II) (*33*). Here, we are interested in quantifying the metal affinity and allosteric response of NmtR to

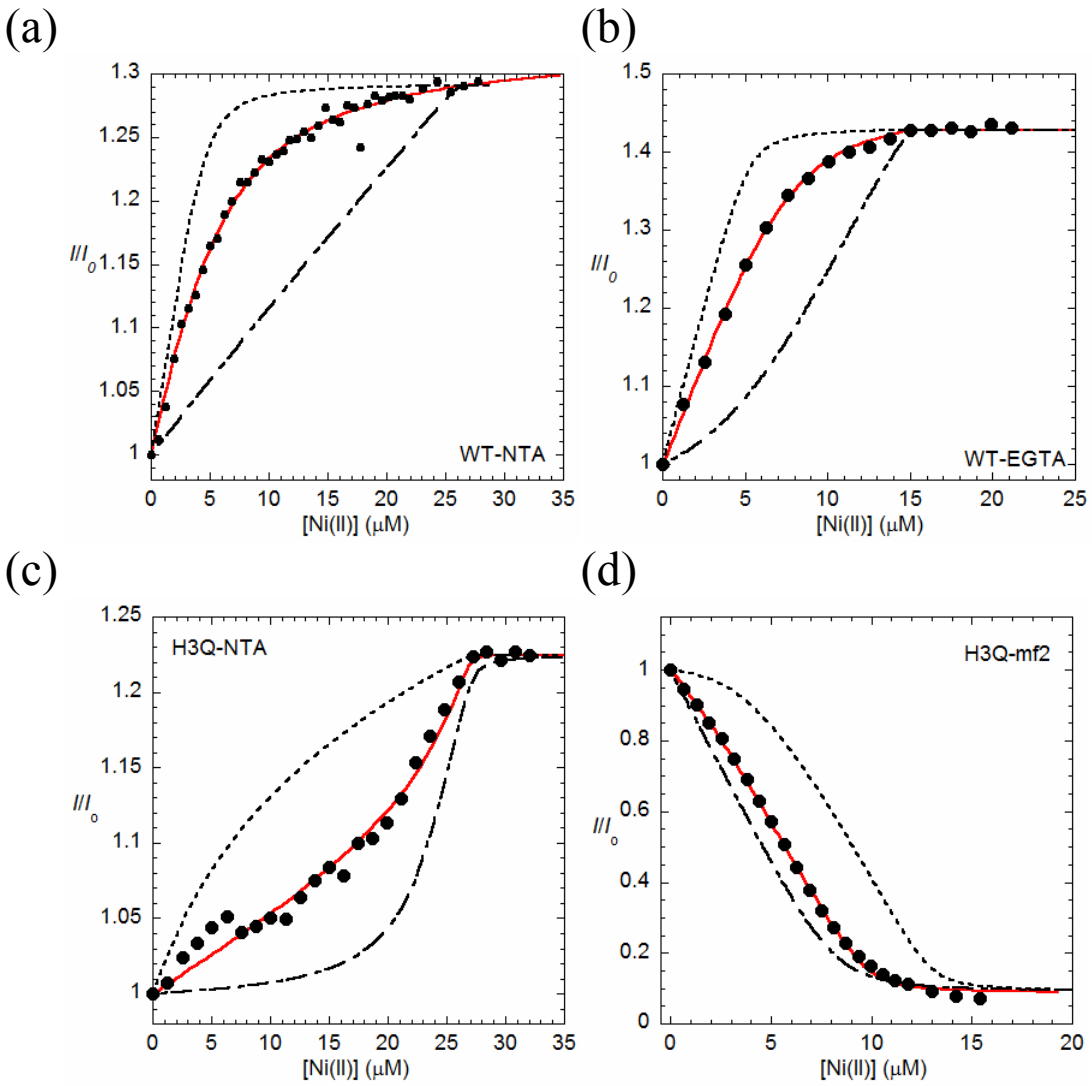

Figure 2.3 Metal-chelator competition experiments with wild-type and H3Q NmtRs. Ni(II) binding isotherm as monitored by the intensity of the intrinsic fluorescence change (*I*/*I*o), in the presence of NTA (a) and (c), EGTA (b) or mf2 (d). The red line represents non-linear least-square fits to a 2:1 (Ni(II):dimer) binding model. The results of the fit are given in the text (Table 2.2). Concentrations (a) 5μM NmtR wild-type and 21μM NTA, (b) 5μM NmtR wild-type and 10μM EGTA, (c) 5μM H3Q and 20μM NTA, (d) 5μM H3Q and 8 μM mf2 . The dashed lines represent simulations if K_{Ni} values were one log higher and lower. Binding affinities K_{Ni1}, K_{Ni2} ($x10^{10}$ M^{-1}); (a) 1.3 (±0.2), 0.3 (±0.04), (b) 1.1 (±0.03), 1.10 (± 0.03) (c) 0.073 (± 0.0008), 0.001(± 0.0004) (d) 0.010 (± 0.005), 0.001 (± 0.0001).

Table 2.2 Ni(II) binding affinities of NmtR wild-type and mutant variants

NmtR	K_{Ni1}(x10^{10} M^{-1})	K_{Ni2}(x10^{10} M^{-1})
Wild-type [a]	1.15 (±0.10)	0.70 (±0.40)
H3Q [b]	0.042 (±0.03)	0.001 (±0.0001)
D91Q[c]	0.0120 (±0.0005)	0.001 (±0.0001)
H93Q[c]	0.0031 (±0.0001)	0.001 (±0.0001)
H104Q[c]	0.0004(±0.00003)	0.001 (±0.0001)
H107Q[c]	0.0034 (±0.0002)	0.001 (±0.0001)
H109Q[a]	0.75 (±0.25)	1.00 (±0.01)
D114Q[a]	0.76 (±0.04)	0.60 (±0.13)
H116Q[a]	0.77 (±0.18)	0.55 (±0.05)
Δ111NmtR[a]	2.43 (±1.6)	- [d]

Conditions: 10mM Hepes pH 7.0, 0.2 M NaCl, 25 ^{o}C
[a]Average of K_{Ni} measured in presence of NTA or EGTA as competitor.
[b]Average of K_{Ni} measured in presence of NTA or mf2 as competitor.
[c]mf2 competition experiments
[d]not detected, e.g., stoichiometry of one per dimer

different metals and the extent to which single substitution mutants affect this response. Ni(II) affinities are compiled in Table 2.2 and DNA-binding parameters are presented in Table 2.3. We employed an anisotropy-based experiment to measure allosteric regulation using a 30 bp fluorescein-labeled duplex DNA that harbors the quasi-perfect inverted repeat sequence to which NmtR binds (*33*). To our surprise, Ni(II) was found to reduce the binding affinity by only 20 fold with respect to apo-NmtR, *vs*. the expected 200-300 fold observed previously at higher monovalent salt concentration (0.4 M NaCl) (Table 2.3) (*99*). This finding suggest that Ni(II)NmtR forms a DNA complex characterized by appreciable non-specific binding interactions at 0.2 M NaCl. To test this we measured the DNA binding affinity of NmtR for its operator at 0.4 M NaCl in the presence and absence of nonspecific DNA, in an effort to decrease the nonspecific electrostatic component of the interaction. To choose the appropriate model to fit the anisotropy data, the dimerization equilibrium constant previously measured was taken into account (*99*), consistent in a model in which the binding of NmtR to DNA at sub-micromolar concentrations is linked to a monomer-dimer equilibrium. In addition, the change in anisotropy that results from titrating apo-NmtR in to the DNA probe, (Δr_{obs}) is 0.016 consistent with previous stoichiometric determinations of binding one dimer per DNA of similar length (*99, 109, 135*). Therefore, a model that describes the binding of a dissociable NmtR dimer to DNA was used to analyze the data.

These data (Figure 2.4(a), Table 2.3) reveal that apo-NmtR binds to DNA with a K_{DNA} of 9.0 (±0.3) x 10^9 M^{-1} at 0.4 M NaCl independent of the presence of the competitor DNA; thus this is the specific binding affinity of apo-NmtR for its operator

Table 2.3 NmtR wild-type DNA binding affinities for different metal complexes

NmtR WT	Δr_{max} [a]	K_{DNA} ($x10^9$ M^{-1})	ΔG_c [b] (kcal mol^{-1})
1=0.2			
apo[c]	0.027	28.6 (±0.4)	-
Ni(II)[d]	0.027[a]	1.5 (±0.1)	1.7 (±0.04)
1=0.4 and Nonspecific competitor[e]			
apo[c]	0.016	9.2 (±1.0)	-
Ni(II)[d]	0.016[a]	0.06 (±0.01)	2.9 (±0.1)
1=0.4			
apo[c]	0.020	8.70 (±1.0)	-
Ni(II)[f]	0.020[a]	0.10 (±0.01)	2.7 (±0.1)
Co(II)[f]	0.020[a]	0.21 (±0.03)	2.2 (±0.1)
Zn(II)[f]	0.027	1.5 (±0.2)	1.1 (±0.1)

Conditions: 10mM Hepes, pH 7.0, 25 °C

[a] Δr_{max} = maximum fitted anisotropy

[b] $\Delta G_c = -RT \ln(K_{DNA\text{-}Ni}/K_{DNA\text{-}apo})$

[c] For determination of *apo* K_{DNA} 500μM EDTA was added to the binding reaction.

[d] For determination of Ni(II) K_{DNA} 100μM Ni(II) was added to the binding reaction.

[e] Salmon sperm DNA

[f] For determination of metal K_{DNA} 10μM Ni(II), Co(II) or Zn(II) was added to the binding reaction

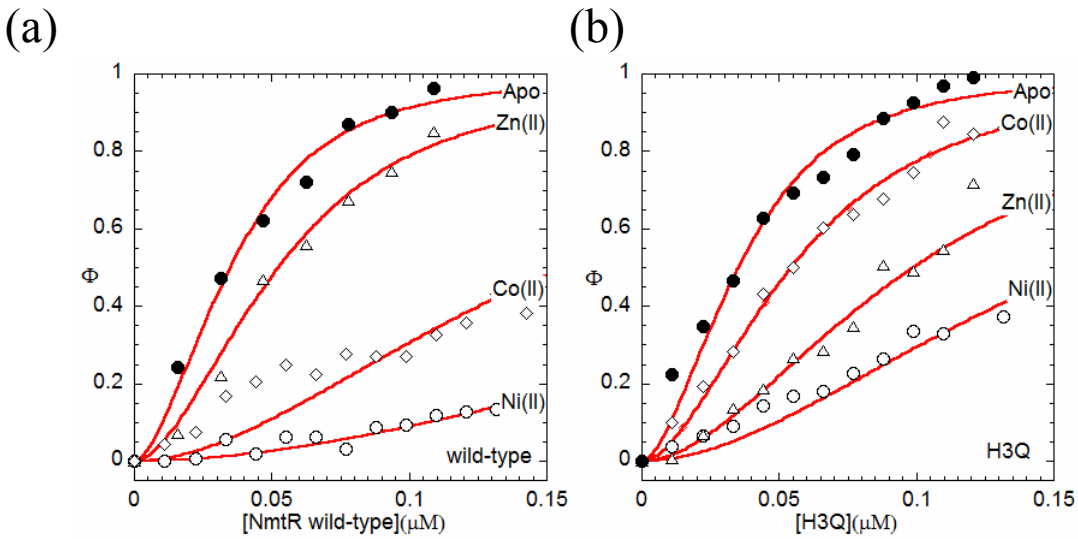

Figure 2.4 Allosteric regulation of DNA binding by wild-type (a) and (b) H3Q NmtR variants. Representative data points of binding isotherms depicted by open and closed symbols for metal or apo-form respectively. The red line represents non-linear least-square fits to a model where a dissociable dimer binds to a single DNA. The total anisotropy change is normalized to the apo-NmtR value (Δr_{max}) so for each instance the anisotropy change observed (Δr_{obs}) is a fraction of that for apo-NmtR. Table 2.3 and 2.4 gives the K_{DNA} values calculated from this analysis, along with values of Δr_{max}. Key to notation (as indicated in the figure): Ni(II); open circles, Co(II); diamonds, Zn(II); triangles. NmtR H3Q depict are data from experiments with 10 μM metal added.

sequence. Addition of Ni(II) to the binding reaction shifts the binding equilibrium to higher concentrations, decreasing the affinity by ~100 fold to 8.0 (±2.0) $x10^7$ M^{-1}. The magnitude of this response in thermodynamic terms is given by the coupling free energy ΔG_c (Figure 1.5) (*15*), which defines effectiveness of the communication between DNA operator and Ni(II) binding sites which leads to allosteric inhibition of DNA binding. For wild-type NmtR ΔG_c = 2.8 (±0.1) kcal mol^{-1}, with the positive sign indicative of negative heterotropic linkage. The specific DNA binding affinity of NmtR is decreased by addition of other metals, but the magnitude of their regulation is quantitatively less effective. Co(II), an inducer of the *nmtA* transcription *in vivo* (*33*), is characterized by a ΔG_C = 2.2 kcal mol^{-1} which is followed by Zn(II), which reduces the affinity of NmtR for DNA 6 fold. We note that the anisotropy change observed for Zn(II) NmtR is 1.4 times larger than for the apoprotein (Δr_{obs}= 0.026), which suggests that Zn(II) binding lead to higher order NmtR-DNA complex. This was not investigated further.

His3 contributes to the stability of the metal binding site. Some members of the ArsR/SmtB family use metal ligands from the N-terminal extension to coordinate metal to the α3 helix (α3N subfamily) (*14*) and crystallographic studies suggest that this "tail" is not likely to be structurally organized (*192*). In the N-terminal domain of NmtR, the conserved residue His3 is an excellent candidate for a Ni(II) ligand (Figure 2.1), based on precedents in the literature. This histidine is flanked to each side by Gly, forming a specific sequence (Gly-His-Gly) that can coordinate Ni(II) with one or two deprotonated main chain amide, the α-amino terminal and the side chain histidine Nδ1 or Nε2 atoms

(*193-197*). A metalloregulator thought to utilize such an arrangement is found in *E. coli* RcnR, a Ni(II) dependent metalloregulator from the CsoR family (*56*).

The N-terminal residue Met1 is processed during the expression of NmtR as corroborated by ESI-MS (Materials and Methods), as a result little steric clash is expected from the backbone Gly2-His3-Gly4 sequence, if indeed it is used to coordinate the metal. The importance of this residue as Ni(II) ligand and/or regulation in NmtR was investigated using a Gln substitution mutant. NmtR H3Q binds Ni(II) with a stoichiometry of 1:1 (Ni(II):protomer) like wild-type NmtR; with a concomitant increase of 30% fluorescence intensity and a lower limit of K_{Ni} of ~ 10^8 M^{-1} observed from direct titration in the absence of chelator (Figure 2.2(b)). However, in the chelator competition experiments, the Ni(II) binding isotherm depicts a shape that is indicative of dramatically decreased affinity with respect to wild-type NmtR (Figure. 2.3 (c)-(d)). The stepwise binding affinities of H3Q NmtR are reduced by ~20 and ~700 fold for K_{Ni1} and K_{Ni2} relative to wild-type NmtR (Table 2.2). Nevertheless, the DNA binding experiments show that apo H3Q binds DNA similarly to wild-type, with a change in anisotropy that is comparable to the wild-type NmtR (Figure 2.4(b), Table 2.4). H3Q binding to DNA is still strongly regulated by Ni(II), but with ΔG_C^{Ni}= 2.8 kcal mol^{-1} and identical to that of wild-type protein NmtR. This mutant is significantly more sensitive to Zn(II) mediated inhibition relative to Co(II). These data suggest that His3 directly influence binding and Ni(II)/Co(II) selectivity of this switch (see Discussion).

Conserved residues in the α5 putative helix are essential for Ni(II) binding affinity and allosteric regulation. Mutations in the α5 helix of sensors CzrA and SmtB

Table 2.4 DNA binding affinities of H3Q NmtR with different metal complexes

NmtR H3Q	Δr_{max} [a]	K_{DNA} ($x10^9$ M^{-1})	ΔG_c [b] (kcal mol^{-1})	*Wt*. ΔG_c [c] (kcal mol^{-1})
apo[d]	0.019	8.40 (±1.00)	-	-
10 μM metal				
Ni(II)	0.019	0.07 (±0.01)	2.8 (±0.1)	2.7 (±0.1)
Co(II)	0.019	1.33 (±0.20)	1.1 (±0.1)	2.2 (±0.1)
Zn(II)	0.019	0.35 (±0.02)	2.0 (±0.1)	1.1 (±0.1)

Conditions: 10mM Hepes, pH 7.0, 0.4 M NaCl, 25 °C

[a] Δr_{max} = maximum fitted anisotropy

[b] $\Delta G_c = -RT \ln(K_{DNA\text{-}Ni}/K_{DNA\text{-}apo})$

[c] Wild-type NmtR values show for comparison

[d] For determination of *apo* K_{DNA} 500μM EDTA was added to the binding reaction.

are characterized by loss of function and/or decrease of Zn(II) binding affinity (*45*). NmtR is predicted to coordinate Ni(II) with the four ligands conserved in the α5 helix relative to the CzrA sequence (D91, H93, H104 and H107), and all were, as expected, found to be essential for regulation in an *in vivo* experiment (*33*). Here we substitute, each of these residues with a non-liganding Gln to test their requirement for stabilization of the metal complex and/or to quantify the loss of allosteric regulation. An increase in intrinsic Tyr fluorescence in response to Ni(II) binding was not detected for any of these α5-site NmtR variants, suggestive of non-native structure found in each case. Therefore, the fluorescent indicator mag-fura-2 (mf2) was used instead to monitor binding of Ni(II) in competition experiments analogous to an approach used previously to measure Ni(II) affinity in other systems (*56, 58*). In our hands, calibration of the mf2 with NTA give an affinity $K_{\text{-Mf2-Ni}} = 2.0\ (\pm 0.1)\ \text{x}10^7\ \text{M}^{-1}$ (Figure 2.5) that is in reasonable agreement with the previously tabulated affinity $K_{\text{Ni-Mf2}} = 7.7\ \text{x}\ 10^6\ \text{M}^{-1}$ measured at the same salt concentration(*56, 58*). The results of these competition experiments (Figure 2.6) are clearly indicative of significant competition with mf2, albeit a pronounced reduction of K_{Ni1} and K_{Ni2}, in each α5-site variants (Table 2.2).

The Ni(II) dependent allosteric regulation of DNA binding was quantified by measuring DNA binding curves in the absence and presence of 0.1 mM Ni(II), a concentration sufficient to saturate Ni(II) sites on this regulators (Figure 2.7, Table 2.5). Surprisingly, the presence of excess metal increases the value of Δr_{max} two to three-fold, with the possible exception of H104Q NmtR in which binds with an affinity and Δr consistent with wild-type apo NmtR, perhaps indicative of a different assembly state on

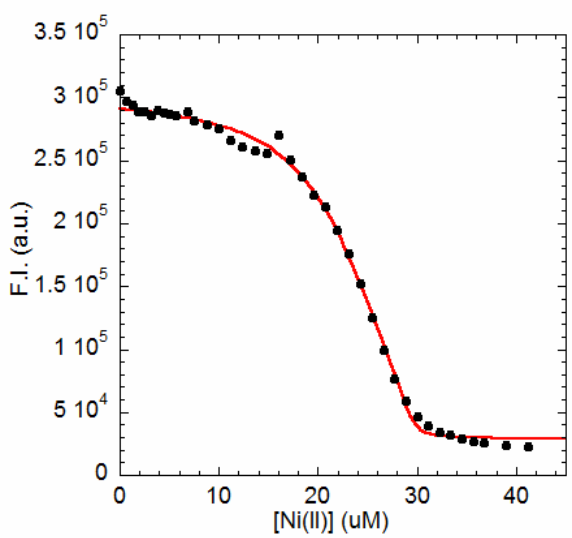

Figure 2.5 Calibration of mag-fura-2 binding affinity for Ni(II). Binding affinity of mf2 for Ni(II) was obtained from competition experiments with NTA. The binding isotherm of Ni(II) titration into mf2 depict as the total fluorescence intensity (F.I.) quenching. The red line represents a non-linear least-square fits to a 1:1 Ni(II):mf2 binding model. The calculated value $K_{Mf2\text{-}Ni} = 2.0 (\pm 0.1) \times 10^7\ M^{-1}$. [NTA] = 20 μM and [mf2] = 9.7 μM.

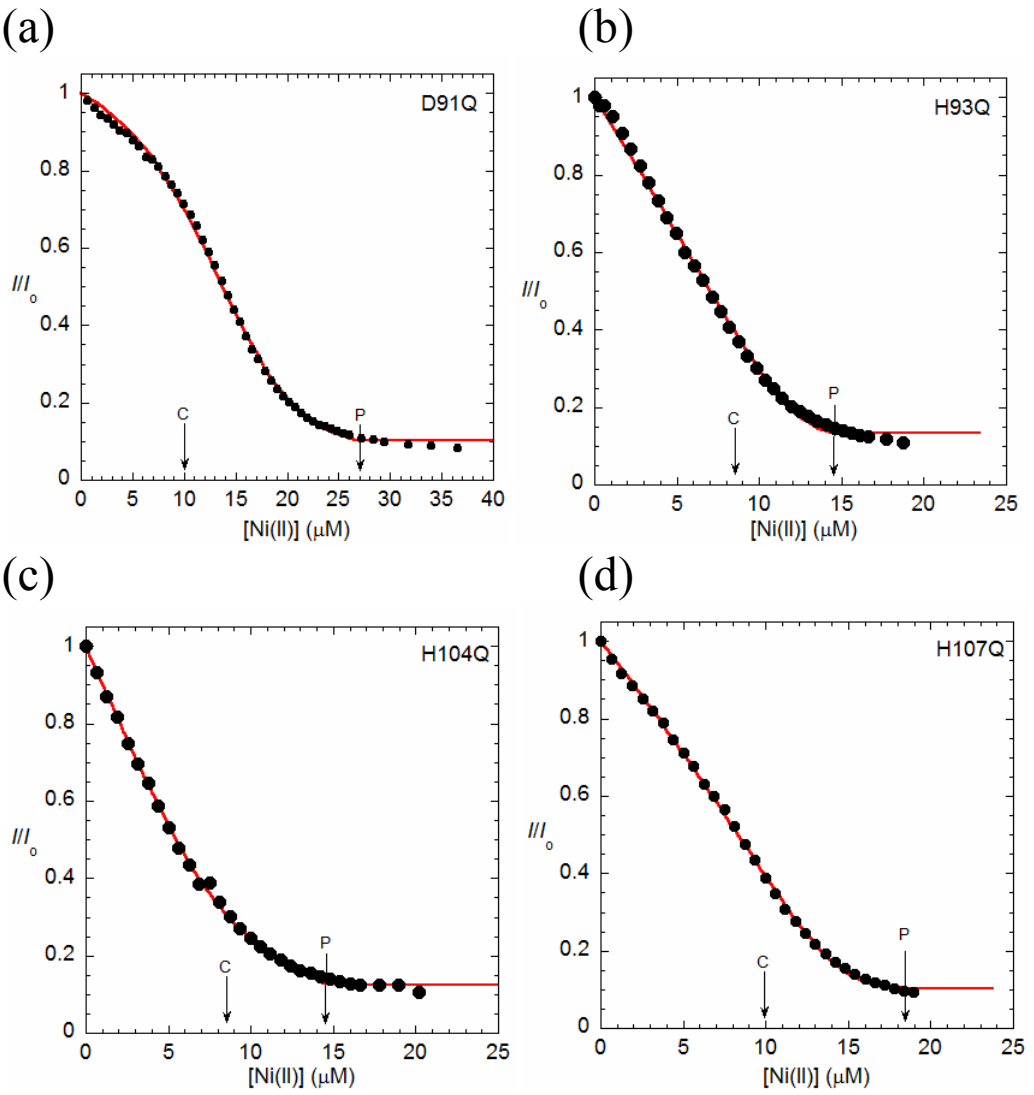

Figure 2.6 Ni(II) binding to α5-siste Gln substitution mutant NmtRs variants. Binding is monitored by mf2 fluorescence quenching. Red lines represent non-linear least square fit to a 2:1(Ni(II):dimer) binding model. All the *K* values are given in Table 2.2. An arrow labeled C indicates the number of Ni(II) sites for chelator alone and an arrow labeled P points at the total number of sites (μM). [Concentrations](μM); (a) [D91Q] = 17 [mf2] = 10, (b) [H93Q] = 6, [mf2] = 8.5, (c) [H104Q] = 6, [mf2] = 8.5, (d) [H107Q] = 7.5, [mf2] = 10.

Table 2.5 DNA binding affinities of α5 missense mutant NmtRs in presence of Ni(II)

NmtR	Δ *r* max.[a]	Δ *r* obs.[b]	K_{DNA} (x10^9 M^{-1})	ΔG_c[c,d] (kcal mol^{-1})
D91Q				
apo[e]	0.026	0.026	5.0 (±0.4)	-
Ni(II)[f]	0.046	0.046	7.5 (±0.1)	–0.2 (±0.1)
H93Q				
apo[e]	0.019	0.019	4.2 (±0.7)	-
Ni(II)[f]	0.050	0.050	16 (±3.0)	–0.8 (±0.1)
H104Q				
apo[e]	0.004	0.003	0.85 (±0.22)	-
Ni(II)[f]	0.012	0.010	0.77 (±0.10)	–0.1 (±0.2)
H107Q				
apo[e]	0.025	0.024	50.0 (±1.0)	-
Ni(II)[f]	0.044	0.043	24.0 (±0.5)	0.4 (±0.01)

Conditions: 10mM Hepes, pH 7.0, 0.4 M NaCl, 25°C.

[a] Δ *r* max = anisotropy fix as maximal response in the fit and normalization

[b] Δ *r* obs = Δ *r* max

[c] $\Delta G_c = -RT \ln(K_{DNA\text{-}Ni}/K_{DNA\text{-}apo})$

[d] For comparation $\Delta G_{c\ Ni(II)NmtR\ wild\text{-}type} = 2.7$ (±0.2) kcal mol^{-1}

[e] For determination of *apo* K_{DNA} 500μM EDTA was added to the binding reaction.

[f] For determination of Ni(II) K_{DNA} 100 μM Ni(II) was added to the binding reaction.

the DNA relative to wild-type NmtR. Thus not only are these mutants refractive to Ni(II) regulation, but Ni(II) increases the apparent assembly state and in some cases the affinity, reversing sign on ΔG_C. This observation was further explored in NmtR H104Q, since this NmtR mutant presents a binding isotherm with a very small change in anisotropy, but still easily distinguished from no binding (Figure. 2.7 (c)). The presence of other metals also appears to stabilize DNA complex formation, with the results showing that Ni(II) and Co(II) were the most efficient in increasing the anisotropy of the DNA in a way that is dependent on metal concentration (Figure. 2.8, Table 2.6). Interestingly, this binding has residual elements of DNA specificity since an excess of nonspecific DNA reduces the affinity by ~10 fold if an unrelated DNA probe is used.

C-terminal variants. On the basis of arginine substitution mutants His109 and His116 in the C-terminal extension of NmtR was reported to be essential for metal dependent regulation *in vivo* (*33*). Here we investigate Ni(II) binding affinity and metal-dependent regulation of DNA binding of Gln-substitution mutants of H109, D114, H116 and a truncated C-terminal NmtR that deletes residues 112-120 designated Δ111NmtR. For Δ111NmtR, intrinsic fluorescence experiments conducted in absence of chelator, reveal a metal stoichiometry of just one metal per dimer for Ni(II) and Zn(II), with the second binding event undetected by this method. The change in fluorescence intensity are half that of wild-type NmtR, this is consistent with Ni(II) occupancy at 1 of 2 sites in the dimer (Figure 2.9 (a)). Interestingly, Co(II) binding monitored by UV electronic absorption suggest a stoichiometry of 1.4 equivalents per dimer (Figure 2.9 (b)). These results suggest a perturbation of the structural symmetry in the regulatory metal binding

Table 2.6 Metal induced DNA binding by H104Q NmtR

NmtR H104Q	Δr_{max} [a]	Δr_{obs} [b]	K_{DNA} ($x10^9$ M^{-1})	ΔG_c [c,d] (kcal mol^{-1})
apo[e]		0.004	0.14 (±0.01)	-
10 μM metal				
Ni(II)		0.007	0.37 (±0.04)	-0.6 (±0.1)
Co(II)		0.008	0.42 (±0.04)	-0.6 (±0.01)
Zn(II)		0.007	0.33 (±0.01)	-0. 5 (±0.04)
100 μM metal				
Ni(II)	0.011	0.010	1.0 (±0.1)	-1.2 (±0.1)
Co(II)		0.007	0.23 (±0.01)	-0.29 (±0.04)
Zn(II)		0.010	0.13 (±0.01)	0
Unrelated DNA, [f] *100 μM metal*				
Ni(II)		0.001	0.01(±0.002)	-

Conditions: 10mM Hepes, pH 7, 0.4 M NaCl, 25°C. Excess salmon sperm DNA.

[a] Δr_{max} = anisotropy fix as maximal response in the fit and normalization

[b] Δr_{obs} = anisotropy change at maximum protein concentration

[c] $\Delta G_c = -RT \ln(K_{DNA\text{-}Ni}/K_{DNA\text{-}apo})$

[d] For comparation $\Delta G_{c\ Ni(II)NmtR\ wild\text{-}type} = 2.7$ (±0.15) kcal mol^{-1}

[e] For determination of *apo* K_{DNA} 500μM EDTA was added to the binding reaction.

[f] Sequence in the oligo is not related to NmtR

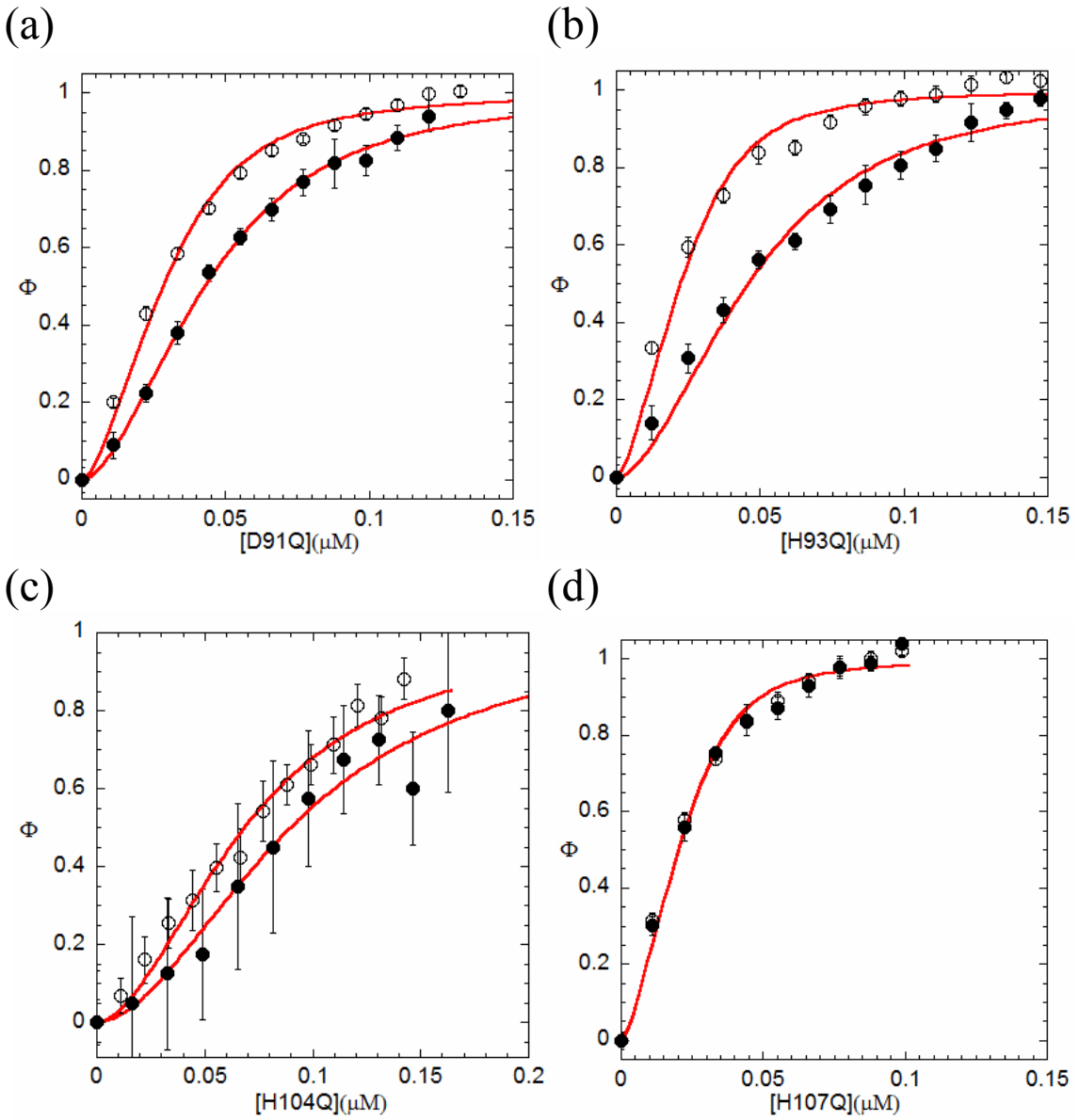

Figure 2.7 Lack of allosteric regulation of α5 missense mutant NmtRs. This variants are defective in Ni(II) dependent allosteric regulation of DNA binding. Depict are binding isotherms of fluorescence anisotropy experiments used to monitor DNA binding. Experiments in presence (open symbols) or absence (closed symbols) of Ni(II). The red line represents non-linear least-square fits to a model where a dissociable dimer binds to a single DNA probe. The data is normalized to the maximum anisotropy change (Δr_{max}) of each metal/apo protein so the plots depict differences in affinity not in total change in anisotropy. Table 2.5 gives the K_{DNA} values calculated from this analysis, along with values of Δr max. (a) NmtR D91Q, (b) NmtR H93Q, (c) NmtR H107Q,(d) NmtR H104Q. The anisotropy standard deviation for each point is depict in the *y* axes.

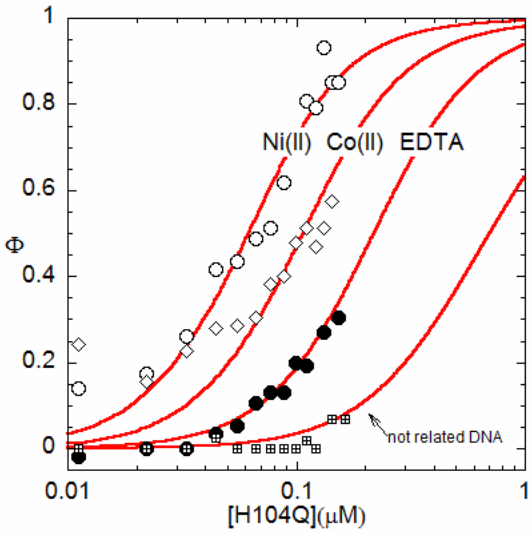

Figure 2.8 Distinct allosteric regulation of H104Q Ni(II)NmtR. Depict are binding isotherms of fluorescence anisotropy experiments used to monitor DNA binding. Open and closed symbols represent metal or apo- form, respectively. The red line represents non-linear least-square fits to a model where a dissociable dimer binds to a single DNA probe. The total anisotropy change is normalized to the Ni(II) NmtR value (Δr_{max}) so for each instance the anisotropy change observed (Δr_{obs}) is a fraction of that for Ni(II)-NmtR. Table 2.6 gives the K_{DNA} values calculated from this analysis, along with Δr_{max}. Key to notation (as indicated in the figure): Ni(II); open circles, Co(II); diamonds, Non related DNA prove; crossed squares. The experiments were performed in excess of nonspecific DNA competitor and illustrated is data obtain in excess of (100μM) metal

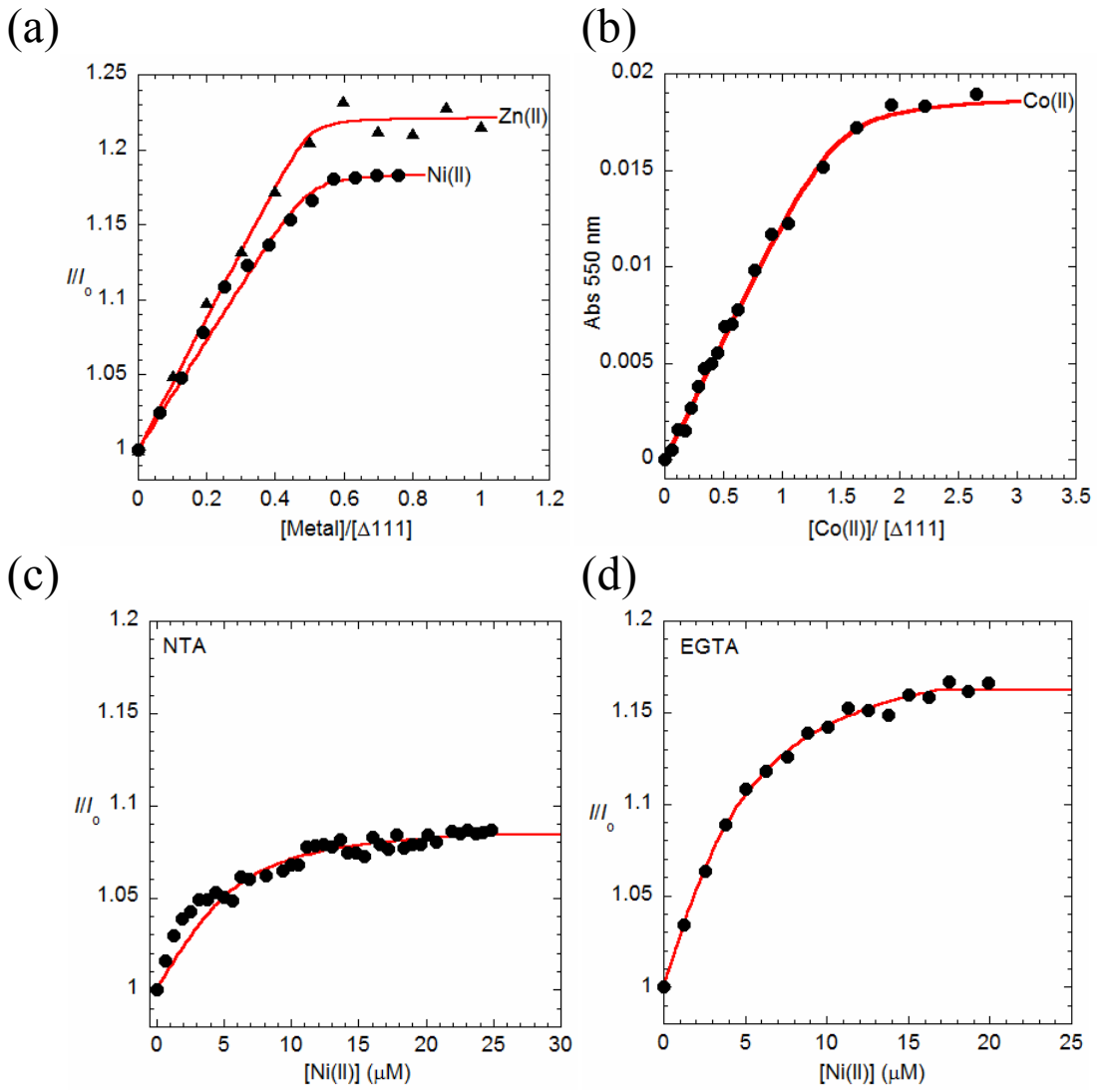

Figure 2.9 Ni(II) binding stoichiometry and affinity for different metals of Δ111 NmtR (a) Ni(II) (circles) and Zn(II) (triangles) binding to Δ111NmtR were monitored by the intrinsic fluorescence intensity change (*I*/*I*o). The red line represents non-linear least-square fit to 0.5:1 (metal:monomer). $K_{\text{NmtR-Zn(II)}} \sim 1.38 \times 10^{8}\ M^{-1}$, $K_{\text{NmtR-Ni(II)}} \sim 9.12 \times 10^{7}\ M^{-1}$ (b) Co(II) binding was monitored by U.V. absorption at 550 nm. The red line represents non-linear least-square fits to 1.5:1 (Co(II):monomer). $K_{\text{NmtR-Coi(II)}} \sim 8.44 \times 10^{7}\ M^{-1}$. Ni(II) monitored by the intrinsic fluorescence intensity change (*I*/*I*o) in presence of a chelator, (c) [NTA] (20μM) and (d) [EGTA] (12μM). The red line represents non-linear least-square fit to 0.5:1 (metal:monomer). The result are given in the text (Table 2.2). [Δ111NmtR](μM); (a) 5, (b) 140, (c) 5, (d) 5. Binding affinities K_{Ni1} ($\times 10^{10}\ M^{-1}$); (c) 0.86 (±0.06) (d) 4.0 (±0.30)

site upon deletion of the tail. The first step wise affinity constant for Ni(II) is obtained for Δ111NmtR in the presence of competitors is very similar to that of wild-type NmtR, with the expected smaller change in I/Io relative to wild-type NmtR (Figure 2.9(c)-(d), Table 2.2).

Apo-Δ111NmtR binds DNA less tightly than wild-type NmtR, which suggest that the truncation may not be structurally silent (see the figure on page 71 and table on page 73). However, this mutant is largely refractive to Ni(II) mediated regulation, with the coupling free energy decreased to a level comparable to that of non cognate metal Zn(II). Interestingly, Co(II) is still capable of regulate DNA binding to a degree similar to wild-type NmtR; this suggest that the stoichiometry of metal binding may well be a primary determinant of regulation in this mutant rather than the identity of the residues in the tail. To test this we examine individually all the putative metal ligands in the C-terminal that may be responsible for this reduced binding stoichiometry. We used the Gln substitution mutants H109Q, D114Q and H116Q to address this. To our surprise each of the single C-terminal mutant variants binds stoichiometric Ni(II) (Figure. 2.10) and the competition experiments are characterized by an affinity indistinguishable to that of wild-type NmtR (Figure 2.11 and Table 2.2). The Ni(II) dependent negative allosteric regulation of DNA by these variants are also wild-type like (Figure 2.12 and Table 2.7), with metal effectively decreasing the affinity for DNA to the same degree as wild-type NmtR in constrat to what is observed for Δ111NmtR (Figure 2.13 and Table 2.8).

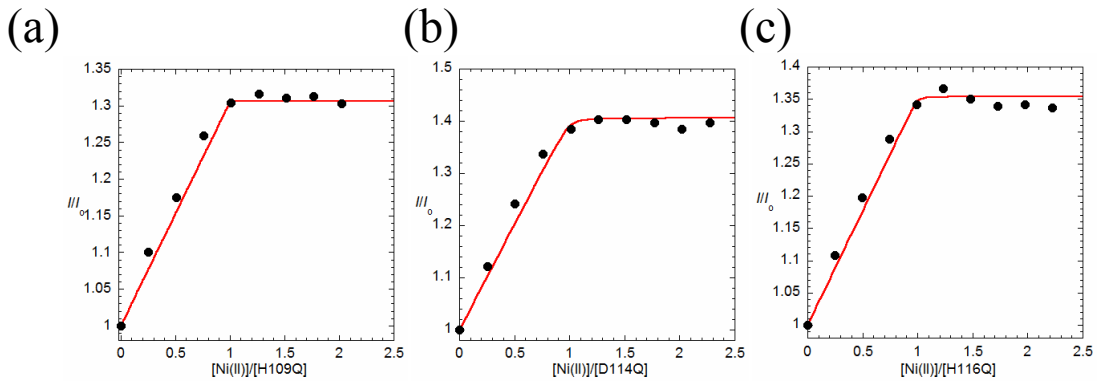

Figure 2.10 Binding of Ni(II) to C-terminal NmtR variants. Ni(II) binding isotherm as monitored by the intrinsic fluorescence intensity change (*I*/*I*o). The red line represents non-linear least-square fits to a 1:1 (Ni(II):monomer) binding model. (a) H109Q (K_{Ni}~ 1.65 x 10^8 M^{-1}), (b) D114Q (K_{Ni}~ 6.4 x 10^8 M^{-1}), (c) H116Q (K_{Ni} ~3.30 x 10^8 M^{-1}). [Concentrations](μM): (a) –(c) 5.

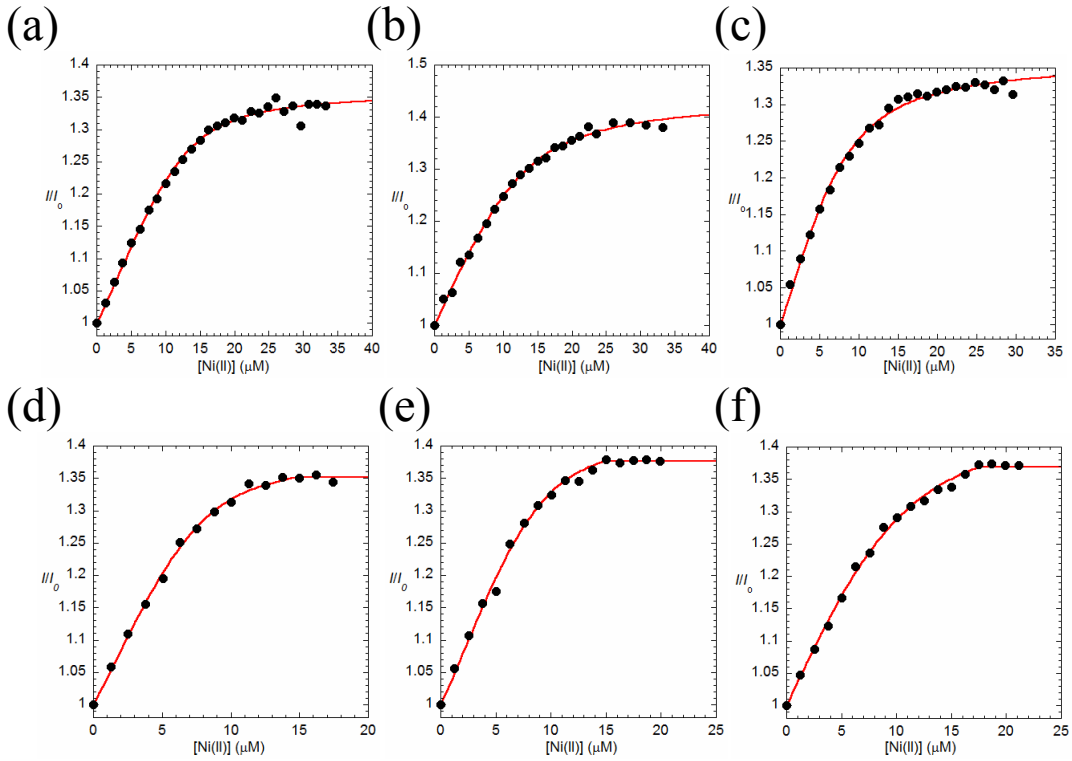

Figure 2.11 NTA and EGTA metal competition experiments with C-terminal missense mutant NmtRs. Ni(II) binding isotherm as monitored by the intensity of the intrinsic fluorescence change (*I*/*I*o), in the prescense of NTA (a)-(c) or EGTA (d)-(f). The red line represents non-linear least-square fits to a 2:1 (Ni(II):dimer) binding model. The results of the fits are given in the text (Table 2.2). a) 10μM H109Q and 20 μM NTA, (b) 10 μM D114Q and 20 μM NTA, (c) 5μM H116Q and 12.5μM NTA, (d) 5μM H109Q and 10 μM EGTA, (e) 5μM D114Q and 10 μM EGTA, (f) 5μM H116Q and 12.5 μM EGTA. Binding affinities K_{Ni1}, K_{Ni2} (x10^{10} M^{-1}); (a) 0.50 (±0.10), 1.00 (±0.01), (b) 0.80 (±0.10), 0.45 (±0.04), (c) 0.60 (±0.10), 0.60 (±0.05), (d) 1.00 (±0.04), 1.00 (±0.04), (e) 0.72 (±0.04), 0.72 (±0.04), (f) 0.95 (±0.01), 0.50 (±0.07).

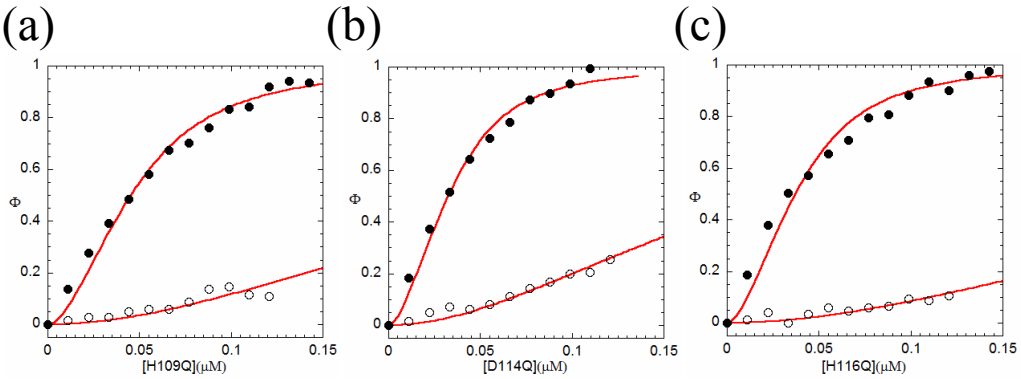

Figure 2.12 Ni(II) dependent allosteric regulation of NmtR C-terminal variants. The allosteric regulation is wild-type like. Depict are binding isotherms of fluorescence anisotropy experiments used to monitor DNA binding. Experiments in presence (open symbols) or absence (closed symbols) of Ni(II). The red line represent non-linear least-square fits to a model where a dissociable dimer binds to a single DNA probe. The data is normalized to the maximum anisotropy change (Δr_{max}) that correspond to apo-protein. Table 2.7 gives the K_{DNA} values calculated from this analysis, along with values of Δr_{max}. (a) NmtR H109Q, (b) NmtR D114Q, (c) NmtR H116Q.

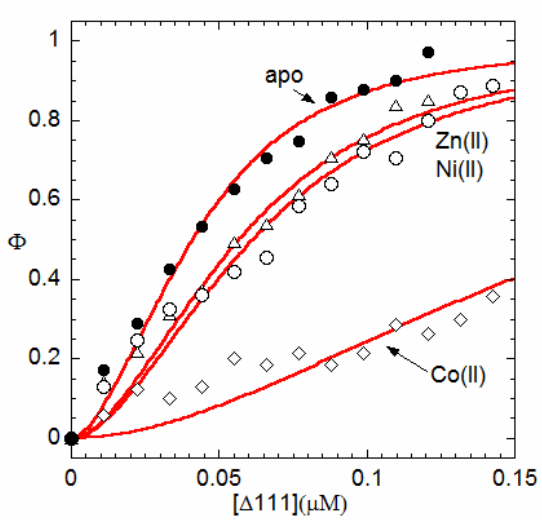

Figure 2.13 Δ111 NmtR is nearly refractive to Ni(II)-dependent regulation but not to Co(II) regulation. Fluorescence anisotropy experiments were used to monitor DNA binding of the truncated variant. Open and closed symbols represent metal or apo- form, respectively. The red line represents non-linear least-square fits to a model where a dissociable dimer binds to a single DNA probe. The total anisotropy change is normalized to the Δr_{max} so for each instance the anisotropy change observed Δr_{obs} is a fraction of Δr_{max}. Table 2.8 gives the K_{DNA} values calculated from this analysis, along with Δr_{max}. Key to notation (as indicated in the figure): Ni(II); open circles, Zn(II); triangles, Co(II); diamonds. The experiments were performed in excess of (100μM) metal.

Table 2.7 DNA binding affinities of C-terminal NmtR variants.

NmtR	Δr_{max} [a]	Δr_{obs} [b]	K_{DNA} ($x10^9$ M^{-1})	ΔG_c [c,d] (kcal mol^{-1})
H109Q				
apo[e]	0.014	0.013	4.3 (±0.6)	-
Ni(II)[f]	0.014 [b]	0.001	0.04 (±0.01)	2.8 (±0.2)
D114Q				
apo[e]	0.020	0.019	10.0 (±0.2)	-
Ni(II)[f]	0.020 [b]	0.005	0.08 (±0.004)	3.0 (±0.03)
H116Q				
apo[e]	0.017	0.017	7.3 (±0.1)	-
Ni(II)[f]	0.017 [b]	0.002	0.02 (±0.002)	3.5 (±0.1)

Conditions: 10mM Hepes, pH 7.0, 0.4 M NaCl, 25°C.

[a] Δr_{max} = anisotropy fix as maximal response in the fit and normalization

[b] Δr obs = Δr max

[c] $\Delta G_c = -RT \ln(K_{DNA\text{-}Ni}/K_{DNA\text{-}apo})$

[d] For comparation $\Delta G_{c\ Ni(II)NmtR\ wild\text{-}type} = 2.7$ (±0.2) kcal mol^{-1}

[e] For determination of *apo* K_{DNA} 500μM EDTA was added to the binding reaction.

[f] For determination of Ni(II) K_{DNA} 100μM Ni(II) was added to the binding reaction.

Table 2.8 DNA binding affinities of Δ111 NmtR complexed with various metals ions

Δ111NmtR	Δr_{max} [a]	Δr_{obs} [b]	K_{DNA} (x10^9 M^{-1})	ΔG_c [c] (kcal mol^{-1})	*W.t.* ΔG_c [d] (kcal mol^{-1})
apo[e]	0.014	0.013	5.61 (±1.00)	-	
100 μM metal					
Ni(II)		0.012	1.00 (±0.02)	1.0 (±0.1)	2.7 (±0.1)
Co(II)		0.005	0.12 (±0.01)	2.4 (±0.1)	2.2 (±0.1)
Zn(II)	0.024	0.020	1.20 (±0.20)	0.9 (±0.1)	1.1 (±0.1)

Conditions: 10 mM Hepes, 0.4 M NaCl, 25°C

[a] Δr max = anisotropy fix as maximal response in the fit and normalization

[b] Δr obs = anisotropy change at maximum protein concentration used in the fitting

[c] $\Delta G_c = -RT \ln(K_{DNA\text{-}Ni}/K_{DNA\text{-}apo})$

[d] Wild-type NmtR values show for comparison

[e] For determination of *apo* K_{DNA} 500μM EDTA was added to the binding reaction.

U.V. absorption spectroscopy. The U.V. absorption spectrum of Co(II)-substituted wild-type NmtR is consistent with a six-coordinate Co(II)-NmtR complex (*46, 99*). Strikinly, the shape and intensity of the U.V.-visible ligand–charge transition region of Co(II)- Δ111NmtR is characterized by two maxima at 475 and 570 nm, and a molar absorptivity of $\varepsilon_{c570} = 140\ M^{-1}\ cm^{-1}$ (Figure 2.14(a)). In contrast to wild-type NmtR the magnitude of the peaks at 570 nm is reduced about 1.5 fold, which is indicative of a change in coordination number to four/five ligands. However all the single substitute variants in the C-terminal that were examined by this technique (H109Q, D114Q, and H116Q) show wild-type like visible absorption spectra (Fig. 2.14(c)-(e)). In contrast, the spectra of Co(II) substitute H3Q NmtR (Figure 2.14 (b)) is red-shifted relative to wild-type NmtR, suggestive of a non native coordination number of some kind whose structure cannot be discerned from this data. It is interesting to note that this mutant have the poorest Co(II) regulation (see discussion).

DISCUSSION

The structural basis of metal selectivity by a metal sensor protein is key establishing the affinities of distinct metal sites on an otherwise quite constant molecular scaffold characterized by a protein family. In this work, we use a glutamine-scanning mutagenesis with the Ni(II) sensor NmtR to investigate cognate Ni(II) vs. Co(II) regulation and how the sensing site in NmtR has evolved to functionally discriminate against a high competitive metal like Zn(II). Biochemical and structural studies of α5 prototype Zn(II) sensing members from the ArsR/SmtB family, *e.g.* SmtB and CzrA

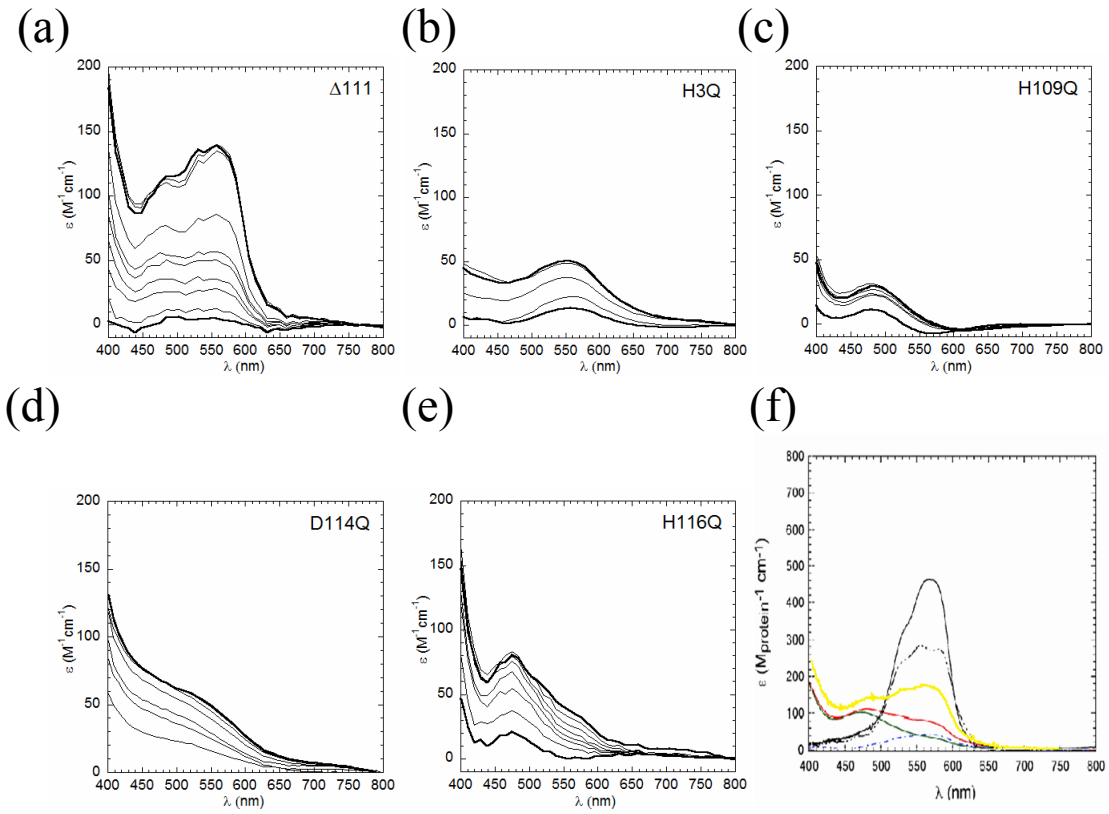

Figure 2.14 Co(II) electronic absorption spectra of H3Q and C-terminal variant NmtRs. Concentrations (μM); (a) [Δ111NmtR] 140, (b)[H3Q] 50, (c) [H109Q] 50, (d) [D114Q] 50, (e) [H116Q] 50. (f) Overlap spectrum of Δ111NmtR (yellow) and previously published data. Ni_1-NmtR wild-type (green), Ni_2-NmtR wild-type (red), Ni_2-Ni_1 subtraction (blue), Zn(II)-$SmtB^{\alpha 3}$ (dashed line), Zn(II)-CzrA (solid dark) (*99*).

(*46, 111*), reveal that two Zn(II) bind to a pair of 2-fold symmetric tetrahedral sites that straddle the C-terminal α5 helices of the dimerization domain. Previous studies established a model of selectivity based on coordination geometry. The results showed that binding of noncognate metal Ni(II) to CzrA in a non native octahedral geometry abolish allosteric regulation of protein-DNA interactions. In support of this model, CzrA single substitution mutants in the α5 helix regulatory binding center that bind Zn(II) in non native tetrahedral geometry have a reduced allosteric coupling free energy, similar to that observed when Ni(II) is bound (*99*). The allosteric regulation by cognate metal in other families of metalloregulatoy proteins are consistent with this model, metal specificity depends on the metal native coordination geometry (Figure 1.2).

In this chapter, we corroborate the previous observations (*33*) that NmtR binds two metal ions per dimer in a way that modifies the local structure of the near flanking tyrosines in the α5 helix, such that it provides a convenient reporter on the affinity and stoichiometry of metal binding by NmtR (Figure 2.2). We show that the affinity of NmtR for Ni(II) in its octahedral center (*99*) is on the order of 10^{10} M^{-1}, a value approximately between that the two other characterized Ni(II) metalloregulators. *E. coli* NikR binds Ni(II) in a square planar geometry, coordinated by 3 His and 1 Cys with a $K_{Ni}= 10^{12}$ M^{-1} (*72*), while its functional counterpart, RcnR binds Ni(II) with an octahedral geometry with a low affinity ~ 10^{7} M^{-1}. In RcnR, the Ni(II) is bound by a Cys and one His at the periphery of what is anticipated to be a 4-helix bundle, as well His3 and the αNH_2 from the N-terminal and perhaps a soluble molecule (*56*). Co(II), a metal inducer of RcnR *in vivo*, binds in a octahedral coordination with Cys as a ligand donor,

analogous to Ni(II) RcnR, but this residue is essential only for Co(II) *in vivo* regulation (*56*). This indicates that although both metals are sensed by RcnR, the coordination structure may not be precisely identical.

KmtR is the second Ni(II) sensor from the ArsR/SmtB family that is expressed in in *M. tb.* cytoplasm (*76*). KmtR binds Ni(II) with an as yet uncharacterized coordination geometry, although mutagenesis experiments suggest that Ni(II) is six-coordinate with a mixture of carboxylate and imidazole ligands (*76*). In a experiment to estimate the relative affinities of KmtR and NmtR for Ni(II), it was shown that the former has a ≥100-fold higher affinity for Ni(II) (*76*). Thus, based on the binding affinity reported here for NmtR, KmtR should bind Ni(II) with an affinity of no less than ~10^{12} M^{-1}. The presence of two regulators in the same cytoplasm has been hypothesized to be used to sense metals at distinct concentration ranges (sensitivities) that allows for a greater metal response (*76*). For example, *M. tb.* encodes two structurally homologs Cu(I) sensors which regulates distinct genes on response to Cu(I) stress at distinct extracelullar Cu(I) regimes (B. Kester and D. Giedroc, unpublished results)(*198*). It is expected that *in vivo* de-repression will be observed only after Ni(II) concentrations have reached their activation threshold, which for NmtR means at three orders of magnitude higher concentration than KmtR. Whether or not this is relevant to the biology of *M tb*. is not known at present.

The allosteric negative heterotropic linkage that characterizes Ni(II) NmtR (ΔG_c ~ 2.8 kcal mol^{-1}) is of a similar magnitude relative to other ArsR/SmtB members including the α3N Cd(II) sensor CadC (*94*), and α5N $BxmR^{\alpha 3}$ Zn(II) sensor (*48*), which

recruit one or more ligands from the N-terminal region to coordinate their respective metals. However, this allosteric energy coupling is small relative to the α5 paradigm zinc sensor CzrA, ΔG_c ~ 6 kcal mol^{-1} (*45, 98*). The origin of this difference is not yet known but strongly suggests that the structural mechanism may well differ between CzrA and NmtR as anticipated based on their distinct metal specificity profile. In any case, we report here that all the anticipated metal ligands in the α5 helix are necessary, but not sufficient, to establish a native-like metal site structure, and each is required to drive allosteric regulation of DNA operator binding. Actually, the metallated NmtR α5 variants seem to stabilize the formation of higher order DNA complexes, which may be indicative of metal mediated stabilization (*199, 200*) of an allosterically impaired dimeric interface. Taken together, these findings suggest that the α5 derived ligands play a major role in stabilizing the NmtR dimer in a weak DNA-binding conformation. These observations establish a functional difference with the α5 Zn(II) sensing CzrA, where conservation of just two of the four metal ligands is sufficient for maintenance of tetrahedral complex and the Zn(II)-mediated allosteric switching mechanism (*45*).

Our characterization of H3Q NmtR provides strong support for the proposal that His3 and perhaps other determinant in N-terminus are a direct ligand to the Ni(II) since K_{Ni} is greatly decreased. However, provided sufficient Ni(II) is present, H3Q NmtR exhibited wild-type ΔG_c. A primary role of His3 may be to prevent adventitious inhibition of DNA binding by Zn(II), the lost of His3 allows NmtR to revert to a prototype Zn(II) activated α5 sensor like CzrA. H3Q NmtR also exhibited an attenuated Co(II) absorption spectrum and poor Co(II) regulation, consistent with the idea that the

Co(II) complex may well be functionally dependent on His3 for wild-type activity. There is precedent for distinct coordination complexes found by pairs of cognate metals, *e.g.* Co/Ni in *E.coli* RcnR (*56*). It is also interesting to note that Co(II) binds much weaker than Ni(II) ($K_{Co} \sim 10^5$ M^{-1}) to NmtR (*33*) and lost of His3 may destabilized the complex to a degree that all the binding sites are not saturated at 10μM Co(II) (Table 2.3). All we can conclude at the moment is that XAS reveals a Ni(II) center in NmtR containing a mixture of histidines and other as yet not defined N/O ligands (*99*). If His3 is indeed a ligand to the Ni(II) ion, this would be a unique structural future among the ArsR/SmtB members containing a core α5 metalloregulatory site. Based on the structure of CzrA, the NmtR N-terminal extension would be expected to extend for 13 residues from Gly2 to Pro 14 (*14*). A flexible linker of this length can indeed span the total required distance between the residues analogous to Pro14 and the C-terminal α5 helix (*135*), which is less than 9 Å from inspection of the solution structure of Zn(II) CzrA (*109*). NMR studies of apo, Ni(II)-bound and DNA-bound NmtR are in progress to more fully elaborate this hypothesis.

If indeed this is the case, a plausible mechanism of allosteric regulation may involved a reorganization of the N-terminal residues which maybe in direct contact with the DNA in the apo form (*e.g.* Arg8 and Arg10). In fact, in the solution structure of CzrA in complex with DNA, residues in the N-terminal of α1 helix contact the intertwining minor groove of consecutive major grooves which harbor TGAA recognition element (*109*). Although little structural information is available for members of the α3N family in complex with DNA, other metalloregulators like

Helicobacter pylori NikR, possess a flexible region called the N-terminal "arm" of the RHH (ribbon-helix-helix) DNA binding domain that enables specific DNA interactions (*201, 202*).

Our results do not provided direct support for the direct involvement of individual side chain in the C-terminal coil as directly involved in metal binding and allosteric regulation in contrast to a previous report (*33*) which show that H116R NmtR but not D114A NmtR loss *in vivo* Ni(II) regulation. This discrepancy may be due to two possible explanations and structural studies would be required to discriminate between these two. One possibility is the insertion of a bulky and positively charge arginine residue near the metal binding site that can compete for binding with the metal ion (steric inhibition) or create an electrostatic repulsive interaction for it (charge repulsion). A precedent exist in an arginine substitution of a non-Ni(II) ligand of RcnR that inhibit *in vivo* allosteric response (*56*). The second explanation is the recruitment of a non-native ligand from multiple ligands donors available, similar to what is believe to happen in other metal sensors like the Zn(II) sensor SmtB and RcnR (*56, 89*).

The C-terminal is essential to maintain two Ni(II) binding events and a native coordination geometry, thus the Δ111NmtR truncation mutant results in decreased metal mediated allosteric regulation (ΔG_c = 1 kcal mol^{-1}) relative to wild-type NmtR. A Zn(II) sensor CzrA (fCzrA) was previously engineered by the fusion of the N- and C-terminal domains by a flexible peptide inter-dimeric linker, with the objective of measuring the effects of the perturbations in the dimeric interface on allosteric regulation (*135*). In a fCzrA variant where the shortest linker was used and the strongest perturbation in the

dimer interface is expected, binding of only one Zn(II) per dimer was detected, analogous to the Δ111NmtR. However this fCzrA variant is competent to Zn(II) regulation, in contrast to the results show for Ni(II) Δ111NmtR. However, the truncation can bind Co(II) with four or five ligands and a stoichiometry of up to three metals per dimer which efficiently activates de-repression (ΔG_c = 2.4 kcal mol^{-1}) to the extent observed for Co(II) in wild-type NmtR. Thus, based on our observations, we conclude that the C-terminal is essential for Ni(II) coordination in the competent allosteric state, but perhaps not for Co(II).

CHAPTER III

BIOCHEMICAL STUDIES OF *Streptococcus pneumoniae AdcR**

INTRODUCTION

Streptococcus pneumoniae (*S. pneumoniae*) is a Gram-positive respiratory pathogen that colonizes the upper respiratory tract (the nasopharynx) as a commensal organism. At some frequency, *Spn* becomes invasive and spreads to infect lung tissues where it causes pneumonia, and can ultimately migrate to the bloodstream to induce sepsis(*203*). Acute respiratory diseases, mainly pneumonia, are the causative agents of 17% of all infant deaths per year worldwide according to the World Health Organization and plans to provide patient care and preventive measures in countries with a high rate of pneumonia-related mortality have been put forward (*204-206*). With a natural ability for genetic transformation (competence) and genome plasticity, *Spn* had evolved rapidly, acquiring antibiotic resistance and genetic variability that facilitates host invasion, colonization and vaccine escape (*207, 208*). Knowledge of the molecular basis of host-pathogen interactions that allow a successful colonization and infection may well lead to the discovery of new drug therapies and more effective vaccines and prevention methods (*209*).

The *adcRCBA* operon is conserved in all *Streptococci* and encodes an ABC

---

*This chapter is reproduced with permission from "The Metalloregulatory Zinc Site in Streptococcus pneumoniae AdcR, a Zinc-activated MarR Family Repressor" by Reyes-Caballero, H., Guerra, A. J., Jacobsen, F. E., Kazmierczak, K. M., Cowart, D., Koppolu, U. M. K., Scott, R. A., Winkler, M. E., and Giedroc, D. P.(2010), *J. Mol. Biol. 403*, 197-216. doi: 10.1016/j.jmb.2010.08.030. Copyright [2010] by Elsevier Ltd.

(ATP-binding cassette) transporter, AdcCBA, that is believed to function as a high affinity importer for Zn(II) (*210*). AdcCBA is a member of the Cluster IX family of metal specific transporters (*210-212*), and may well mediate uptake of noncognate Mn(II) at high extracellular concentrations (*210*). AdcR is a proposed Zn(II)-sensing transcriptional regulator (*62*) which sequence analysis suggests is a MarR family repressor. MarR proteins are known to regulate aromatic catabolism, the expression of virulence factors (*79, 213*), and the response to antibiotic and antimicrobial stress and oxidative stress. Multiple crystallographic structures are available that provide insights into MarR-family architecture and in some cases, the mechanism of regulation of operator DNA binding (*214-219*).

The *adc* operon is reported to be expressed during active *S. pneumoniae* infection and is essential for genetic transformation, although the molecular basis of this requirement remains unclear (*210, 212, 220*). AdcA, the extracellular, metal (solute)-binding lipoprotein component of AdcCAB is strongly immunogenic in mice and is an excellent vaccine candidate for the porcine pathogen *Streptococcus suis* (*221*). In *S. suis* an *adcR* deletion mutant exhibits attenuated virulence (*222*). Antibodies raised against a number of solute binding components from ABC transporters found in the Gram-negative pathogen *Yersina pestis* and other bacterial pathogens are also protective against bacterial infection (*223, 224*). An *adcB* mutant *S. pneumoniae* strain shows attenuated binding to human epithelial cells *in vitro* (*225*) and AdcB is a documented virulence factor in a signature-tagged mutagenesis screen (*226*). In *Streptococcus*

gordonii, an oral plaque pathogen, AdcR is reported to play an essential role in biofilm formation (*227, 228*).

Genomically unlinked AdcR-regulated genes were first predicted on the basis of *in silico* analysis of the *S. pneumoniae* genome for what is now known to be the AdcR operator sequence (*62*). One predicted AdcR-regulated gene in *Streptococcus pyogenes* is a paralog of 30S ribosomal subunit S14 (*rpsN*) that has a disrupted C-terminal Zn-ribbon domain similar to those under transcriptional control of the master Zn(II) uptake regulator Zur (Fur family) in *Streptomyces coelicolor* (*229*) and *Bacillus subtilis* (*63*) during zinc starvation. Another *adcR*-regulated locus predicted in *Streptococcus pyogenes* is *pht* (pneumococcal histidine triad proteins) which consists of four homologous genes (*phtA, phtB, phtD, phtE*) which encode highly immunogenic pneumococcal surface proteins (*230*) each of which contains up to five repeats of the sequence $Dx_{(20)}HxxHxH$ now known to coordinate Zn(II) tetrahedrally (*231*). Pht proteins play a role in immune evasion and may inhibit complement deposition thereby impairing opsonization and phagocytosis, although these effects appear to be strain-specific with the mechanism still under investigation (*232*). AdcAII, an orphan metal binding receptor of known structure that is homologous to AdcA (*233*) is also regulated transcriptionally by AdcR. In *Streptococcus pyogenes*, the AdcA homolog Lbp functions in colonization as an adhesin that binds to the extracellular matrix protein laminin, with zinc suggested to play a role in this interaction (*234*). An Lbp mutant shows attenuated virulence in a murine model of infection and defective growth in zinc depleted media (*235*).

The clear importance of Zn(II) homoeostasis in *Streptococcus* stands in sharp contrast with the degree to which we understand AdcR structure and function. Zur, the Fur-family (*122*) transcriptional regulator of Zn(II) uptake in *Escherichia coli* (*43, 236*) and Gram-positive organisms *Bacillus subtilis* and *Mycobacterium tuberculosis* (*108, 237*), is encoded by some *Streptococci* with a primary role in regulating Zn(II) homeostasis clearly demonstrated (*238*). In contrast, Zur is not encoded by any sequenced *S. pneumoniae* strain, with zinc uptake regulation handled exclusively by AdcR (*239*) which is functionally analogous to *Lactobacillus lactis* ZitR (*240*). SczA, a predicted tetracycline repressor (TetR)-family transcriptional regulator controls the expression of a divalent metal ion efflux transporter encoded by *czcD* (*80, 241*) which belongs to the cation diffusion facilitator (CDF) family of transporters (*242, 243*). As such, *S. pneumoniae* encodes a complete Zn(II) homeostasis system controlled by novel regulators from well-known protein structural families (*14*). This homeostasis system likely allows *S. pneumoniae* to effectively respond to changes in external zinc availability during the course of a bacterial infection of the human host, with zinc concentrations reported to vary from the low μM in the nasopharynx, to ≈220 μM in lung tissue to 15 μM in the serum (*244*), while during inflammation [Zn] is known to increase in the blood and other tissues (*245*).

In this report we identify candidate Zn(II)-coordinating residues on AdcR and measure its relevance for the allosrteric regulation. These studies reveal that Zn(II) strongly activates DNA binding by the AdcR homodimer upon formation of a high affinity, five-coordinate nitrogen/oxygen-rich Zn(II) complex via His108 and H112 in

the C-terminal regulatory domain, and His42 in the N-terminal winged helical DNA-binding domain. Other non-cognate metals, Mn(II) and Co(II), also activate DNA binding *in vitro*, the functional implications of which are discussed.

MATERIALS AND METHODS

Chemicals and reagents. All water used in these experiments was Milli-Q deionized (>18MΩ) and the buffers were obtained from Sigma. All glassware was acid washed before use and rinsed exhaustively with metal-free water. Indicator dyes mag-fura-2 and quin-2 were obtained from Invitrogen and Sigma, respectively. Metal stocks made with Ultra Pure Alfa Aesar metals. All other reagents are as indicated in the text. For all the chromatography steps an Ätka 10 purifier (GE) was used. All metal binding experiments were performed under anaerobic conditions. Dialysis into experimental buffer was under an Argon saturated atmosphere of no more than 8 ppm of oxygen.

ICP-MS analysis. 1 mL aliquots of *S. pneumoniae* cells in exponential phase were centrifuged and washed twice with BHI containing 5 mM nitrilotriacetic acid (Aldrich), then once with PBS that had been treated overnight with chelex (Biorad) according to the manufactures' protocol. The cell pellets were dried overnight in a rotary evaporator. 400 µL of 2.5% v/v nitric acid (Ultrapure, Sigma-Aldrich) with 0.1% v/v Triton-X 100 were added to the cell pellets which were then lysed for 10 min at 95 ºC with shaking at 500 rpm followed by vigorous vortexing for 20 s. 200 µL of the lysed cell solution was added to 1.3 mL of 2.5% v/v nitric acid for ICP-MS analysis. Analyses were performed using a Perkin Elmer ELAN DRCII ICP-MS. The instrument

was equipped with a Microflow PFA-ST concentric nebulizer with a 100 μL/min self-aspiration capillary, a cyclonic spray chamber, a quartz torch and platinum sampler/skimmer cones. Germanium at 50 ppb was added as an internal standard using an EzyFit glass mixing chamber. Metal content was determined per cell using the OD_{620} to obtain the number of cells analyzed. Molar metal content was determined assuming a cell volume of 0.644×10^{-15} L (*246*) and 10 cells per chain.

Cloning and mutations. The AdcR gene was PCR-amplified from *S. pneumoniae* D39 genomic DNA using the cloning oligonucleotides (Integrated DNA Technologies) 5'- CCGGATCCTCTACCGTAATATATCTCATTATTTGATTTCTC and 5'-CCCATATGAGACAGCTAGCAAAGGATATCAATGCTTTTTTG (BamHI and NdeI restriction sites are underlined, respectively) and cloned into the expression vector pET3a. The final construction has the entire native sequence of the AdcR gene under the control of a T7 promoter. AdcR single residue mutants were obtain using the protocol supplied by QuikChange from Stratagene using pET-AdcR as the template for PCR and appropriate mutagenic primers. All expression constructs were sequenced to verify the integrity of the plasmids on an ABI 3730 DNA Analyzer (Applied Biosystems) located in the Indiana Molecular Biology Institute. The plasmids were transformed into either BL21(DE3) or BL21 pLysS cells for protein expression.

Overexpression and purification. Growth was performed as previously described (*247*). Overexpression of AdcR was accomplished by induction of 1 L mid-log LB cultures with IPTG (Inalco) to a final concentration of 0.4 mM for 4 h at 37 °C or 30 °C overnight. The cells were harvested and resuspended in 25 mM MES, pH 6.0, 0.5 M

NaCl, 5 mM EDTA, and 5 mM DTT. The cell suspension was lysed by sonication. After centrifugation, 10% PEI (polyethylenimine) pH 6 was added to the supernatant to a final concentration of 0.015% (v/v) and stirred for 2 h at 4°C. The supernatant was fractionated with two $(NH_4)_2SO_4$ cuts (35% and 70%) and the pellet was resuspended and equilibrated in 25 mM MES pH 6, 0.1 M NaCl, 5 mM EDTA and 2 mM TCEP (GoldBio). Dialysis to remove excess $(NH_4)_2SO_4$ was performed with at least four 1 L buffer exchanges over 16 h. This fraction was loaded on an SP-Sepharose Fast Flow column and fractions eluted in a salt gradient from 0.1-1 M NaCl. The cleanest fractions as determined by SDS-PAGE gels, were pooled and equilibrated in 25 mM Tris, pH 8.0, 50 mM NaCl, and 2 mM TCEP and loaded into a Q-Sepharose column. The cleanest fractions were then pooled, concentrated using centrifugal filter units (Millipore) and loaded on a Superdex 75 gel preparative grade column as the last step in the purification. The identity of AdcR wild-type and variant proteins was confirmed by LC-ESI/MS mass spectrometry at the Indiana University Department of Chemistry Mass Spectrometry Facility. Samples for LC-ESI-MS were prepared in the glove box under anaerobic conditions and passed through a Micro Bio Spin P6 desalting column (BioRad). The concentration of the AdcR monomer was determined for all variants using an ε_{280} of 2980 M^{-1} cm^{-1}.

Zinc-binding experiments. All zinc binding experiments were carried out by using a Hewlett-Packard model 8452A spectrophotometer. Two different zinc chelator indicator dyes were used as apo-AdcR competitors under anaerobic conditions, mag-fura-2 (mf2) and quin-2. Protein was diluted in 800 μL of buffer (25 mM Bis-Tris, pH

6, 0.2 M NaCl or 25 mM Tris, pH 8, 0.5 M NaCl) that was passed through a Chelex (Bio-Rad) column to remove contaminating metals. These chelator competition experiments were carried out and the data corrected as previously described (*45, 89, 248*). The mf2 isotherm was fit to the model indicated in the text using a $K_{D,Zn}$ = 0.022 μM for mf2 (*249*). To corroborate the affinity of quin-2 for Zn(II) at pH 8.0 and 0.5 M NaCl, a series of measurements were done using 10, 20 and 28 μM EDTA (K_{Zn} = $2.7x10^{14}$ M^{-1}, pH 8.0, 25.0 ^{o}C) (*189*) competing for Zn(II) in presence of 20 μM quin-2. The affinity was fit to a K_{Zn} = 2.9 x 10^{11} M^{-1}, which is in agreement to the previously reported value of 2.7 x 10^{11} M^{-1} (*250*). All data was fit to a simple competition model using Dyna-Fit (*187*).

Fluorescence anisotropy experiments. A 28 mer double stranded 3'-fluorescein labeled DNA (5'-TGATATAATTAACTGGTAAACAAAATGT) and its complementary strand containing the native operator-promotor sequence found upstream AdcR were synthesized using a 3'-fluorescein CPG column (Glen Research) on a MerMade 4 oligonucleotide synthesizer (Bio Automation Corporation), and purified and annealed as described before (*46, 98*). All anisotropy experiments were carried out with an ISS PC1 spectrofluorometer operating in steady-state mode fitted with Glan-Thompson polarizers in the L format (excitation wavelength set at 495 nm with 1 mm slit and the emission collected through a 515 nm filter). The G-factor was set to 0.99 and the average light intensity was $1x10^{5}$ (a.u) with a decrease of no more than 5% at the end of the titration with all the components in solution. The average of 10 iterations of 40 s each for each *i*th addition of protein measured with a corresponding standard

deviation that was ≤ 0.001. All experiments were carried out with 10 nM DNA in 50 mM Bis-Tris, pH 6.0, 0.2 M NaCl, 0.005% Tween-20, 1 mM TCEP and 80 μg/mL DNA sodium salt from salmon testes (Sigma) as an unspecific competitor in a volume of 1.8 mL. A solution containing 1-10 μM of AdcR and AdcR variants was titrated into the cuvette containing the DNA and allowed to mix for 3 min. To measure the allosteric effect of metals ions, one molar equivalent per monomer of the indicated metal was preincubated with the protein titrant. The binding reaction contained either 100 μM of Zn(II) or 10 μM Mn(II) or Co(II). The anisotropy of the apo-protein was measured in presence of 0.5 mM EDTA and was under the limit of detection. The buffer used to measured the anisotropy of Co(II) / Mn(II)-AdcR was passed through a Chelex (Bio-Rad) column and no anisotropy change was detected in absence of metal, assuring that no metal contaminants were present in the buffer or protein. The data, normalized as described previously (*52, 109*), were fit to a binding model as indicated in the text. The maximal change in anisotropy for wild-type AdcR of 0.023, is consistent with that expected for one dimer bound per DNA duplex when taking into account the effect of the DNA length on Δr_{obs} (*45, 109, 248*).

Atomic absorption spectroscopy. All the Zn(II) and Co(II) metal stocks were measured as before using metal specific hollow cathode lamps (*45*) and Mn(II) was detected at 279.5 nm (slit-width of 0.2 nm) in a Perkin-Elmer AAnalyst spectrometer. Zn(II) contents of the wild-type and AdcR apoprotein variants ranged from 0.01-0.08 monomer mol equiv. Mn(II) and Co(II) concentrations were negligible.

Quantitation of free thiol. DTNB was used to determine the total concentration of free thiol as previously described (*89*). The total concentration of free thiols ranged from 80-90% in all the AdcR and AdcR variants as purified. Glu-C in-gel digestion and LC-MS/MS analysis of the sample was done as previously described (*52*) with the exception that 25 μL of a 20 ng/μL GluC was used to digested the samples. The LC-MS/MS was performed in Indiana University, Chemistry Department at the National Center for Glycomics and Glycoproteomics.

Derivatization of thiols. MMTS (methyl methanethiosulfonate) converts free sulfhydryl groups of cysteines side chains into –S-SCH_3.(*251*) Wild-type AdcR (100 μL, 690 μM) was modified by incubation with 100 fold molar excess of MMTS for 1 h. The protein was then passed through a Bio-Spin P6 (Bio-Rad) gel filtration column, concentrated using centrifugal filter membranes (Millipore) and buffer exchanged by dialysis to remove any unreacted MMTS. The modified protein was verified by LC-ESI-MS where AdcR (16,649 amu, MW= 16,605 + 2Na) forms a product after MMTS reaction of 16,697 (AdcR+ 2Na + 46 amu, the latter consistent with a single –S-SCH_3 derivatization on Cys30).

NMR Experiments. NMR spectra were acquired on a Varian DDR 800 MHz spectrometer equipped with a cryogenic probe at the Indiana University MetaCyt Biomolecular NMR laboratory. NMR spectra were processed and analyzed using NMRPipe(*252*) and SPARKY†. Typical solution conditions were 250-600 μM ^{15}N-labeled or ^{15}N/^{13}C-labeled protein, pH 6.0, MES-d_{13} (Sigma), 50 mM NaCl, 1 mM tris(2-carboxyethyl)phosphine (TCEP; Gold Biotechnology), 0.02% NaN_3 (Fisher) and 10%

(v/v) $^{2}H_2O$ (CIL) at a level of 70% random deuteration. Zn(II)-AdcR samples contained 2 monomer mol equiv of Zn(II) and 1 mM imidazole. All spectra were acquired at 35 ˚C. Chemical shift referencing is relative to 2,2-dimethyl-2-silapentene-5-sulfonic acid (DSS; Sigma).(*253*) Sequential resonance assignments (to be reported elsewhere) for the apo and Zn(II) forms were obtained using ^{1}H-^{15}N HSQC, and triple resonance HNCA, HN(CO)CA, HN(CA)CB, HN(COCA)CB and HNCO spectra.(*254-256*)

Zn(II) X-ray Absorption Spectroscopy. Samples were loaded into a polycarbonate XAS cuvette containing five 10-µL wells covered with a Mylar-tape front window and immediately frozen in liquid nitrogen. Zinc K-edge XAS data were collected at Stanford Synchrotron Radiation Lightsource (SSRL) on beam line 9-3 with the SPEAR storage ring operating at 3.0 GeV, 60-100 mA. X-ray absorption spectra were recorded with the sample at 10 K using a 1×1 mm beam incident on a fully tuned Si[220] double-crystal monochromator, downstream of a harmonic rejection mirror set for a 15-keV cutoff. XAS data were collected using a 30-element intrinsic Ge detector windowed to Zn K_α emission with a 6-absorption length Cu fluorescence filter backed by Soller slits. Energies were calibrated using an internal zinc standard, with the first inflection point assigned at 9660.7 eV. *k* values were calculated using a threshold ($k = 0$) energy of 9670 eV. The averaged XAS data for a sample represent 6-8 scans, each of 21 min duration, collected on several replicate sample wells. Data reduction and analysis were performed with EXAFSPAK software (www-ssrl.slac.stanford.edu/exafspak.html) according to standard procedures as described previously.(*257*) Fourier transforms of the EXAFS spectra were generated using sulfur-based phase correction. The multiple-

scattering model, based on zinc-bound imidazole, was calculated using FEFF version 8.0 (*258, 259*). Debye-Waller factors for the multiple-scattering legs were optimized by fitting a structural model of $Zn(imid)_4^{2+}$ and were fixed during curve-fitting. Optimal imidazole coordination numbers were chosen based on the size of the 3- and 4-Å FT peaks arising from outer-shell C,N atoms of the imidazole ring. Zn-(N,O) distances and Debye-Waller factors of additional first-shell ligands were then optimized for the final fits.

RESULTS

Microarray determination of the AdcR regulon in Streptococcus pneumoniae. Relative transcript amounts of 15 genes increased or decreased (Appendix A) with $p \leq 0.001$ in D39 Δ*adcR* (IU2594) compared to *adcR*$^+$ (IU1781). As anticipated and previously observed using RT-PCR in *Streptococcus pyogenes* (*260*), each of the genes encoding the Zn(II)-specific ABC uptake system *adcCBA* (SPD_1999, SPD_1998, SPD_1997, respectively) increased in transcript abundance in the Δ*adcR* strain. In addition, as was predicted in a genomic analysis (*62*) and shown by RT-PCR analysis (*232*), transcript amounts of the pneumococcal histidine triad (Pht) proteins also increased in the Δ*adcR* strain. These Pht genes include *phtA* (SPD_1038), *phpA* (SPD_1037), *phtD* (SPD_0889), *phtE* (SPD_0890), and a *pht* truncation (SPD_0892) and frameshift (SPD_0891) gene. In addition, the cell surface proteins *adcAII* (SPD_0888), which had previously been hypothesized to be regulated by AdcR in *S. pneumoniae*,(*233*) and *pspC* (SPD_2017) are increased in transcript abundance in the

Δ*adcR* strain. Interestingly, two putative zinc-containing alcohol dehydrogenases are down-regulated in the Δ*adcR* strain, SPD_0265 and SPD_1865 (Appendix A). Although it is unknown if this is a direct or indirect effect of the deletion, the intergenic region upstream of the promoter for SPD_1865 harbors one near-consensus AdcR operator sequence.

AdcR residues H112 and H108 are essential for AdcR function in vivo. Growth analysis was done comparing *adcR*$^+$ parent (IU1781), Δ*adcR* (IU2594), *adcR* H112Q (IU2600), *adcR* C30A (IU2657), *adcR* H111Q (IU2661), and *adcR* H108Q (IU4036) strains (Appendix B). The strains were grown in brain heart infusion media (BHI) overnight and then diluted to an OD_{620} of 0.001 in BHI with 200 μM $ZnSO_4$ added. Under this moderate zinc stress a difference in lag time and yield can be observed in the parent *adcR*$^+$ and Δ*adcR* strains. The Δ*adcR* strain reproducibly exhibits a slightly longer lag phase and a lower overall growth yield. Sequence changes in *adcR* generating amino acid substitutions H112Q and H108Q in AdcR replicate the growth effect observed for Δ*adcR*, while strains encoding substitutions H111Q and C30A grow similarly to the parent strain *adcR*$^+$. This implicates H108 and H112 as essential for the function of AdcR *in vivo*.

ICP-MS analysis (Appendix B) shows that the Δ*adcR* strain has a 2-fold higher cell-associated zinc concentration compared to the *adcR*$^+$ parent strain (0.4 mM vs. 0.8 mM, respectively). A two-fold elevated zinc concentration is also observed in the *adcR* H112Q and H108Q mutants, which indicates that these residues are essential for the in *vivo* functionality of AdcR. The strains with *adcR* C30A and H111Q mutations have

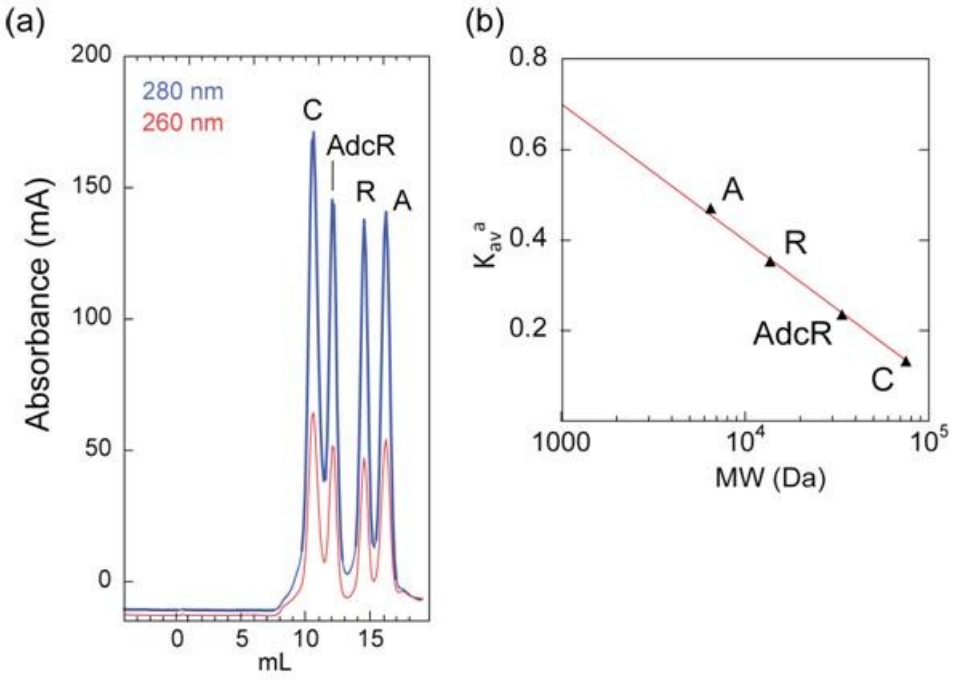

Figure 3.1 Sephadex G75 gel filtration chromatography of apo-AdcR. (a) AdcR elutes with a retention volume that corresponds to a dimer molecular weight. Internal molecular weight standards are aprotinin (A) 6.5×10^3 Da, ribonuclease A (R) 1.3×10^4 Da, and conalbumin (C) 7.5×10^5 Da. (b) Plot of partition coefficient, K_{av} *vs*. log molecular weight. The solid line corresponds to a linear fit from where the molecular weight of AdcR was calculated to be 3.3×10^4 Da (expected value: 16,605.9 Da per subunit; 33,211.8 Da homodimer). Conditions: 10 mM Hepes pH 7.0, 0.2 M NaCl, 2 mM TCEP. $K_{av} = V_e\text{-}V_0/V_C\text{-}V_0$, where V_0 is the column void volume, calculated for the elution volume of dextran as 8.4 mL, V_e is the elution volume of individual samples, and V_c is the geometric column volume or 24 mL.

near wild type levels of zinc, which when in combination with the growth data indicate that they are non-essential residues for *in vivo* AdcR function.

Wild-type AdcR is a homodimer in solution. Purified wild-type *S. pneumoniae* AdcR elutes from a gel filtration column (pH 7.0, 0.2 M NaCl) with an elution volume corresponding to a molecular weight of 33 kD or that of a homodimer (monomer MW=16,605.9 D) (Figure. 3.1). This result is consistent with sedimentation velocity ultracentrifugation experiments (pH 6.0, 0.05 M NaCl, 25.0 ºC) which reveal that the predominant apo-AdcR species is a homodimer characterized by $s_{20,w}$=3.65 S and a frictional coefficient, f/f_o, near 1.0, indicative a nearly spherical hydrodynamic particle (Table 3.1). The same is true for Zn(II)-complexed AdcR. AdcR monomer was not visible within these boundaries, thus placing a lower limit of K_{dimer} of 10^6 M^{-1} under these conditions. A small fraction of apo-AdcR stored at –80 ºC becomes resistant to reduction by dithiothreitol or TCEP and migrates on an overloaded denaturing SDS-PAGE gel as a dimer (Figure 3.2). Although the chemical nature of this presumed covalent linkage is unknown, crosslinked AdcR dimer can be detected by ESI-MS, the formation of which is lost in the C30A AdcR mutant (Table 3.2). These data taken collectively are consistent with the interpretation that both wild-type and C30A AdcRs are stable homodimers with and without bound Zn(II).

Zinc binding properties of wild-type AdcR. It was of interest to quantify the Zn(II) binding affinity, stoichiometry and coordination chemistry of Zn(II) in the wild-type and mutant AdcR homodimers. Since the C-terminal region of *S. pneumoniae* AdcR contains a cluster of five consecutive His residues in an eight amino acid sequence

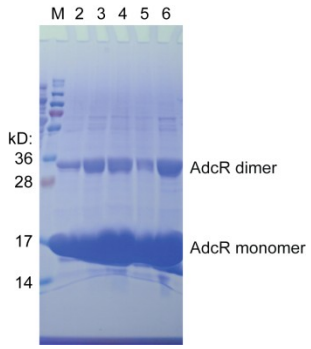

Figure 3.2 A small fraction of apo-AdcR forms a covalent dimer by denaturing SDS-PAGE analysis. An aliquot (10 μL) of apo-AdcR concentrated to 600 μM was mixed with loading buffer containing 30% β-mercaptoethanol and electrophoresed through an 18% denaturing SDS-PAGE gel (lanes 2 and 3, different preparations Av2 an Av3, respectively) or treated by boiling only (lane 4) or boiled followed by incubation with 20 mM dithiothreitol (DTT) (lane 5) or 20 mM TCEP (lane 6) for 1 hr followed by electrophoresis.

Table 3.1 Hydrodynamic parameters of wild-type AdcR obtained from sedimentation velocity experiments[a]

AdcR	% Dist.[b]	MW_{obs} (Da)	*s* (s) $x10^{-13}$	*D* (cm^2/s) $x10^{-7}$	f/f0	MW_{obs}/MW_{mon}[c]
apo (0.3 OD_{230}; 4 μM)	80	35858	3.65	9.93	1.0	2.2
apo (0.8 OD_{230}; 10.7 μM)	81	34101	3.65	9.93	1.0	2.1
1:1 Zn(II) (0.3 OD_{230})	73	32570	3.54	10.1	1.0	2.0
1:1 Zn(II) (0.8 OD_{230})	72	31061	3.42	10.2	1.0	1.9

[a]Conditions: 10 mM phosphate buffer, 25.0 °C, pH 6.0, 0.05 M NaCl and 45,000 rpm rotor speed. *s*, *D* and MW_{obs} fits were derived using the unconstrained genetic algorithm analysis using the Monte Carlo analysis tool in Ultrascan (*261*). [b]Percentage of total protein with a sedimentation coefficient that corresponds to the molecular weight expected for a dimer. [c]Ratio of observed molecular weight over calculated molecular weight of monomeric AdcR (16,605.9 Da). These fits reveal that the predominant quaternary structure of wild-type AdcR in the presence and absence of Zn(II) under these conditions is homodimeric with both forms characterized by a rather spherical hydrodynamic particle shape under thesis conditions. These findings are consistent with the results from gel permeation chromatography (see figure on page 95).

Table 3.2 Electrospray ionization-mass spectrometry (LC-ESI-MS) of apo-wild-type and C30A AdcR.[a]

AdcR variant	Expected MW (Da)	Fractional Intensity (au)	MW observed (amu)	Δ (amu)
WT	16605.9	0.75	16607.1	1.2
WT dimer	33211.8	0.25	33213.4	1.6
C30A	16572.3	1.0	16572.3	0
C30A dimer	33144.6	ND[b]	ND	ND

[a]Conditions: Protein concentration 30 μM, C4 column filtered. [b]ND, not detected

(^{107}E**HHHHHH**EH^{114}) we anticipated a potentially strong pH-dependence on the binding affinity and stoichiometry, and therefore measured these parameters at pH 6.0 and pH 8.0 as representative of conditions below and above the pK_a of a typical His residue (neglecting coupling between His side chains) (*262, 263*). Zn(II) binding was measured indirectly using a chelator competition experiment with two different chelators, Mag-fura-2 (mf2; K_{Zn}=5.0x10^7 M^{-1}) (*46*) and Quin-2 (K_{Zn}=2.7 x 10^{11} M^{-1}) (*250*), whose affinities are not strongly dependent on pH (*111, 264*). Mf2 allows an estimation of the zinc binding affinity, K_i, between ≈10^6 and ≈10^9 M^{-1} while quin-2 effectively brackets ≈10^{10} and 10^{13} M^{-1} (*46, 265*).

Figure 3.3(a)-(b) shows representative zinc binding titrations for wild-type AdcR at pH 6.0, while Fig. 3.3(c)-(d) shows representative data for wild-type AdcR at the higher pH 8.0, with mf2 competitions shown in panels (a) and (c) and corresponding quin-2 competitions shown in panels (b) and (d). At pH 6.0, analysis of the mf2 titration reveals K_{Zn1} of ≥10^9 M^{-1} and K_{Zn2}≈10^9 M^{-1}, since virtually all of the added Zn(II) is bound to AdcR until both protomers are saturated; only then does mf2 coordinate metal giving an absorption change (Fig. 3.3(a)).(*48*) A third binding event could be also be detected in these experiments (K_{Zn3}>10^6 M^{-1}) (Table 3.3). In order to better estimate K_{Zn1}, Zn(II) was titrated into a solution of AdcR and quin-2 (Fig. 3.3(b)). These data reveal that K_{Zn1}≈1.0 x 10^{10} M^{-1}. Thus, AdcR binds two mol equiv of Zn(II) per dimer strongly with step-wise affinity constants, K_{Zn1} and K_{Zn2}, that differ by no more than a factor of 10, with a third Zn(II) binding much more weakly (Table 3.3). At pH 8.0, up to five stepwise binding events were required to fit the data, K_{Zn1}, K_{Zn2}, K_{Zn3}, K_{Zn4} and K_{Zn5}.

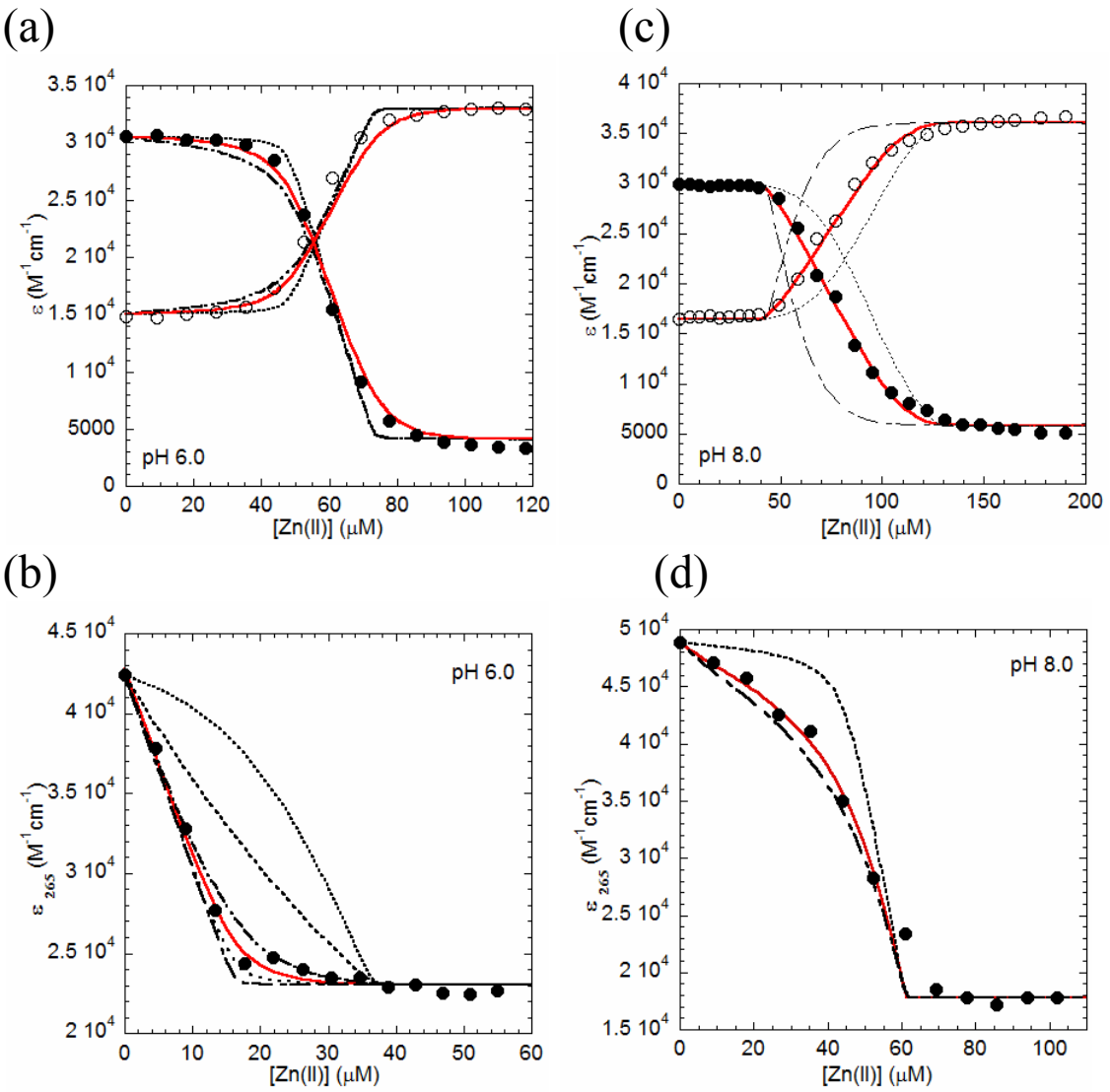

Figure 3.3 Zn(II) binding to AdcR in the presence of competitor chelators. Representative binding isotherms obtained from titrating Zn(II) into a mixture of AdcR wild-type and competitor (mag-fura-2 or quin-2) at pH 6.0 (a-b) or pH 8.0 (c-d). In the mag-fura-2 experiments, filled symbols represent ε_{366} values which are maximal in the apo-mf2 and open symbols represent ε_{325} values that are maximal in the Zn(II)-mf2 complex. For quin-2 experiments, filled circles represent ε_{265} values that are maximal in apo-quin-2. (a) 47.6 μM AdcR and 25 μM mf2. The continuous red line represents non-linear least-square fit to a Zn(II):$AdcR_{dimer}$, 3:1 binding model with the K_{Zn1} stepwise binding affinity fixed to $\geq 10^9$ M^{-1} (a lower limit) and optimized to K_{Zn2}=1.2 (±0.3) x 10^9 M^{-1}, K_{Zn3}=1.7 (±0.1) x 10^6 M^{-1}. The black dot and dash lines are simulated data to K_{Zn1} = 10^{10} and 10^9 M^{-1}, respectively. (b) 41 μM AdcR and 16 μM quin-2. The continuous red line represent non-linear least-square fit to a Zn(II):$AdcR_{dimer}$, 0.5:1 binding model, where K_{Zn1} = 8.3 (±0.2) x 10^9 M^{-1}. Simulated data is represented by discontinuous black lines, with K_{Zn1} = 10^{12}, 10^{11}, 10^{10}, 10^9, 10^8 M^{-1}, descending from right to left. (c) 42.5 μM AdcR and 17.7 μM mf2. The solid red line represent non-linear least-square fit to a Zn(II):$AdcR_{dimer}$, 5:1 binding model with K_{Zn1}=K_{Zn2} = 10^{11} M^{-1}, K_{Zn3}=1.4 (±0.2) x 10^8 M^{-1}, K_{Zn4}=3.00 (±0.03) x 10^7, K_{Zn5}=3.8 (±0.8) x 10^6 M^{-1}. The dot and dash black lines are simulated curves one order of magnitude larger and lower, respectively. (d) 44 μM AdcR and 17.1 μM quin-2. The solid red line represent non-linear least-square fit to a Zn(II):$AdcR_{dimer}$, 2:1 binding model with K_{Zn1}=K_{Zn2} = 1.4 (±0.2) x 10^{12} M^{-1}. The black dot and dashed line are simulated data to K_{Zn1}=K_{Zn2}=10^{13} and 10^{12} M^{-1}, respectively.

Table 3.3 Binding affinities of Zn(II) ($x10^9$ M^{-1}) and other metal ions for wild-type and selected mutant AdcR homodimers[a]

			pH 8.0[c]		
AdcR	K_{Zn1}	K_{Zn2}	K_{Zn3}	K_{Zn4}	K_{Zn5}
WT	1400 (±200)[d]	1400 (±200)[d]	0.14 (±0.02)	0.030 (±0.003)	0.0038 (±0.0008)
C30A	710 (±70)	710 (±70)	0.071 (±0.001)	0.087 (±0.001)	0.014 (±.001)
H42A	7.3 (±1.0)	≥1.0	0.23 (±0.07)	0.036 (±0.007)	–
H108A	1.2 (±0.1)[d]	1.2 (±0.1)[d]	0.017 (±0.001)	0.009 (±0.001)	0.0020 (±0.0005)
H111A	903 (±90)[d]	903 (±90)[d]	0.030 (±0.004)	0.007 (±0.002)	–
H112A	32 (±10)	1.2 (±0.5)	0.090 (±0.001)	0.009 (±0.001)	0.0020 (±0.0006)
H112Q	6.2 (±1.0)	0.012 (±0.001)	0.0020 (±0.001)	–[e]	–[e]
	K_{Co1}[g]	K_{Co2}[g]	K_{Co3}[g]	K_{Co3}[g]	
C30A	6.7 (±0.7) x 10^6	6.7 (±0.7) x 10^6	3.0 (±0.1) x 10^4	3.0 (±0.1) x 10^4	
	K_{Mn1}[h]	K_{Mn2}[h]			
	1.3 (±0.2) x 10^5	1.3 (±0.2) x 10^5	1.0 (±0.1) x 10^4	1.0 (±0.1) x 10^4	
	4.6 (±0.1) x10^5[i]	4.6 (±0.1) x10^5[i]	–[e]	–[e]	

	pH 6.0[b]		
AdcR	K_{Zn1}	K_{Zn2}	K_{Zn3}
WT	8.3 (±0.5)	1.2 (±0.3)	0.0017 (±0.001)
C30A	1.2 (±0.1)	0.055 (±0.001)	0.001 (±0.0001)
H42A	0.012 (±0.004)	–[e]	–
H108A	–	–	–
H111A	3.4 (±0.9)	0.22 (±0.02)	0.001 (±0.0006)
H112A	–	–	–
H112Q	0.010 (±0.004)	–	–
	K_{Co1}[f]		
C30A	2.4 (±0.4) x 10^5	–	–

[a]25 mM bis-Tris, pH 6.0, 0.2 M NaCl, 25.0 ºC or 25 mM Tris-HCl, pH 8.0, 0.5 M NaCl, 25.0 ºC. Measured as shown by representative plots in Fig. 3.3 (see text for details) by chelator (mf2 and quin-2) competition assays.
[b]Fit to 2 (K_{Zn1}, K_{Zn2}) or 3 (K_{Zn1}, K_{Zn2}, K_{Zn3}) step-wise binding events on a nondissociable AdcR dimer ([AdcR monomer]≥25 μM in all cases.
[c]Fit to 4 (K_{Zn1}–K_{Zn4}) or 5 (K_{Zn1}–K_{Zn5}) step-wise binding events (see text for details).
[d]Constrained K_{Zn1}=K_{Zn2} since goodness-of-fit did justify otherwise.
[e]–, binding event not detected with mf2 (K_{Zn3}<$5x10^5$ M^{-1}).
[f]Determined by direct titration of wild-type AdcR (Fig. 3.5)
[g]Determined by isothermal titration calorimetry (Fig. 3.6(b)) with the constraint that K_{Co1}= K_{Co2} and K_{Co3}= K_{Co4}.
[h]Determined by ITC (see Fig. 3.6(a)) with the constraint that K_{Mn1}= K_{Mn2} and K_{Mn3}= K_{Mn4} (Fig. 3.5).
[i]Determined using a chelator competition experiment with mf2 where $K_{Mn\text{-}mf2}$ was fixed to 1.0 x 10^6 M^{-1} (Fig. 3.5).[60]

K_{Zn1} and K_{Zn2} are presumed to represent binding to one pair of symmetry related sites on the dimer, whereas K_{Zn3} and K_{Zn4} are predicted to represent binding to a second pair of sites on the dimer. The mf2 competition curve (Figure 3.3(c) is best fit K_{Zn1} and $K_{Zn2} \geq 10^9$ M^{-1}, with K_{Zn3}=1.4 (±0.2) x 10^8 M^{-1}, K_{Zn4}=3.0 (±0.3) x 10^7 M^{-1} and K_{Zn5}=3.8 (±0.8) x 10^6 M^{-1}. Competition experiments carried out with quin-2 (Figure. 3.3(d)) allow an estimate of the highest affinity sites with $K_{Zn1} = K_{Zn2}$ = 1.4 (±0.2) x 10^{12} M^{-1}. All zinc binding affinities of AdcR are larger at pH 8.0 relative to pH 6.0, with the highest affinity sites (sites 1 and 2) increasing by 100-1000-fold; in addition, the appearance of several lower affinity sites are detectable at the highest pH.

Analogous methods were used to extract Zn(II) binding affinities and stoichiometries for mutant AdcRs (Figure. 3.4, Table 3.3). Substitution of the lone Cys in AdcR with Ala (C30A) results in a protein that exhibits properties like wild-type-like AdcR (Table 3.3). H111A AdcR, like C30A AdcR, is also essentially wild-type in these assays (Table 3.3). In contrast, H42A, H108A and H112A/Q AdcRs exhibit very weak or no detectable Zn(II) binding at pH 6.0 ($K_{Zn1} \leq 10^7$ M^{-1}) with ≈100-1000-fold decreases in zinc affinities of the first two mol equivalents of metal bound at pH 8.0 (Figure. 3.4, Table 3.3). These data reveal that introduction of substitutions specifically at conserved residues His42, His108 and His112 leads to a loss of high affinity Zn(II) binding by AdcR.

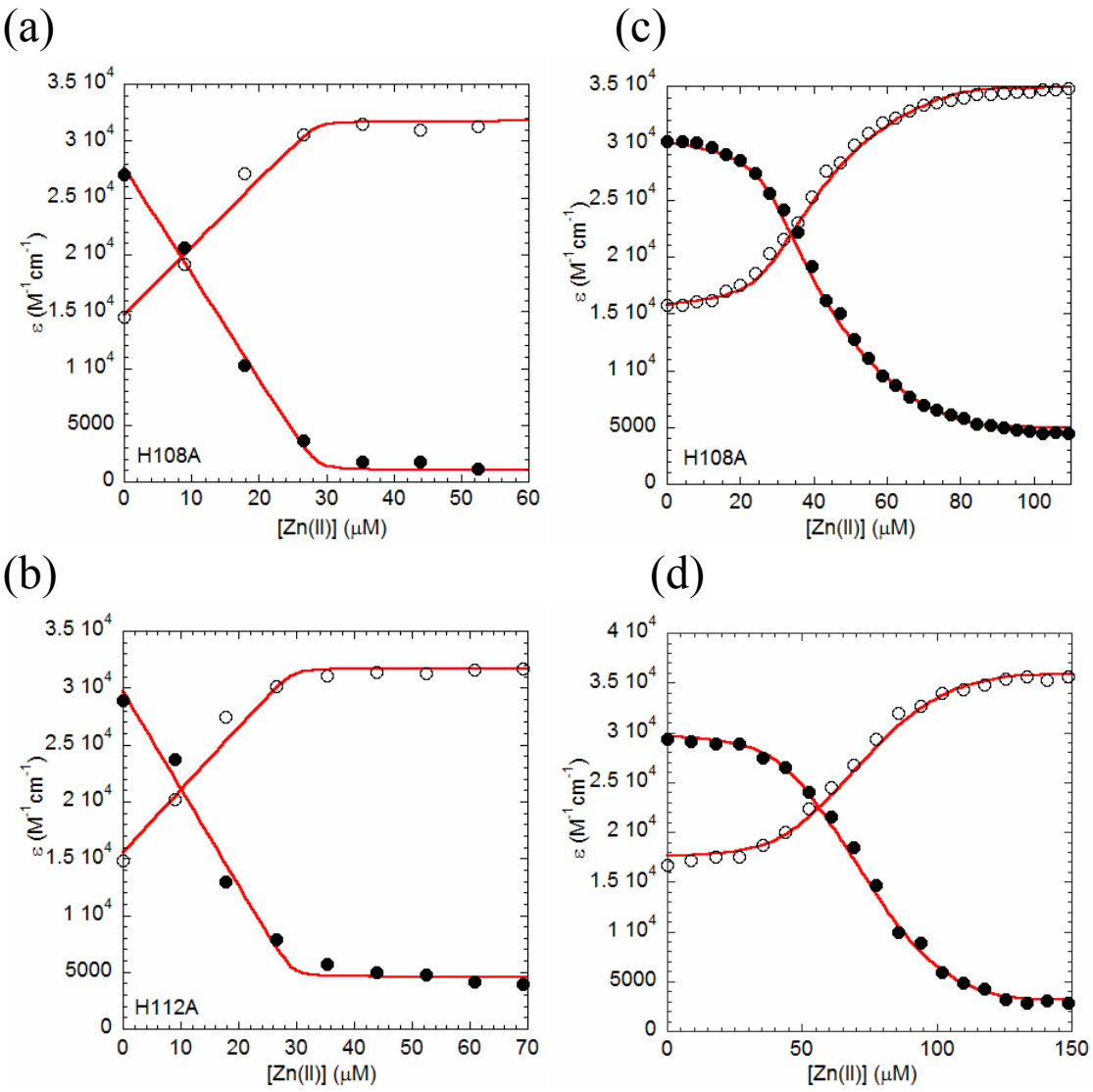

Figure 3.4 Zn(II) binding to AdcR variants in the presence of competitor chelators. Binding isotherms obtained from titrating Zn(II) into a mixture of AdcR variants and competitor mag-fura-2 at pH 6.0 (a-b) or pH 8.0 (c-d). Closed markers represent ε_{366} values which are maximal in the apo-mf2 and open markers represent ε_{325} values that are maximal in the Zn(II)-mf2 complex. (a) 34.4 μM H108A AdcR and 28.6 μM mf2 and (b) 30 μM H112A AdcR and 30 μM mf2. The red solid line represent a non-linear least-square fit to stoichiometric binding of Zn(II) to mf2. (c) 25.3 μM H108A and 22.1 μM mf2. The red solid line represents a non-linear least-square fit to Zn(II):$AdcR_{dimer}$, 5:1 binding model where K_{Zn1}=K_{Zn2}=1.17x10^9 M^{-1}, K_{Zn3}=1.77 (±0.1) x 10^7 M^{-1}, K_{Zn4}=9.0 (±0.9) x 10^6 M^{-1}, K_{Zn5}=1.8 (±0.5) x 10^6 M^{-1}. (d) 41 μM H112A and 27 μM mf2. The red solid line represent a non-linear least-square fit to Zn(II):$AdcR_{dimer}$, 5:1 binding model where K_{Zn1}= 3.5 x 10^9 M^{-1} (fixed), K_{Zn2}=1.2 (±0.5) x 10^9 M^{-1}, K_{Zn3}=9 (±1) x 10^7 M^{-1}, K_{Zn4}=9 (±1) x 10^6 M^{-1}, K_{Zn5}=2.0 (±0.6) x 10^6 M^{-1}.

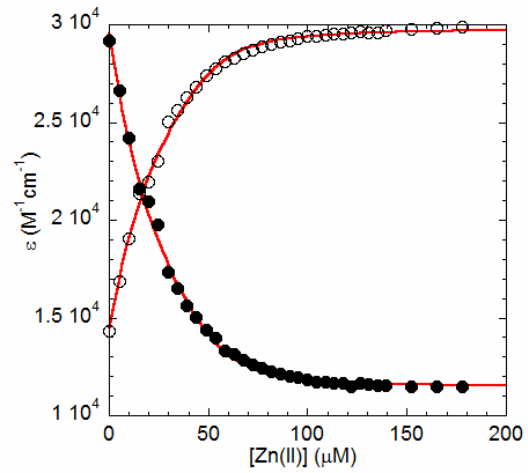

Figure 3.5 Mn(II) binding to C30A AdcR. Representative C30A AdcR-mf2 competition experiment with Mn(II) at pH 8.0. $K_{Mn\text{-}mf2}$ was fixed to 1.0 x 10^6 M^{-1}.(*58*) [C30A AdcR]=33 μM (monomer), [mf2]=18.5 μM. Solid line is a best fit to a simple competition model in which K_{Mn1} and K_{Mn2} are constrained to be identical. Conditions: 25 mM Tris-HCl, pH 8.0, 0.5 M NaCl, 25.0 ºC.

Presumed non-cognate transition metal ions Mn(II) and Co(II) were also tested for their ability to bind to apo-AdcR (Table 3.3). Titration of Mn(II) into a solution of apo-AdcR and mf2 at pH 8.0 gives two (Figure 3.5) higher affinity sites $K_{Mn1,2}$ of $\approx 10^5$ M^{-1}; by ITC, two pairs of Mn(II) sites are observed with $\approx 10^5$ M^{-1} and $\approx 10^4$ M^{-1} affinities (Figure 3.6(a)). The Mn(II) affinity of AdcR is therefore approximately six orders of magnitude weaker than Zn(II) under the same solution conditions (Table 3.3). The cobalt binding affinity was estimated by direct titration at pH 6.0 (Figure 3.7), and gives K_{Co1} of 2.4 x 10^5 M^{-1}, with two pairs of Co(II) binding sites clearly observed by ITC at pH 8.0, with step-wise affinities of 6.7 x 10^6 and 3.0 x 10^4 M^{-1} (Fig. 3.6(b)). Thus, at pH 8.0, metal stoichiometries for both Mn(II) and Co(II) are consistent with that observed for Zn(II) at pH 6.0, and are characterized by relative affinities largely as expected from the trend of stability of small molecule-metal complexes known as the Irving-Williams series (*58, 61, 266*). The molar (monomer) absorptivity of the Co(II) complex in the visible region which reports on *d-d* electronic transitions of d^7 Co(II) ion is weak, ≈60 M monomer^{-1} cm^{-1} (Figure. 3.7) and most consistent with a distorted five-coordinate complex lacking a cysteine ligand, rather than a tetrahedral complex observed in virtually all previously characterized bacterial zinc sensors (*49, 89, 108, 267*).

X-ray absorption spectroscopy reveals a five-coordinate Zn(II) complex for the high affinity sites. Unlike Co(II), Zn(II) is spectroscopically silent due to a filled *d*-shell (d^{10}); as a result, we used x-ray absorption spectroscopy (*89, 268*) to investigate the coordination geometry of the high affinity site(s) in wild-type AdcR (at pH 6.0 and 8.0)

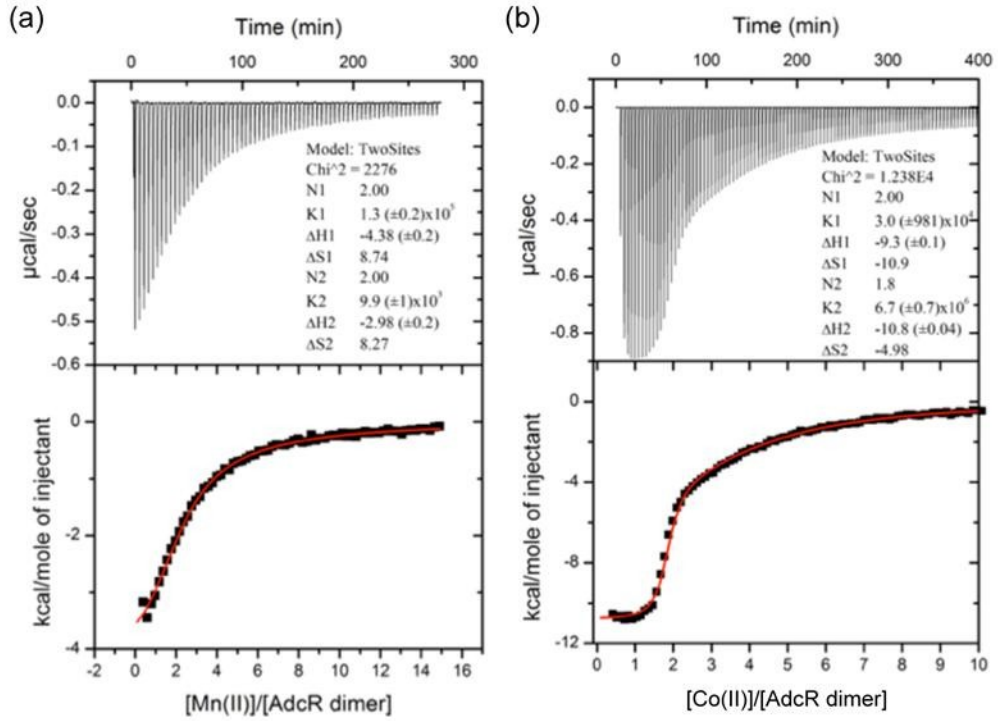

Figure 3.6 The binding of Mn(II) and Co(II) to AdcR as monitored by isothermal titration calorimetry. Representative Mn(II) (a) and Co(II) (b) binding curves for C30A AdcR as measured by isothermal titration calorimetry (ITC) at pH 8.0. [C30A AdcR]=34 µM (monomer) (a) and 32 µM (monomer) (b), with fitted parameters defined by the *solid red* curve compiled in the *inset*. In each case, small additions from a 1.2 mM metal stock solution were made. The stoichiometry of metal binding was fixed as indicated, justified on the basis of the binding of Zn(II) to AdcR under these conditions. Under these conditions, C30A AdcR is presumed to be fully dimeric, based on the behavior of wild-type AdcR under the same conditions (see figure on page 95). K_i are compiled in Table 2 (main text). Note that the binding of Mn(II) is so weak, that a fit to a single pair of identical sites is not statistically different (K_{Mn1}=K_{Mn2}=4.6 (±0.7) x 10^4 M^{-1}) from the fit shown. Conditions: 25 mM Tris-HCl, pH 8.0, 0.5 M NaCl, 25.0 ºC.

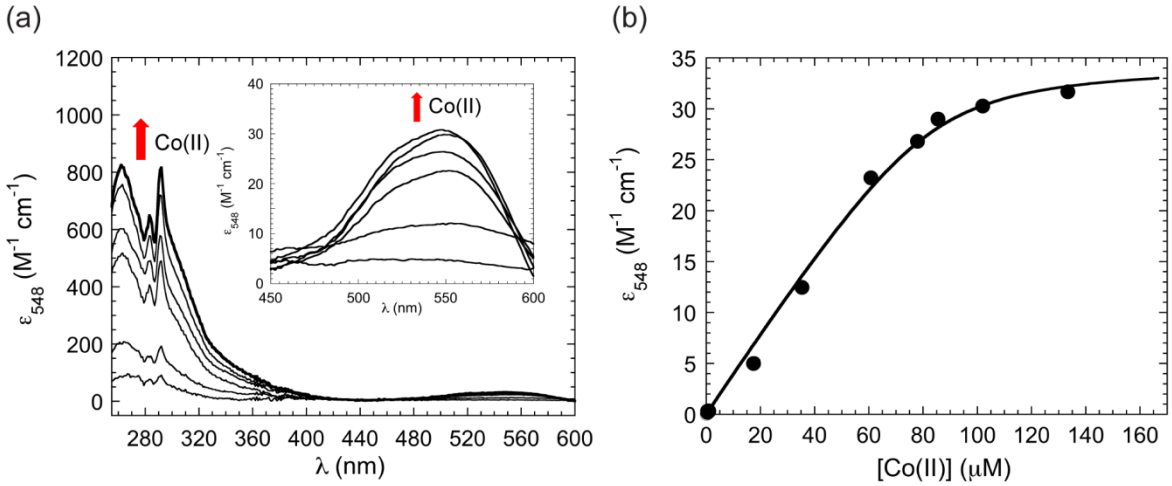

Figure 3.7 Co(II) electronic absorption spectra of AdcR. A representative Co(II) titration of wild-type apo-AdcR. (a) Electronic absorption spectra of AdcR titrated with a stock solution of $CoSO_4$. *Inset:* Magnification of the spectral region that shows *d-d* electronic transition envelope (450-600 nm). (b) Binding isotherm obtained by plotting the change in monomer molar extinction coefficient ε_{548} of 140 μM AdcR (monomer) titrated with Co(II). The solid line represents a nonlinear least-squares fit to a simple 1:1 binding model, where the concentration of AdcR was fitted to 83 μM (n=0.6), and K_{Co}=2.7 (±0.4) x 10^5 M^{-1}. These data reveal that Co(II) adopts a 5- or 6-coordinate complex devoid of thiolate ligands, and binds with measurable negative homotropic cooperativity under these conditions given the apparent stoichiometry of ≈0.5. Conditions: 25 mM Bis-Tris, pH 6.0, 0.2 M NaCl, 25.0 ºC.

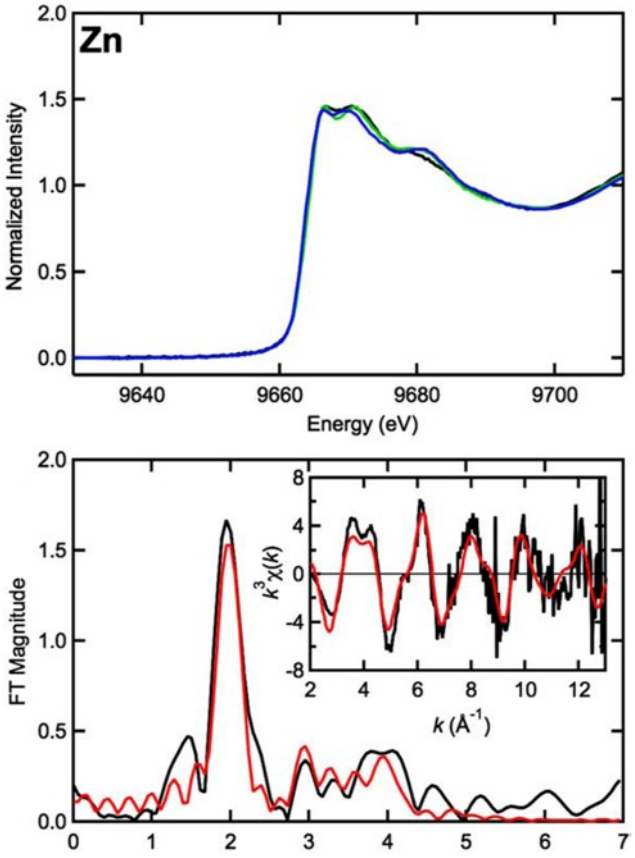

Figure. 3.8 X-ray absorption spectroscopy of Zn(II)-bound AdcR. (Top) Zn K-edge X-ray absorption spectra of Zn(II)-bound WT AdcR at pH 6 (black), C30A mutant (green), and WT AdcR at pH 8 (blue). (Bottom) EXAFS Fourier transform (k^3-weighted, k = 2-13 Å^{-1} of WT AdcR at pH 6. (Inset) k^3-weighted EXAFS spectra for WT AdcR at pH 6. For bottom panel, experimental data are black and best-fit simulations (Table 3, Fit 1) are red.

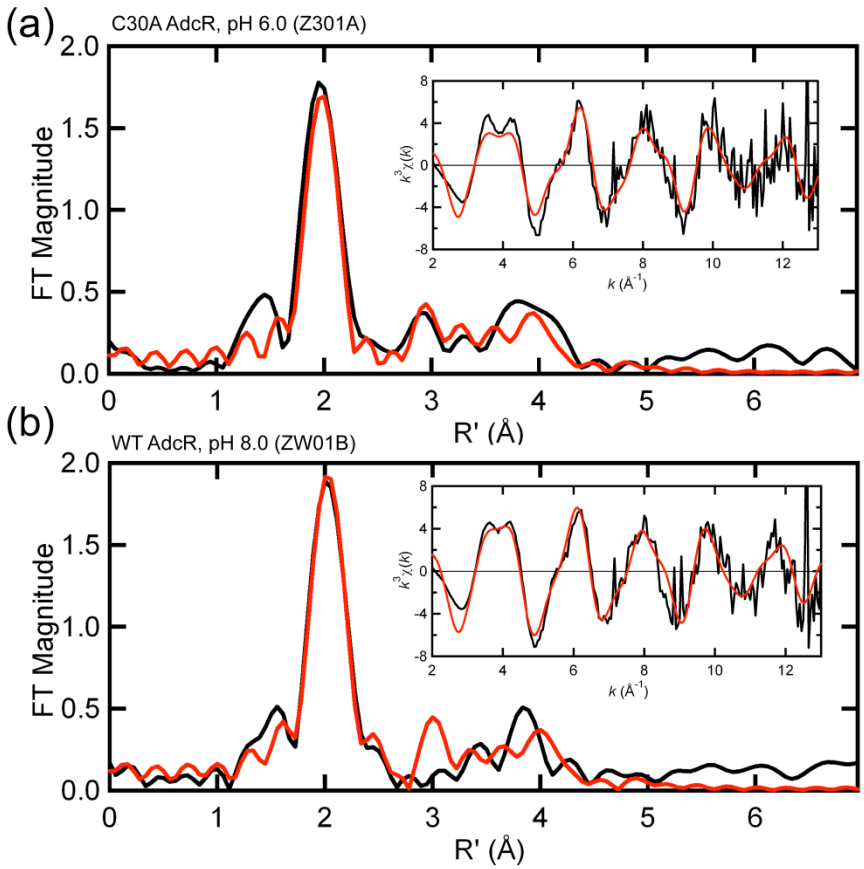

Figure. 3.9 X-ray absorption spectroscopy of Zn(II) bound C30A and wild-type AdcRs. (a) C30A AdcR, pH 6.0 and (b) WT AdcR, pH 8.0. Experimental EXAFS (*inset*), and FT (k = 2−13 Å^{-1}, k^3 weighting) spectra are shown (*black* lines) along with the best fit (*bold red* line) defined by the fitting parameters compiled in Table 3 (main text).

and C30A AdcR (at pH 6.0) that result upon addition of ≈0.8 monomer mol equiv Zn(II). Zn near-edge spectra for all three species are shown in Figure. 3.8(a), with best-fits of the EXAFS and Fourier transforms (FTs) of the EXAFS data shown in Fig. 3.8(b) for wild-type AdcR (pH 6.0) or in Figure 3.9. Parameters that derive from all three fits are also given (Table 3.4). The near-edge spectra for all three complexes are very similar, as are the fits to each data set; these data unambiguously reveal that Cys30 does not donate a thiolate ligand to the Zn(II) complex, and the structure of the chelate is not detectably changed as a result of the C30A substitution or a change in pH. All three data sets are best-fit with a five-coordinate (N/O) complex, modeled with three histidine ligands, and two additional N/O ligands. Although we could not obtain a clear determination of the number of coordinated histidine residues, histidine coordination is consistent with significant FT intensity in the 3-4 Å region (Figure. 3.8(b)).

Zinc binding by AdcR activates adc operator DNA binding. In *S. pneumoniae* D39, an imperfect 5-2-5 inverted repeat sequence 5'- TTAACTGGTAAA is positioned between the *adcR* translation start codon and the -10 region of the promoter that conforms to the consensus 5'-TTAACNRGTTAA sequence.(*62, 221*) This AdcR operator site is identical to that found in ZitR-regulated genes in *Lactobacilis lactis*.(*240*) A standard fluorescence anisotropy-based DNA binding experiment (*45*) was used to measure the affinity of apo- and Zn(II)-bound wild-type and mutant AdcRs for a fluorescein-labeled 28-nucleotide duplex DNA harboring a single *adc* operator (AdcO) derived from the *adcR* gene. In all cases, the binding was measured in presence of non-specific competitor DNA to ensure specificity in either excess Zn(II) or 0.5 mM EDTA

Table 3.4 Curve fitting results for Zn K EXAFS[a]

Sample, filename(k range)$\Delta k^3\chi$	Fit	Shell	R_{as}(Å)	σ_{as}^2(Å^2)	ΔE_0(eV)	f[a]
AdcR WT, pH 6.0, ZW01A	1	Zn-N_2	2.06	0.0039	-0.962	0.149
(k = 2 – 13 Å^{-1})		Zn-N_3	1.98	<u>0.0026</u>	[-0.962]	
$\Delta k^3\chi$ = 12.672		Zn-C_3	[2.96]	[0.0039]	[-0.962]	
		Zn-C_3	[3.01]	[0.0039]	[-0.962]	
		Zn-N_3	[4.14]	[0.0034]	[-0.962]	
		Zn-C_3	[4.19]	[0.0034]	[-0.962]	
AdcR C30A, Z301A	2	Zn-N_2	2.04	0.0037	-0.743	0.147
(k = 2 – 13 Å^{-1})		Zn-N_3	1.98	<u>0.0026</u>	[-0.743]	
$\Delta k^3\chi$ = 12.776		Zn-C_3	[2.96]	[0.0039]	[-0.743]	
		Zn-C_3	[3.01]	[0.0039]	[-0.743]	
		Zn-N_3	[4.14]	[0.0034]	[-0.743]	
		Zn-C_3	[4.18]	[0.0034]	[-0.743]	
AdcR WT, pH 8.0, ZW01B	3	Zn-N_2	2.07	0.0021	0.361	0.154
(k = 2 – 13 Å^{-1})		Zn-N_3	2.00	<u>0.0026</u>	[0.361]	
$\Delta k^3\chi$ = 12.902		Zn-C_3	[3.01]	[0.0039]	[0.361]	
		Zn-C_3	[3.06]	[0.0039]	[0.361]	
		Zn-N_3	[4.19]	[0.0034]	[0.361]	
		Zn-C_3	[4.24]	[0.0034]	[0.361]	

Shell is the chemical unit defined for the multiple scattering calculation. Subscripts denote the number of scatterers per metal. R_{as} is the metal-scatterer distance. σ_{as}^2 is a mean square deviation in R_{as}. ΔE_0 is the shift in E_0 for the theoretical scattering functions. Numbers in square brackets were constrained to be either a multiple of the above value (σ_{as}^2) or to maintain a constant difference from the above value (R_{as}, ΔE_0). Underlined numbers were fixed at the indicated value (not optimized).

[a]f is a normalized error (chi-squared):

$$f = \frac{\left\{ \sum_i \left[k^3 \left(\chi_i^{obs} - \chi_i^{calc} \right) \right]^2 / N \right\}^{1/2}}{\left[\left(k^3 \chi^{obs} \right)_{max} - \left(k^3 \chi^{obs} \right)_{min} \right]}$$

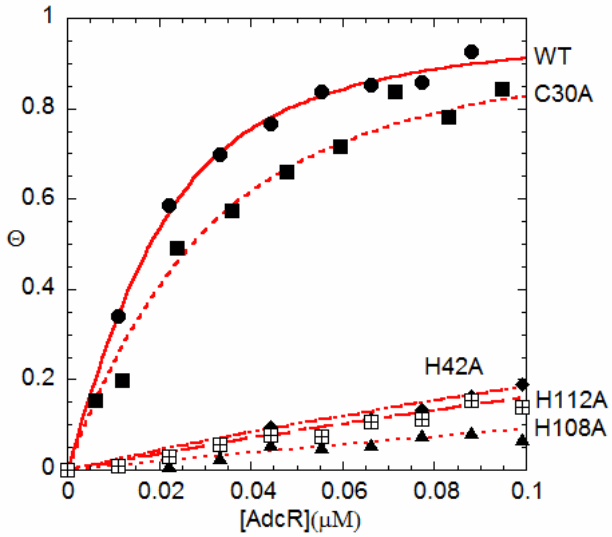

Figure 3.10 DNA binding by wild-type and mutant AdcRs. Representative isotherms of the binding of Zn(II)-AdcR variants to a fluorescein-labeled 28-mer double stranded DNA containing the AdcO sequence. The anisotropy change is normalized to that observed for wild-type AdcR (circles); for all the other variants, C30A (squares), H42A (diamonds), H108A (triangles) and H112A (gridded square) AdcRs, the fractional change in anisotropy was calculated relative to the total change observed for wild-type AdcR. The Zn(II)-activated binding is reversible at the end of the experiment by addition of 500 μM EDTA (not shown). The red continuous lines represent non-linear least-square fits for the binding of a non-dissociable dimer to DNA with the affinities ($K_{\text{DNA Zn}}$) complied in Table 3.5

and the resulting data were fit to a non-dissociable AdcR dimer binding model to obtain $K_{DNA\text{-}Zn}$ or $K_{DNA\text{-}apo}$. Wild-type AdcR binds with an affinity of 2.4 (±0.3) x 10^8 M^{-1} in the presence of Zn(II) ($K_{DNA\text{-}Zn}$) (Figure. 3.10), with no detectable binding observed in the presence of EDTA or chelexed buffer ($K_{DNA\text{-}apo} \leq 10^5$ M^{-1}). These data reveal that AdcR is a Zn(II) activated DNA binding protein, characterized by a lower limit for the allosteric coupling free energy, $\Delta G_c \leq -4.6$ kcal mol^{-1} (Table 3.5) (*52*). Interestingly, non-cognate metal ions Co(II) and Mn(II) also activate AdcR binding to the *adc* operator, with these metals nearly indistinguishable from that of Zn(II) in this assay (Table 3.5). This finding suggests that Co(II) and Mn(II) form coordination complexes that are isostructural with that of Zn(II), at least when bound to the operator DNA (see Discussion).

Exactly analogous DNA binding experiments were carried out with each of the missense mutants with the K_i and $\Delta G_{c,i}$ compiled in Table 3.5 with selected DNA binding curves shown in Figure 3.10 for the indicated Zn(II) complexes (no binding was observed for any mutant in the presence of 0.5 mM EDTA). As expected, all mutant AdcRs that display high affinity Zn(II) binding (C30A, H111A) are strongly activated to bind the AdcO DNA by Zn(II). *S*-methylation of Cys30 also has no effect on Zn(II)-activated DNA binding, further evidence of the non-essentiality of this cysteine in AdcR function. In contrast, H42A, H108A and H112A mutants are all weakly activated by Zn(II) binding, with affinities 50-200-fold reduced in the presence of Zn(II). Zn(II)-bound H112Q AdcR binds to the operator about three-fold more tightly than the other

Table 3.5 Equilibrium binding affinities (K_i) resolved from fluorescein anisotropy-based AdcR operator binding isotherms for individual AdcR derivatives in the presence and absence of Zn(II).

AdcR variant	$K_{DNA\ Zn}$[a] ($\times 10^8\ M^{-1}$)	$K_{DNA\ Me}$[b] ($\times 10^8\ M^{-1}$)	$K_{DNA\ apo}$[c] ($\times 10^8\ M^{-1}$)	ΔG_c[d] (kcal mol^{-1})
Wild-type + Zn	2.4 (±0.3)	–	≤0.002	–4.2
Wild-type + Mn	–	0.82 (±0.05)	≤ 0.002	–3.6
Wild-type + Co	–	1.2 (±0.2)	≤ 0.002	–3.8
S-methylated wild-type	1.1 (±0.1)	–	ND[e]	ND
C30A	1.1 (±0.1)	–	≤ 0.002	–3.7
H42A	0.047 (±0.001)	–	≤ 0.002	–1.9
H108A	0.020 (±0.0007)	–	≤ 0.002	–1.4
H111A	1.4 (±0.1)	–	≤ 0.002	–3.9
H112A	0.038 (±0.001)	–	≤ 0.002	–1.7
H112Q	0.098 (±0.007)	–	≤ 0.002	–2.3

Conditions: 25 mM bis-Tris, pH 6.0, 25.0 ºC, 0.2 M NaCl, 0.005% Tween 20, 0.8 μg/mL of nonspecific deoxyribonucleic acid from salmon sperm. ND, not determined.

[a]For determination of $K_{DNA\ Zn}$, 100 μM $ZnSO_4$ was added to the binding reactions.

[b]For determination of $K_{DNA\ Co}$ and $K_{DNA\ Mn}$, 10 μM of metal was added to the binding reactions.

[c]For determination of $K_{DNA\text{-}apo}$, 500 μM EDTA was present.

[d]$\Delta G_c = -RT \ln(K_{DNA\text{-}Zn}/K_{DNA\text{-}apo})$ and represents a lower limit given the upper limit on $K_{DNA\text{-}apo}$. .

inactive mutants, with an affinity ≈20-fold reduced relative to wild-type AdcR (Figure 3.10).

NMR studies reveal that Zn(II) coordination by His42, His108 and His112 are required to drive a quaternary structural change in the dimer, while His111 is not. The metal binding experiments presented above reveal H42A, H08A and H112Q/A mutants have greatly perturbed Zn(II) binding equilibria and are essential for allosterically activate *adc* operator DNA binding. Uniformly ^{15}N-labeled wild-type AdcR with ≈70% fractional deuteration and selected fully protonated mutant AdcRs were purified and ^{1}H-^{15}N TROSY spectra recorded for each in the presence and absence of Zn(II) at pH 6.0, 35 ºC. In all cases, ≈2 mol equiv of Zn(II) per monomer was added to ensure complete saturation of the two highest affinity zinc sites (if present), as well as any lower affinity sites that might be populated under these conditions (see Table 3.3).

Appendix C shows a ^{1}H-^{15}N TROSY spectrum of apo-AdcR with sequence specific resonance assignments derived from analysis of triple resonance data indicated for each crosspeak (to be reported elsewhere). All but four (of 143) backbone ^{1}H-^{15}N pairs have been assigned, with the spectrum fully consistent with a highly α-helical two-fold symmetric homodimer. Analysis of backbone ^{1}H, ^{15}N, ^{13}Cα, ^{13}Cβ and ^{13}C' chemical shifts with TALOS(*269*) gives the secondary structural analysis of the primary structure of apo-AdcR as shown (Appendix C (c), *top*). These data reveal seven α-helices (labeled α1-α7) and three short β-strands (labeled β0-β2). A comparison of these features with known structures of MarR family regulators(*214-219, 270*) is consistent with an N-terminal winged helical domain consisting of α1–β2, containing an

α3-α4 helix-turn-helix and a β1-β2 hairpin wing, and a C-terminal all α–helical regulatory domain linked by a long α5 helix. His42 is in the N-terminal region of the α2 helix in the DNA binding domain, while the poly-His run containing His108 and His112 is positioned in the middle of the α5 helix (Appendix C (c)).

Appendix C(b) shows a ^{1}H-^{15}N TROSY spectrum of Zn(II) complexed AdcR (*cyan* crosspeaks, labeled) superimposed on the spectrum of apo-AdcR (*red* crosspeaks, single contour line), with a secondary structural analysis of these data shown in Appendix C (c) (*bottom* trace). Zn(II) binding results in large changes in the spectrum that are global in nature extending from the N-terminal α1 to the C-terminal α7 helix (Appendix D, *bottom trace*). Interestingly, while the secondary structure of the core of the molecule is unchanged, the N-terminal α1 helix appears to be shortened by three amino acids, with the α6 and α7 helices apparently making a continuous helix. In some other MarR regulators, these two terminal helical regions derived from opposite subunits (*e.g.,* α1 and α6'-α7') are in close proximity,(*217*) and in AdcR may well reorient as a result of Zn(II) binding. In any case, we reasoned that these spectral changes could be used as a sensitive reporter of quaternary conformational transition in mutant AdcR homodimers upon binding activating metal ions.

Uniformly ^{15}N-labeled H42A, H108A, H111A and H112A AdcRs were purified and a ^{1}H-^{15}N TROSY spectra of apo- and Zn(II) bound forms acquired (spectra not shown). Chemical shift perturbation maps of all four apoproteins relative to the wild-type AdcR (apo-apo) reveals that each mutant is stably folded and adopts a structure very similar to that of apo-wild-type AdcR (Appendix E). The largest perturbations

($\Delta\delta \leq 0.3$ ppm) are obtained with an Ala substitution of H42 in the α2 helix, which influences the chemical shifts of residues not only in the α2 helix, but also in the α5 and α7 helical regions, indicative a long-range perturbations even in the apo-state. Strikingly, addition of Zn(II) to H42A, H108A and H112A results in virtually no spectral changes (Appendix D), direct evidence that Zn(II) binding (albeit weakly; see Table 3.3) to these mutants fails to switch the conformation to a high affinity DNA binding state (see below). This is in contrast to H111A AdcR which gives a perturbation map that is nearly identical to that of wild-type AdcR (Appendix D). These data reveal that loss of a high affinity binding site(s) on the dimer (see Table 3.3) results in loss of the ability to undergo quaternary structural conformational switching. Thus, these structural data provide further evidence that H42, H108 and H112 are direct ligands to the regulatory pair of Zn(II) binding sites on AdcR.

DISCUSSION

Transition metal sensing bacterial repressors comprise a collection of transcriptional regulatory proteins that allow an organism to control the intracellular availability of biological required metal ions (*14, 15*). It is hypothesized that each metalloregulatory protein must be tuned such that it responds only to a single metal ion at a thermodynamic "set-point' in the context of the intracellular milieu. Such a set-point is proposed to correspond to a concentration of "buffered" or "weakly chelated" metal ion in the intracellular compartment in which metalloregulation or sensing occurs. In bacteria, this compartment corresponds to the cytoplasm. It is therefore important to

determine the affinity and stoichiometry of a sensor for cognate and noncognate metal ions, and determine how metal binding allosterically activates or inhibits repressor binding to its DNA operator (*52, 109, 111, 139*).

In this work, we show that *S. pneumoniae* AdcR is a zinc-sensing metalloregulatory protein that is characterized by a strongly pH-dependent affinity for metal ions, and forms a coordination complex that is thus far unique to our knowledge among zinc-specific bacterial regulators. Although the AdcR homodimer harbors two pairs of the zinc binding sites characterized by $K_{Zn} \geq 10^7$ M at pH 8.0 (Table 3.3), the two highest affinity sites appear necessary and sufficient for metalloregulation of DNA binding *in vitro*. This pair of sites likely involves direct coordination of the imidazole side chains of His42 in the α2 helix within the DNA binding domain, and His108 and His112 on opposite ends of a poly-histidine tract in the α5 helix. These residues are absolutely conserved in all known and predicted members of the zinc-sensing AdcR/ZitR subfamily of MarR family regulators, and thus collectively donate three of the five ligand donor atoms to the regulatory Zn(II) ion in each subunit. This follows the predicted trend that two histidine residues separated by four residues apart in a helix (in this case H108 and H112) are used to bind metal ions (*113*). The affinity of this site is $\approx 10^9$-10^{10} M^{-1} at pH 6.0 and increases by approximately two orders of magnitude, to $\approx 10^{12}$ M^{-1} at pH 8.0. The origin of the strong pH-dependence is unknown and has not been directly measured for any other bacterial zinc sensor. For *S. aureus* CzrA, formation of the two regulatory zinc complexes of $K_{Zn1}=10^{12}$ M^{-1} and $K_{Zn2}=10^{11}$ M^{-1}, each composed of three His ligands and a carboxylate residue , occurs with the

concomitant release of a net of ≈1 proton per monomer (or ≈2 per dimer) as measured by isothermal titration calorimetry at pH 7.0 (*98, 111*). On the other hand, the intrinsic pK_a of transition metal ligands can be quite acidic, and thus would be fully deprotonated at neutral pH. However, neighboring non-liganding histidines and local electrostatics may strongly influence the degree of ligand deprotonation in apo-AdcR (*271-273*) and thus the pH-dependence of the metal-binding affinity.

Of the five consecutive His residues in the α5 helix in AdcR, only His108, His111 and His112 are invariant and thus were strong candidates for direct coordination to the regulatory zinc ion. We show here that His108 and His112, predicted to be on the same side of the α5 helix, are required for AdcR function *in vivo* and *in vitro*. X-ray absorption spectroscopy, as well as spectroscopic features of the Co(II) complex, are most consistent with a coordination number (*n*) of five in this chelate; however, *n*=6 can not be rigorously excluded from these data. The identity of the additional ligands to the regulatory site, as well as any of the metal ligands to the second pair of lower affinity sites on the dimer are currently unknown. Zn(II) is most often coordinated by carboxylate, imidazole and/or thiolate ligands and typically adopts a tetrahedral (*n*=4) coordination geometry (*108, 111, 267*). On the basis of sequence conservation, strong candidates for other metal ligands are Glu20 and Glu24 in the α1 helical region, C30 in the α1-α2 loop, Glu41 and Glu107, each of which are immediately adjacent to ligands His42 and His108 (Appendix C). The backbone ^{1}H-^{15}N TROSY crosspeak positions of Glu20 and Glu24 are not strongly perturbed on Zn(II) binding, evidence that this region is unlikely to donate ligands to the regulatory metal. C30 in the α1-α2 loop, Glu41 and

Glu107, each of which are immediately adjacent to ligands His42 and His108. Cys30 also does not donate a ligand to the regulatory pair of sites, since we could not obtain spectroscopic evidence for thiolate coordination in the regulatory site, nor is Cys30 essential for AdcR function. This finding does not rule out an additional regulatory role of Cys30 in an oxidative stress response superimposed on the primary zinc-sensing role of AdcR as recently proposed in *S. suis* (*221, 222*). The physiological significance, if any, of redox chemistry occurring on Cys30 in *S. pneumoniae* AdcR remains unknown and contrasts sharply with *bona fide* MarR family members that sense peroxide or other ROS stress via formation of higher oxidation states of cysteine (*218, 274, 275*).

Glu41 and/or Glu107 are the strongest candidates for donating a carboxylate ligand to the regulatory site in AdcR. Carboxylate side chains can assume monodentate or bidentate coordination, and thus one or both may be involved in Zn(II) coordination. . It is interesting to note that efforts to create *S. pneumoniae* D39 strains harboring E41A and H42Q alleles yielded either wild-type revertants or suppressor mutants (data not shown). High resolution structural studies will be required to obtain a comprehensive picture of the $(N/O)_5$ regulatory coordination complex in AdcR. The pentavalent coordination structure of the activating metal site in AdcR is unusual, as an increased coordination number is often associated with transition metal ions Fe(II) and Mn(II), with biological Zn(II) complexes overwhelmingly tetrahedral (n=4),(*100, 101*) despite the fact that there is no fundamental *a priori* reason why this should be the case (*276*). In fact, this feature alone might be expected to decrease the specificity of this sensor for Zn(II) in the cytoplasm. Other transition metals are capable of activating DNA binding

to an extent quantitatively similar to that of Zn(II) (Table 3.5), a finding that contrasts sharply with non-cognate metal complexes formed by well characterized Ni(II) sensor NikR(*104*), and ArsR and CsoR/RcnR family sensors (*51, 99*). In these cases, non-cognate metal ions nearly always adopt coordination complexes that differ structurally from that formed by the cognate metal ion (*56, 177*). In AdcR, a fundamentally distinct mechanism of specificity is likely operative, with the relative metal binding affinities (Table 3.3) likely controlling AdcR function in the cell, *i.e.,* bioavailable concentrations of Co(II) and Mn(II) never rise to the degree necessary to activate DNA binding in the cell. This ensures that only Zn(II), which may well be buffered to very low (femtomolar) "free" or weakly chelated intracellular concentrations (*29*) far below that of Mn(II), Fe(II), Co(II) and Ni(II), will strongly activate DNA binding in the cytoplasm of *S. pneumoniae* (*13*). For AdcR, $K_{Zn} \approx 10^{12}$ M^{-1} which is two-three orders of magnitude lower than that reported for zinc uptake and efflux regulators *E. coli* Zur and ZntR, respectively (*29*), but comparable to that of *S. aureus* efflux regulator CzrA (*98*). The functional significance of this discrepancy is currently unknown. This model for the zinc specificity of AdcR also partly explains the apparent discrepancy between the ability of Zn(II) to activate AdcO binding *in vitro* vs. that which occurs *in vivo*. All AdcR mutants in which the high affinity Zn(II) sites are destroyed, are activated to small but significant degrees to bind to the operator under standard conditions; furthermore, this binding is sequence-specific since it is measured in the presence of excess non-specific DNA. Thus, substitution of single metal ligands in the regulatory site does not abolish metalloregulation of DNA binding, although the magnitude of the allosteric coupling

free energy (ΔG_c) is significantly decreased, indicative of a perturbation of the communication between metal and DNA binding sites. However, a regulatory K_{Zn} reduced by ≈200-1000 fold renders these AdcR mutants capable of sensing free Zn(II) concentrations only if they rise to nM range, thus making them non-functional *in vivo*.

Elucidation of the structural and dynamical mechanism of allosteric activation of DNA binding by Zn(II) by this novel MarR regulator, particularly in the context of well-studied allosterically inhibited zinc sensors, promises to reveal novel insights into MarR family function (*79*) and zinc homeostasis in *S. pneumoniae* (*80*).

CHAPTER IV

SUMMARY AND PERSPECTIVES

SUMMARY

The studies on metal sensors that focus on metal selectivity and allosteric switching have being summarized in Chapter 1. The interest in metal selectivity follows from the diversity of transition metals as a future of the cytoplasm, and the metal specificity that is required for adequate function of metalloproteins and for metal sensors to efficiently and specifically respond to enviroment changes in metal concentrations. Metal specificity can be dictated in metal sensors by three features; metal binding affinities, ligand preference and coordination geometry. It is satisfying to note that it was required for metal regulatory centers to evolve round intrinsic properties of metals.

With respect to allosteric propagation, it was noted that changes in the structure that are initialized by metal ion binding are propagated by second shell interactions of key allosteric donor ligand histidines. In some instances, it was found that the structural changes that occur on metal binding are observable in crystallographic structures. However, in other cases where observed structural changes are small and localized, it becomes necessary to examine structural dynamics over the widest possible range of different timescales in an effort to explain allosteric switching. In the only extensively studied case available at this time, *S. aureus* CzrA, metal binding appears to stabilize the native structure into a low DNA affinity state(*98, 109*).

NmtR is one of the two Ni(II)/Co(II) sensor members of the ArsR (or ArsR/SmtB) family present in *M. tuberculosis* genome, a feature that could be an advantage for adaptation to high Ni(II) environments. We report structural differences at metal allosteric centers that functionally distinguish NmtR from *S. aureus* CzrA, a well-characterize helix α5 regulated Zn(II) sensor member of this family. These key functional differences may be relevant to Zn(II) homeostasis regulation in *M. tuberculosis* cytoplasm(*123*) by yet another member of the ArsR family, *Mt*SmtB, a canonical helix α5 regulated sensor(*76*)that is specifically activated by Zn(II) *in vivo* (*156*).

For NmtR, integrity of all the donor ligand residues in the α5 helix are required to maintain a native octahedral coordination geometry and wild-type-like allosteric regulation. The N-terminal and C-terminal extensions, lacking in CzrA and other Zn(II)-specific sensors of the ArsR family, are important for metal selectivity and metal induced allosteric regulation, respectively. These findings motivate NMR studies in various allosteric states that are currently ongoing to gain specific insights into NmtR function.

The *S. pneumoniae* AdcR is the first metal sensor of the MarR family of transcriptional regulators to be characterized, although a biological characterization of the homolog from *Lactobacillus lactis*, ZitR, has recently appeared(*277*). The functional state of AdcR is a homodimer that binds two Zn(II) per monomer with affinities that are dependent on pH in the physiological range. The AdcR dimer is capable of binding up to five Zn(II) at pH 8, likely to surface-exposed adventitious sites that have not yet been

identified . Zn(II) binding allosterically activates AdcR to bind operator DNA, as do non-cognate metals Mn(II) and Co(II) *in vitro*; however, non-cognate metal ions bind with far lower affinity relative to Zn(II). It is expected that the *in vivo* metal selectivity is dictated in this case by metal binding affinities. The metal regulatory center of AdcR was found to involve residues in the C-terminal dimerization domain and the DNA binding domain, and thus exhibits properties superficially analogous to Fur family regulators, *e.g., B. subtilis* PerR (*116, 118*). The extent to which Zn(II) drives a quaternary structural change in the dimer is under current investigation in solution using NMR techniques.

PERSPECTIVES

Nowadays one of the key challenges of understanding transition metal homeostasis is to obtain a complete picture of metal speciation in the cellular environment. One objective is to reconcile the i*n vitro* metal concentrations at which efflux and uptake systems are activated by functionally related pairs of metalloregulators (K_{Me}) and the metal concentration at which this systems are activated *in vivo*, which may or may not be the same. One manifestations of this disconnect is, for example, a ~4 *vs*. ~1 order of magnitude difference in range of sensitivity in *E. coli* Ni(II) homeostasis system (*56, 71, 74*) as well as our preliminary studies on the *S. pneumoniae* Zn(II) sensor AdcR and its functional efflux regulator SczA. This might suggest that the *in vivo* situation may be shifted far from the thermodynamic equilibrium found in ideal laboratory experimental conditions. It is proposed that SczA can sense Zn(II) ions in the

cytoplasm at lower concentrations that those sensed *in vitro*, as is speculated for the *E. coli* Ni(II) sensor RcnR(*186*). This could happen if a Zn(II) protein functioned as a chaperone to deliver metal to SczA or the cation diffusion facilitator CzcD, in a process governed more by the kinetics of metal transfer similar to what has been argued for copper chaperones(*65, 278*). On the other hand, a kinetically facile process with low or no barriers to metal transfer will function most efficiently down even a shallow thermodynamic gradient, and support for this latter idea is found in the copper trafficking field as has recently been obtained (*279*). Arguing against this proposal in the case of Zn(II) is that we have no clear evidence in support of a zinc chaperone. However, the AdcR regulon operates on a distal locus that consists of a distinctive group of cell wall attached proteins in *S. pneumoniae*, pneumococcal histidine triad (Pht), that are unique to this species. In *S. pneumoniae* genome are find four copies of this gene in what it seems to be a locus important for pathogenesis. Crystallographic structure of a truncated Pht protein showed that it binds Zn(II) using a HxxHxxH sequence which, is repeated five times in a protein of about 800 residues (*231*). These characteristics make Pht proteins good candidates for a role in Zn(II) transport between the cell wall and metal centers of proteins in the cytoplasm. A biophysical characterization of this protein will bring light to what role, if any, Pht proteins play is in cellular Zn(II) homeostasis. The Zn(II) binding affinities, oligomerization state and characterization of the Zn(II) binding center, can be studied using methodologies outlined in this work.

A unique feature of AdcR that distinguishes it from any other Zn(II) metal sensor is that the regulatory center contains five ligand donors ($His_3(N/O)_2$). In Chapter 3 we

presented evidence that identified three His residues that are donor ligands in the Zn(II) AdcR complex and essential for allosteric regulation. We also showed that XAS indicated the presence of two additional (N/O) ligands. A series of conserved Glu that are good candidates for donor ligand residues in the Zn(II) AdcR complex are listed in Chapter 3. The role of this residues could be defined in a straightforward way by characterizing single Ala substitution mutants and measurement of the Zn(II) binding affinities and coupling free energy of this AdcR variants. If an additional donor ligand is identified, would be expected that the binding affinity for Zn(II) and/or the coupling free energy will be attenuated.

It is hypothesized that unique pentacoordination of Zn(II) by AdcR endows AdcR to be activated by non cognate transition metals of similar ionic radii, *e.g.,* Mn(II) and Co(II) (see Appendix G) under conditions of extreme multiple metal stress. Indeed, at least a subset of Zn(II) metalloregulatory proteins can respond to Co(II) stress *in vivo*, although the physiological significance of this is unknown (refs: CzrA, SmtB). The importance of specific coordination properties in dictating metal specificity of metalloregulators finds a precedent early in the literature of this field. *E. coli* Fe(II) sensor Fur (ferric uptake regulator) was activated *in vivo* by Fe(II) and non cognate Mn(II) (*280-283*), and speculated that this was based on similar physical properties of charge, coordination preference and radii (*35*). Structural determination of the metal regulatory center of AdcR in complex with Zn(II), Co(II) and Mn(II) helps to illustrate this points. Preliminary NMR ^{15}N-HSQC studies conducted on AdcR in complex with non cognate Mn(II) (Guerra, A. and D.P. Giedroc, unpublished results) suggested that

significant chemical shift perturbations (resonance line broadening in this case) are localized to the metal binding site with the rest of the structure relatively unchanged. Interestingly this spectrum is similar to what it is observed in an allosterically non-activated apo-AdcR. These preliminary findings argue in favor of a mechanism of activation characterized in the Zn(II) CzrA sensor from the ArsR/SmtB family (*16*). ITC and NMR based experiments showed that an important contribution to the coupling free energy in CzrA came from dynamic stabilization of the native structure upon Zn(II) binding (*98, 109*). This suggests that the allosteric signal is propagated from the metal regulatory center to the effector domain, in this case the DNA recognition helix, by means of changes in the structure primarily at the level of dynamics, and is proposed that this model may be apply to other metal sensors as well (Chapter 1). It is hypothesized that apo-AdcR exists in a higher-energy state or ensemble with low DNA binding affinity that is stabilized by Zn(II), but also by Mn(II) or Co(II), into a conformational state that allows for high affinity DNA binding. The dynamic fingerprint of the allosterically competent AdcR state should be distinct to the dynamics observed in the allosterically impaired AdcR variants. This will allow us to deconvolute the relative importance of structural vs. dynamical changes in metal-dependent activation of DNA operator binding. In other systems this has been investigated using hydrogen/deuterium-exchange mass spectroscopy (DXMS) (*284*) as well as by detailed NMR and thermodynamic experiments (*109, 285*).

Structural futures found to be important in the metal center of NmtR also represent points of interest for further research. His3 in the N-terminal extension of

NmtR is a Ni(II) donor ligand; more importantly, this residue is essential for maintaining the ability of NmtR to discriminate against Zn(II) as well as enable Co(II)-dependent allosteric regulation. The structural basis of this observation is not known, but the coordination geometries adopted by Ni(II) and Zn(II) in this H3Q NmtR variant are likely different from that of the Co(II) complex. The results in NmtR are consistent with the idea that Co(II) and Ni(II) complexes are not iso-structural although their metal regulatory centers essentially colocalize. However, these differences may allow fine tuning of the metal specificity. This is similar to what is found in a member of the CsoR/RcnR family, the Ni(II) sensor RcnR in complex with Co(II) (*56*). We propose that sensitivity to small differences in coordination geometry, like the ones that could be between a Co(II) and Ni(II) center, are increased in the NmtR variant with a substitution of the N terminal H3 donor ligand. To test this idea high resolution structural information is again required that can differentiate between ligand donor number, bond distances and coordination geometry. Given the difficulties associated with paramagnetic centers, e.g., high-spin Co(II) and Ni(II), in NMR studies, this resolution is most easily achieved in crystallographic structures, which seems feasible since three other structures of the ArsR/SmtB family members, SmtB, CzrA and CadC, have been solved by this method (*111*). In addition, XAS experiments has provided of useful information to differentiate Ni(II) and Co(II) centers in other metal sensors (*56*).

We also provide no direct evidence for the presence of metal ligand donors in the C-terminal extension of NmtR (H109, D114 and H116), which is in direct contrast to a previous report (*33*). However, at least some part of the C-terminal region appears

necessary to bind two Ni(II) or Zn(II) per dimer and for allosteric activation by Ni(II), but in contrast is dispensable for allosteric activation and stoichiometric binding of Co(II). These results support the idea, discussed above, that the Co(II)-NmtR complex possesses features that distinguish it from the Ni(II) complex but more importantly suggests that the C-terminal extension stabilizes a dimeric NmtR-Ni_1 complex intermediate that is fully competent to bind a second Ni(II) or Zn(II) to the dimer. Structural, thermodynamic and biochemical data from studies of the negative homotropic cooperativity of Zn(II) binding to the Zn(II) sensor CzrA provides precedence for this; in this case, these studies reveal that structural changes that occur on binding the first Zn(II) are consistent with reorganization of the dimer interface, with in turn lowers the affinity of the second structurally identical site. An analogous situation may occur in NmtR, and in particular, the Δ111 NmtR mutant. Further structural studies are required to assess the role if any of the C-terminal tail in stabilizing the singly metal-ligated intermediate. Characterization of the intermediate NmtR-Ni_1 complex by NMR will reveal the structural changes relative to the apo and NmtR-Ni_2 complex that can be traced to the C-terminal tail.

REFERENCES

1. Berg, J. M., and Godwin, H. A. (1997) Lessons from zinc-binding peptides, *Annu. Rev. Biophys. Biomol. Struct. 26*, 357-371.

2. Seneque, O., Bonnet, E., Joumas, F. L., and Latour, J. M. (2009) Cooperative metal binding and helical folding in model peptides of treble-clef zinc fingers, *Chemistry-a European Journal 15*, 4798-4810.

3. Auld, D. S. (2001) Zinc coordination sphere in biochemical zinc sites, *Biometals 14*, 271-313.

4. Perry, J. J. P., Shin, D. S., Getzoff, E. D., and Tainer, J. A. (2010) The structural biochemistry of the superoxide dismutases, *BBA-Proteins Proteomics 1804*, 245-262.

5. Denkhaus, E., and Salnikow, K. (2002) Nickel essentiality, toxicity, and carcinogenicity, *Critical Reviews in Oncology/Hematology 42*, 35-56.

6. Davidson, T., Chen, H., Garrick, M. D., D'Angelo, G., and Costa, M. (2005) Soluble nickel interferes with cellular iron homeostasis, *Mol. Cell. Biochem. 279*, 157-162.

7. Chen, H., Davidson, T., Singleton, S., Garrick, M. D., and Costa, M. (2005) Nickel decreases cellular iron level and converts cytosolic aconitase to iron-regulatory protein 1 in A549 cells, *Toxicol. Appl. Pharmacol. 206*, 275-287.

8. Ermler, U., Grabarse, W., Shima, S., Goubeaud, M., and Thauer, R. K. (1998) Active sites of transition-metal enzymes with a focus on nickel, *Curr. Opin. Struct. Biol. 8*, 749-758.

9. Arredondo, M., and Nunez, M. T. (2005) Iron and copper metabolism, *Mol Aspects Med 26*, 313-327.

10. Singleton, C., and Le Brun, N. (2007) Atx1-like chaperones and their cognate P-type ATPases: copper-binding and transfer, *Biometals 20*, 275-289.

11. Hartwig, A. (2001) Zinc finger proteins as potential targets for toxic metal ions: differential effects on structure and function, *Antioxid. Redox Signal. 3*, 625-634.

12. Valko, M., Morris, H., and Cronin, M. T. (2005) Metals, toxicity and oxidative stress, *Curr. Med. Chem. 12*, 1161-1208.

13. Waldron, K. J., Rutherford, J. C., Ford, D., and Robinson, N. J. (2009) Metalloproteins and metal sensing, *Nature 460*, 823-830.

14. Ma, Z., Jacobsen, F. E., and Giedroc, D. P. (2009) Coordination chemistry of bacterial metal transport and sensing, *Chemical Reviews 109*, 4644-4681.

15. Giedroc, D. P., and Arunkumar, A. I. (2007) Metal sensor proteins: Nature's metalloregulated allosteric switches, *Dalton Trans. 7*, 3107-3120.

16. Busenlehner, L. S., Pennella, M. A., and Giedroc, D. P. (2003) The SmtB/ArsR family of metalloregulatory transcriptional repressors: Structural insights into prokaryotic metal resistance, *FEMS Microbiol. Rev. 27*, 131-143.

17. Reyes-Caballero, H., Guerra, A. J., Jacobsen, F. E., Kazmierczak, K. M., Cowart, D., Koppolu, U. M. K., Scott, R. A., Winkler, M. E., and Giedroc, D. P. (2010) The metalloregulatory zinc site in streptococcus pneumoniae Adcr, a zinc-activated MarR family repressor, *J. Mol. Biol. 403*, 197-216.

18. Chen, H., Wu, R., Xu, G., Fang, X., Qiu, X., Guo, H., Tian, B., and Hua, Y. (2010) DR2539 is a novel DtxR-like regulator of Mn/Fe ion homeostasis and antioxidant enzyme in Deinococcus radiodurans, *Biochem. Biophys. Res. Commun. 396*, 413-418.

19. Ernst, F. D., Kuipers, E. J., Heijens, A., Sarwari, R., Stoof, J., Penn, C. W., Kusters, J. G., and van Vliet, A. H. M. (2005) The nickel-responsive regulator NikR controls activation and repression of gene transcription in Helicobacter pylori, *Infect. Immun. 73*, 7252-7258.

20. Danielli, A., and Scarlato, V. (2010) Regulatory circuits in Helicobacter pylori : network motifs and regulators involved in metal-dependent responses, *FEMS Microbiol. Rev. 34*, 738-752.

21. Danielli, A., Roncarati, D., Delany, I., Chiarini, V., Rappuoli, R., and Scarlato, V. (2006) In vivo dissection of the Helicobacter pylori Fur regulatory circuit by genome-wide location analysis, *J. Bacteriol. 188*, 4654-4662.

22. Wang, S. N., Wu, Y., and Outten, F. W. (2011) Fur and the novel regulator yqji control transcription of the ferric reductase gene yqjh in Escherichia coli, *J. Bacteriol. 193*, 563-574.

23. Ahn, B.-E., Cha, J., Lee, E.-J., Han, A.-R., Thompson, C. J., and Roe, J.-H. (2006) Nur, a nickel-responsive regulator of the Fur family, regulates superoxide dismutases and nickel transport in Streptomyces coelicolor, *Mol. Microbiol. 59*, 1848-1858.

24. Puri, S., Hohle, T. H., and O'Brian, M. R. (2010) Control of bacterial iron homeostasis by manganese, *Proceedings of the National Academy of Sciences 107*, 10691-10695.

25. Jacobsen, F. E., Kazmierczak, K. M., Lisher, J. P., Winkler, M. E., and Giedroc, D. P. (2011) Interplay between manganese and zinc homeostasis in the human pathogen Streptococcus pneumoniae, *Metallomics 3*, 38-41.

26. Kloosterman, T. G., Witwicki, R., Pol, M., Bijlsma, J., and Kuipers, E. (2008) Opposite effects of Mn2+ and Zn2+ on the PsaR-mediated expression of the virulence genes pcpA, prtA and psaB(CA) of Streptococcus pneumoniae., *Mol. Microbiol.*

27. Ward, S. K., Abomoelak, B., Hoye, E. A., Steinberg, H., and Talaat, A. M. (2010) CtpV: a putative copper exporter required for full virulence of Mycobacterium tuberculosis, *Mol. Microbiol. 77*, 1096-1110.

28. Wolschendorf, F., Ackart, D., Shrestha, T. B., Hascall-Dove, L., Nolan, S., Lamichhane, G., Wang, Y., Bossmann, S. H., Basaraba, R. J., and Niederweis, M. (2011) Copper resistance is essential for virulence of Mycobacterium tuberculosis, *Proc. Natl. Acad. Sci. U. S. A. 108*, 1621-1626.

29. Outten, C. E., and O'Halloran, T. V. (2001) Femtomolar sensitivity of metalloregulatory proteins controlling zinc homeostasis, *Science 292*, 2488-2492.

30. Deuschle, U., Gentz, R., and Bujard, H. (1986) lac repressor blocks transcribing RNA polymerase and terminates transcription, *Proceedings of the National Academy of Sciences 83*, 4134-4137.

31. Gilbert, W., and Maxam, A. (1973) The nucleotide sequence of the lac operator, *Proceedings of the National Academy of Sciences 70*, 3581-3584.

32. Majors, J. (1975) Initiation of in vitro mRNA synthesis from the wild-type lac promoter, *Proceedings of the National Academy of Sciences 72*, 4394-4398.

33. Cavet, J. S., Meng, W., Pennella, M. A., Appelhoff, R. J., Giedroc, D. P., and Robinson, N. J. (2002) A nickel-cobalt-sensing ArsR-SmtB family repressor. Contributions of cytosol and effector binding sites to metal selectivity, *J. Biol. Chem. 277*, 38441-38448.

34. Chauhan, S., Kumar, A., Singhal, A., Tyagi, J. S., and Krishna Prasad, H. (2009) CmtR, a cadmium-sensing ArsR–SmtB repressor, cooperatively interacts with multiple operator sites to autorepress its transcription in Mycobacterium tuberculosis, *FEBS J. 276*, 3428-3439.

35. Bagg, A., and Neilands, J. B. (1987) Ferric uptake regulation protein acts as a repressor, employing iron(II) as a cofactor to bind the operator of an iron transport operon in Escherichia coli., *Biochemistry 26*, 5471-5477.

36. Hobman, J., Wilkie, J., and Brown, N. (2005) A design for life: prokaryotic metal-binding MerR family regulators, *Biometals 18*, 429 - 436.

37. O'Halloran, T. V., Frantz, B., Shin, M. K., Ralston, D. M., and Wright, J. G. (1989) The MerR heavy metal receptor mediates positive activation in a topologically novel transcription complex, *Cell 56*, 119-129.

38. Lee, P. E., Demple, B., and Barton, J. K. (2009) DNA-mediated redox signaling for transcriptional activation of SoxR, *Proceedings of the National Academy of Sciences 106*, 13164-13168.

39. Williams, R. J. P. (1982) Free manganese(II) and iron(II) cations can act as intracellular cell controls, *FEBS Lett. 140*, 3-10.

40. Waldron, K. J., and Robinson, N. J. (2009) How do bacterial cells ensure that metalloproteins get the correct metal?, *Nat Rev Micro 7*, 25-35.

41. Williams, R. J. P., and da Silva, J. (2000) The distribution of elements in cells, *Coord. Chem. Rev. 200*, 247-348.

42. Jin-Won, L., and John, D. H. (2007) Functional specialization within the Fur family of metalloregulators, *Biometals 20,* 485-499.

43. Patzer, S. I., and Hantke, K. (1998) The ZnuABC high-affinity zinc uptake system and its regulator Zur in Escherichia coli, *Molecular Microbiology 28*, 1199-1210.

44. Outten, C. E., Outten, F. W., and O'Halloran, T. V. (1999) DNA distortion mechanism for transcriptional activation by ZntR, a Zn(II)-responsive MerR homologue in Escherichia coli, *J. Biol. Chem. 274*, 37517-37524.

45. Pennella, M. A., Arunkumar, A. I., and Giedroc, D. P. (2006) Individual metal ligands play distinct functional roles in the zinc sensor Staphylococcus aureus CzrA, *J Mol Biol 356*, 1124-1136.

46. VanZile, M. L., Chen, X., and Giedroc, D. P. (2002) Structural characterization of distinct alpha3N and alpha5 metal sites in the cyanobacterial zinc sensor SmtB, *Biochemistry 41*, 9765-9775.

47. Liu, T., Golden, J. W., and Giedroc, D. P. (2005) A zinc(II)/lead(II)/cadmium(II)-inducible operon from the Cyanobacterium anabaena is regulated by AztR, an alpha3N ArsR/SmtB metalloregulator, *Biochemistry 44*, 8673-8683.

48. Liu, T., Chen, X. H., Ma, Z., Shokes, J., Hemmingsen, L., Scott, R. A., and Giedroc, D. P. (2008) A Cu-I-sensing ArsR family metal sensor protein with a relaxed metal selectivity profile, *Biochemistry 47*, 10564-10575.

49. Changela, A., Chen, K., Xue, Y., Holschen, J., Outten, C. E., O'Halloran, T. V., and Mondragon, A. (2003) Molecular basis of metal-ion selectivity and zeptomolar sensitivity by CueR, *Science 301*, 1383-1387.

50. Jian, X., Wasinger, E. C., Lockard, J. V., Chen, L. X., and He, C. (2009) Highly sensitive and selective Gold(I) recognition by a metalloregulator in Ralstonia metallidurans, *J. Am. Chem. Soc. 131*, 10869-10871.

51. Ma, Z., Cowart, D. M., Scott, R. A., and Giedroc, D. P. (2009) Molecular insights into the metal selectivity of the Copper(I)-sensing repressor Csor from Bacillus subtilis, *Biochemistry 48*, 3325-3334.

52. Ma, Z., Cowart, D. M., Ward, B. P., Arnold, R. J., DiMarchi, R. D., Zhang, L., George, G. N., Scott, R. A., and Giedroc, D. P. (2009) Unnatural amino acid substitution as a probe of the allosteric coupling pathway in a mycobacterial Cu(I) sensor, *Journal of the American Chemical Society 131*, 18044-18045.

53. Grossoehme, N., Kehl-Fie, T. E., Ma, Z., Adams, K. W., Cowart, D. M., Scott, R. A., Skaar, E. P., and Giedroc, D. P. (2011) Control of copper resistance and inorganic sulfur metabolism by paralogous regulators in Staphylococcus aureus, *J. Biol. Chem. 286*, 13522-13531.

54. Wang, S. C., Dias, A. V., Bloom, S. L., and Zamble, D. B. (2004) Selectivity of metal binding and metal-induced stability of Escherichia coli NikR, *Biochemistry 43*, 10018-10028.

55. Li, Y. J., and Zamble, D. B. (2009) pH-Responsive DNA-binding activity of Helicobacter pylori NikR, *Biochemistry 48*, 2486-2496.

56. Iwig, J. S., Leitch, S., Herbst, R. W., Maroney, M. J., and Chivers, P. T. (2008) Ni(II) and Co(II) sensing by Escherichia coli RcnR, *J. Am. Chem. Soc. 130*, 7592-7606.

57. Mills, S. A., and Marletta, M. A. (2005) Metal binding characteristics and role of iron oxidation in the ferric uptake regulator from Escherichia coli, *Biochemistry 44*, 13553-13559.

58. Golynskiy, M. V., Gunderson, W. A., Hendrich, M. P., and Cohen, S. M. (2006) Metal binding studies and EPR spectroscopy of the manganese transport regulator MntR, *Biochemistry 45*, 15359-15372.

59. Sen, K. I., Sienkiewicz, A., Love, J. F., vanderSpek, J. C., Fajer, P. G., and Logan, T. M. (2006) Mn(II) binding by the anthracis repressor from Bacillus anthracis, *Biochemistry 45*, 4295-4303.

60. Dittmer, P. J., Miranda, J. G., Gorski, J. A., and Palmer, A. E. (2009) Genetically encoded sensors to elucidate spatial distribution of cellular zinc, *J. Biol. Chem. 284*, 16289-16297.

61. Irving, H., and Williams, R. J. P. (1948) Order of stability of metal complexes, *Nature 162*, 746-747.

62. Panina, E. M., Mironov, A. A., and Gelfand, M. S. (2003) Comparative genomics of bacterial zinc regulons: Enhanced ion transport, pathogenesis, and rearrangement of ribosomal proteins, *Proc. Natl. Acad. Sci. U. S. A. 100*, 9912-9917.

63. Gabriel, S. E., and Helmann, J. D. (2009) Contributions of Zur-controlled ribosomal proteins to growth under zinc starvation conditions, *J. Bacteriol. 191*, 6116-6122.

64. Nanamiya, H., and Kawamura, F. (2010) Towards an elucidation of the roles of the ribosome during different growth phases in Bacillus subtilis, *Biosci. Biotechnol. Biochem. 74*, 451-461.

65. Robinson, N. J., and Winge, D. R. (2010) Copper metallochaperones, *Annu. Rev. Biochem. 79*, 537-562.

66. Dainty, S. J., Patterson, C. J., Waldron, K. J., and Robinson, N. J. (2009) Interaction between cyanobacterial copper chaperone Atx1 and zinc homeostasis, *J Biol Inorg Chem 15*, 77-85.

67. Chivers, P. T., and Sauer, R. T. (2002) NikR repressor: High-affinity nickel binding to the C-terminal domain regulates binding to operator DNA, *Chem. Biol. 9*, 1141-1148.

68. Schreiter, E. R., Sintchak, M. D., Guo, Y., Chivers, P. T., Sauer, R. T., and Drennan, C. L. (2003) Crystal structure of the nickel-responsive transcription factor NikR, *Nat. Struct. Mol. Biol. 10*, 794-799.

69. De Pina, K., Desjardin, V., Mandrand-Berthelot, M.-A., Giordano, G., and Wu, L.-F. (1999) Isolation and characterization of the nikr gene encoding a nickel-responsive regulator in Escherichia coli, *J. Bacteriol. 181*, 670-674.

70. Dosanjh, N. S., and Michel, S. L. J. (2006) Microbial nickel metalloregulation: NikRs for nickel ions, *Curr. Opin. Chem. Biol. 10*, 123-130.

71. Iwig, J. S., Rowe, J. L., and Chivers, P. T. (2006) Nickel homeostasis in Escherichia coli - the rcnR-rcnA efflux pathway and its linkage to NikR function, *Mol. Microbiol. 62*, 252-262.

72. Wang, S. C., Dias, A. V., and Zamble, D. B. (2009) The "metallo-specific" response of proteins: A perspective based on the Escherichia coli transcriptional regulator NikR, *Dalton Trans.*, 2459-2466.

73. Wang, S. C., Li, Y., Ho, M., Bernal, M.-E., Sydor, A. M., Kagzi, W. R., and Zamble, D. B. (2010) The response of Escherichia coli NikR to nickel: A second nickel-binding site, *Biochemistry 49*, 6635-6645.

74. Iwig, J. S., and Chivers, P. T. (2010) Coordinating intracellular nickel-metal-site structure-function relationships and the NikR and RcnR repressors, *Nat. Prod. Rep. 27*, 658-667.

75. Osman, D., and Cavet, J. S. (2010) Bacterial metal-sensing proteins exemplified by ArsR-SmtB family repressors, *Nat. Prod. Rep. 27*, 668-680.

76. Campbell, D. R., Chapman, K. E., Waldron, K. J., Tottey, S., Kendall, S., Cavallaro, G., Andreini, C., Hinds, J., Stoker, N. G., Robinson, N. J., and Cavet, J. S. (2007) Mycobacterial cells have dual nickel-cobalt sensors, *J. Biol. Chem. 282*, 32298-32310.

77. Shin, J.-H., Oh, S.-Y., Kim, S.-J., and Roe, J.-H. (2007) The zinc-responsive regulator Zur controls a zinc uptake system and some ribosomal proteins in Streptomyces coelicolor A3(2), *J. Bacteriol. 189*, 4070-4077.

78. Shin, J.-H., Jung, H. J., An, Y. J., Cho, Y.-B., Cha, S.-S., and Roe, J.-H. (2011) Graded expression of zinc-responsive genes through two regulatory zinc-binding sites in Zur, *Proceedings of the National Academy of Sciences 108*, 5045-5050.

79. Wilkinson, S. P., and Grove, A. (2006) Ligand-responsive transcriptional regulation by members of the MarR family of winged helix proteins, *Curr Issues Mol Biol 8*, 51-62.

80. Kloosterman, T. G., van der Kooi-Pol, M. M., Bijlsma, J. J., and Kuipers, O. P. (2007) The novel transcriptional regulator SczA mediates protection against Zn2+ stress by activation of the Zn2+-resistance gene czcD in Streptococcus pneumoniae, *Molecular microbiology 65*, 1049-1063.

81. Pearson, R. G. (1968) Hard and soft acids and bases, HSAB, part 1: Fundamental principles, *J. Chem. Educ. 45*, 581.

82. Pearson, R. G. (1963) Hard and soft acids and bases, *J. Am. Chem. Soc. 85*, 3533-3539.

83. Schmitt, M. P. (2002) Analysis of a DtxR-like metalloregulatory protein, MntR, from Corynebacterium diphtheriae that controls expression of an ABC metal transporter by an Mn2+-dependent mechanism, *J. Bacteriol. 184*, 6882-6892.

84. Que, Q., and Helmann, J. D. (2000) Manganese homeostasis in Bacillus subtilis is regulated by MntR, a bifunctional regulator related to the diphtheria toxin repressor family of proteins, *Mol. Microbiol. 35*, 1454-1468.

85. Glasfeld, A., Guedon, E., Helmann, J. D., and Brennan, R. G. (2003) Structure of the manganese-bound manganese transport regulator of Bacillus subtilis, *Nat. Struct. Biol. 10*, 652-657.

86. Lieser, S. A., Davis, T. C., Helmann, J. D., and Cohen, S. M. (2003) DNA-binding and oligomerization studies of the manganese(II) metalloregulatory protein MntR from Bacillus subtilis, *Biochemistry 42*, 12634-12642.

87. Golynskiy, M. V., Davis, T. C., Helmann, J. D., and Cohen, S. M. (2005) Metal-induced structural organization and stabilization of the metalloregulatory protein MntR, *Biochemistry 44*, 3380-3389.

88. Stoll, K. E., Draper, W. E., Kliegman, J. I., Golynskiy, M. V., Brew-Appiah, R. A. T., Phillips, R. K., Brown, H. K., Breyer, W. A., Jakubovics, N. S., Jenkinson, H. F., Brennan, R. G., Cohen, S. M., and Glasfeld, A. (2009) Characterization and structure of the manganese-responsive transcriptional regulator ScaR, *Biochemistry 48*, 10308-10320.

89. VanZile, M. L., Cosper, N. J., Scott, R. A., and Giedroc, D. P. (2000) The zinc metalloregulatory protein Synechococcus PCC7942 SmtB binds a single zinc ion per monomer with high affinity in a tetrahedral coordination geometry, *Biochemistry 39*, 11818-11829.

90. Liu, T., Ramesh, A., Ma, Z., Ward, S. K., Zhang, L. M., George, G. N., Talaat, A. M., Sacchettini, J. C., and Giedroc, D. P. (2007) CsoR is a novel Mycobacterium tuberculosis copper-sensing transcriptional regulator, *Nat. Chem. Biol. 3*, 60-68.

91. Chen, K., Yuldasheva, S., Penner-Hahn, J. E., and O'Halloran, T. V. (2003) An atypical linear Cu(I)-S2 center constitutes the high-affinity metal-sensing site in the CueR metalloregulatory protein, *J. Am. Chem. Soc. 125*, 12088-12089.

92. An, Y. J., Ahn, B. E., Han, A. R., Kim, H. M., Chung, K. M., Shin, J. H., Cho, Y. B., Roe, J. H., and Cha, S. S. (2009) Structural basis for the specialization of Nur, a nickel-specific Fur homolog, in metal sensing and DNA recognition, *Nucleic Acids Res. 37*, 3442-3451.

93. Phillips, C. M., Schreiter, E. R., Guo, Y., Wang, S. C., Zamble, D. B., and Drennan, C. L. (2008) Structural basis of the metal specificity for nickel regulatory protein NikR, *Biochemistry 47*, 1938-1946.

94. Busenlehner, L. S., Weng, T. C., Penner-Hahn, J. E., and Giedroc, D. P. (2002) Elucidation of primary (alpha N-3) and vestigial (alpha(5)) heavy metal-binding sites in Staphylococcus aureus pI258 CadC: Evolutionary implications for metal ion selectivity of ArsR/SmtB metal sensor proteins, *J. Mol. Biol. 319*, 685-701.

95. Wang, Y., Hemmingsen, L., and Giedroc, D. P. (2005) Structural and functional characterization of Mycobacterium tuberculosis CmtR, a PbII/CdII-sensing SmtB/ArsR metalloregulatory repressor, *Biochemistry 44*, 8976-8988.

96. Guedon, E., and Helmann, J. D. (2003) Origins of metal ion selectivity in the DtxR/MntR family of metalloregulators, *Mol. Microbiol. 48*, 495-506.

97. Kliegman, J. I., Griner, S. L., Helmann, J. D., Brennan, R. G., and Glasfeld, A. (2006) Structural basis for the metal-selective activation of the manganese transport regulator of Bacillus subtilis, *Biochemistry 45*, 3493-3505.

98. Grossoehme, N. E., and Giedroc, D. P. (2009) Energetics of allosteric negative coupling in the zinc sensor S. aureus CzrA, *J. Am. Chem. Soc. 131*, 17860-17870.

99. Pennella, M. A., Shokes, J. E., Cosper, N. J., Scott, R. A., and Giedroc, D. P. (2003) Structural elements of metal selectivity in metal sensor proteins, *Proc. Natl. Acad. Sci. U. S. A. 100*, 3713-3718.

100. Maret, W., and Li, Y. (2009) Coordination dynamics of zinc in proteins, *Chemical Reviews 109*, 4682-4707.

101. Patel, K., Kumar, A., and Durani, S. (2007) Analysis of the structural consensus of the zinc coordination centers of metalloprotein structures, *Biochimica et Biophysica Acta (BBA) - Proteins & Proteomics 1774*, 1247-1253.

102. Dudev, T., and Lim, C. (2003) Principles governing Mg, Ca, and Zn binding and selectivity in proteins, *Chemical Reviews 103*, 773-787.

103. Kuppuraj, G., Dudev, M., and Lim, C. (2009) Factors governing metal-ligand distances and coordination geometries of metal complexes, *The Journal of Physical Chemistry B 113*, 2952-2960.

104. Leitch, S., Bradley, M. J., Rowe, J. L., Chivers, P. T., and Maroney, M. J. (2007) Nickel-specific response in the transcriptional regulator, Escherichia coli NikR, *J. Am. Chem. Soc. 129*, 5085-5095.

105. Bloom, S. L., and Zamble, D. B. (2004) Metal-selective DNA-binding response of Escherichia coli NikR, *Biochemistry 43*, 10029-10038.

106. Ahmad, R., Brandsdal, B. O., Michaud-Soret, I., and Willassen, N. P. (2009) Ferric uptake regulator protein: Binding free energy calculations and per-residue free energy decomposition, *Proteins: Struct., Funct., Bioinf. 75*, 373-386.

107. DeLano, W. L., Lam, J.W. (2005) PyMol: A communications tool for computational models, *Abtracts of Papers of the American Chemichal Society 230*, U1371-U1372.

108. Lucarelli, D., Russo, S., Garman, E., Milano, A., Meyer-Klaucke, W., and Pohl, E. (2007) Crystal structure and function of the zinc uptake regulator FurB from Mycobacterium tuberculosis, *J. Biol. Chem. 282*, 9914-9922.

109. Arunkumar, A. I., Campanello, G. C., and Giedroc, D. P. (2009) Solution structure of a paradigm ArsR family zinc sensor in the DNA-bound state, *Proc. Natl. Acad. Sci. U. S. A. 106*, 18177-18182.

110. Schreiter, E. R., Wang, S. C., Zamble, D. B., and Drennan, C. L. (2006) NikR-operator complex structure and the mechanism of repressor activation by metal ions, *PNAS 103*, 13676-13681.

111. Eicken, C., Pennella, M. A., Chen, X., Koshlap, K. M., VanZile, M. L., Sacchettini, J. C., and Giedroc, D. P. (2003) A metal-ligand-mediated intersubunit allosteric switch in related SmtB/ArsR zinc sensor proteins, *J. Mol. Biol. 333*, 683-695.

112. Arunkumar, A. I., Pennella, M. A., Kong, X. M., and Giedroc, D. P. (2007) Resonance assignments of the metal sensor CzrA in the apo-, Zn-2- and DNA-bound (42 kDa) states, *Biomolecular Nmr Assignments 1*, 99-101.

113. Chakrabarti, P. (1990) Geometry of interaction of metal-ions with histidine-residues in protein structures, *Protein Eng. 4*, 57-63.

114. Alberts, I. L., Nadassy, K., and Wodak, S. J. (1998) Analysis of zinc binding sites in protein crystal structures, *Protein Sci. 7*, 1700-1716.

115. Bhattacharyya, R., Saha, R. P., Samanta, U., and Chakrabarti, P. (2003) Geometry of interaction of the histidine ring with other planar and basic residues, *J. Proteome Res. 2*, 255-263.

116. Jacquamet, L., Traore, D. A. K., Ferrer, J. L., Proux, O., Testemale, D., Hazemann, J. L., Nazarenko, E., El Ghazouani, A., Caux-Thang, C., Duarte, V., and Latour, J. M. (2009) Structural characterization of the active form of PerR: insights into the metal-induced activation of PerR and Fur proteins for DNA binding, *Mol. Microbiol. 73*, 20-31.

117. Lee, J.-W., and Helmann, J. D. (2006) The PerR transcription factor senses H2O2 by metal-catalysed histidine oxidation, *Nature 440*, 363-367.

118. Traoré, D. A. K., El Ghazouani, A., Ilango, S., Dupuy, J., Jacquamet, L., Ferrer, J. L., Caux-Thang, C., Duarte, V., and Latour, J. M. (2006) Crystal structure of the apo-PerR-Zn protein from Bacillus subtilis, *Mol. Microbiol. 61*, 1211-1219.

119. Traore, D. A. K., Ghazouani, A. E., Jacquamet, L., Borel, F., Ferrer, J.-L., Lascoux, D., Ravanat, J.-L., Jaquinod, M., Blondin, G., Caux-Thang, C., Duarte, V., and Latour, J.-M. (2009) Structural and functional characterization of 2-oxo-histidine in oxidized PerR protein, *Nat. Chem. Biol. 5*, 53-59.

120. Won, Y. B., Ji, C. J., Cho, J. H., and Lee, J. W. (2010) Mutational analysis of the metal-binding sites of peroxide sensor PerR, *Bull. Korean Chem. Soc. 31*, 1573-1576.

121. Giedroc, D. P. (2009) Hydrogen peroxide sensing in Bacillus subtilis: it is all about the (metallo)regulator, *Mol. Microbiol. 73*, 1-4.

122. Lee, J. W., and Helmann, J. D. (2007) Functional specialization within the Fur family of metalloregulators, *Biometals 20*, 485-499.

123. Lucarelli, D., Vasil, M. L., Meyer-Klaucke, W., and Pohl, E. (2008) The metal-dependent regulators FurA and FurB from Mycobacterium tuberculosis, *International Journal of Molecular Sciences 9*, 1548-1560.

124. Pohl, E., Haller, J. C., Mijovilovich, A., Meyer-Klaucke, W., Garman, E., and Vasil, M. L. (2003) Architecture of a protein central to iron homeostasis: crystal structure and spectroscopic analysis of the ferric uptake regulator, *Mol. Microbiol. 47*, 903-915.

125. Sheikh, A., and Taylor, G. L. (2009) Crystal structure of the Vibrio cholerae ferric uptake regulator (Fur) reveals insights into metal co-ordination, *Mol. Microbiol. 72*, 1208-1220.

126. Dian, C., Vitale, S., Leonard, G. A., Bahlawane, C., Fauquant, C., Leduc, D., Muller, C., de Reuse, H., Michaud-Soret, I., and Terradot, L. (2011) The structure of the Helicobacter pylori ferric uptake regulator Fur reveals three functional metal binding sites, *Mol. Microbiol. 79*, 1260-1275.

127. Liu, Q., Wang, P. B., Ma, Y., and Zhang, Y. X. (2007) Characterization of the Vibrio alginolyticus fur gene and localization of essential amino acid sites in Fur by site-directed mutagenesis, *J. Mol. Microbiol. Biotechnol. 13*, 15-21.

128. Lewin, A. C., Doughty, P. A., Flegg, L., Moore, G. R., and Spiro, S. (2002) The ferric uptake regulator of Pseudomonas aeruginosa has no essential cysteine residues and does not contain a structural zinc ion, *Microbiology 148*, 2449-2456.

129. Bsat, N., and Helmann, J. D. (1999) Interaction of Bacillus subtilis Fur (ferric uptake repressor) with the dhb operator in vitro and in vivo, *J. Bacteriol. 181*, 4299-4307.

130. Tsai, C.-J., del Sol, A., and Nussinov, R. (2008) Allostery: Absence of a change in shape does not imply that allostery is not at play, *J. Mol. Biol. 378*, 1-11.

131. Popovych, N., Sun, S., Ebright, R. H., and Kalodimos, C. G. (2006) Dynamically driven protein allostery, *Nat. Struct. Mol. Biol. 13*, 831-838.

132. Kern, D., and Zuiderweg, E. R. P. (2003) The role of dynamics in allosteric regulation, *Curr. Opin. Struct. Biol. 13*, 748-757.

133. Zotin, A. I. (1972) Thermodynamic aspects of developmental biology, *Monographs dev. Biol. 5*, 1-159.

134. Reinhart, G. D. (2004) Quantitative analysis and interpretation of allosteric behavior, in *Energetics of Biological Macromolecules, Pt E*, pp 187-203, Academic Press Inc, San Diego.

135. Lee, S., Arunkumar, A. I., Chen, X., and Giedroc, D. P. (2006) Structural insights into homo- and heterotropic allosteric coupling in the zinc sensor *S. aureus* CzrA from covalently fused dimers, *J. Am. Chem. Soc. 128*, 1937-1947.

136. Fenton, A. W. (2008) Allostery: an illustrated definition for the 'second secret of life', *Trends Biochem. Sci. 33*, 420-425.

137. Hilser, V. J., and Thompson, E. B. (2007) Intrinsic disorder as a mechanism to optimize allosteric coupling in proteins, *Proceedings of the National Academy of Sciences 104*, 8311-8315.

138. Sen, K. I., Logan, T. M., and Fajer, P. G. (2007) Protein dynamics and monomer-monomer interactions in AntR activation by electron paramagnetic resonance and double electron-electron resonance, *Biochemistry 46*, 11639-11649.

139. Golynskiy, M. V., Sheng, L., Virgil, L. W., and Seth, M. C. (2007) Conformational studies of the manganese transport regulator (MntR) from Bacillus subtilis using deuterium exchange mass spectrometry, *Journal of Biological Inorganic Chemistry*. *12*, 699-709.

140. Delany, I., Spohn, G., Rappuoli, R., and Scarlato, V. (2001) The Fur repressor controls transcription of iron-activated and -repressed genes in Helicobacter pylori, *Mol. Microbiol. 42*, 1297-1309.

141. Delany, I., Pacheco, A. B. F., Spohn, G., Rappuoli, R., and Scarlato, V. (2001) Iron-dependent transcription of the frpB gene of Helicobacter pylori is controlled by the Fur repressor protein, *The Journal of Bacteriology 183*, 4932-4937.

142. Harris, A. G., Hinds, F. E., Beckhouse, A. G., Kolesnikow, T., and Hazell, S. L. (2002) Resistance to hydrogen peroxide in Helicobacter pylori: role of catalase (KatA) and Fur, and functional analysis of a novel gene product designated 'KatA-associated protein', KapA (HP0874), *Microbiology 148*, 3813-3825.

143. Ernst, F. D., Bereswill, S., Waidner, B., Stoof, J., Mader, U., Kusters, J. G., Kuipers, E. J., Kist, M., van Vliet, A. H. M., and Homuth, G. (2005) Transcriptional profiling of Helicobacter pylori Fur- and iron-regulated gene expression, *Microbiology 151*, 533-546.

144. Ernst, F. D., Homuth, G., Stoof, J., Mader, U., Waidner, B., Kuipers, E. J., Kist, M., Kusters, J. G., Bereswill, S., and van Vliet, A. H. M. (2005) Iron-responsive regulation of the Helicobacter pylori iron-cofactored superoxide dismutase SodB is mediated by Fur, *J. Bacteriol. 187*, 3687-3692.

145. Vitale, S., Fauquant, C., Lascoux, D., Schauer, K., Saint-Pierre, C., and Michaud-Soret, I. (2009) A ZnS4 structural zinc site in the Helicobacter pylori ferric uptake regulator, *Biochemistry 48*, 5582-5591.

146. Carpenter, B. M., Gancz, H., Benoit, S. L., Evans, S., Olsen, C. H., Michel, S. L. J., Maier, R. J., and Merrell, D. S. (2010) Mutagenesis of conserved amino acids of Helicobacter pylori Fur reveals residues important for function, *J. Bacteriol. 192*, 5037-5052.

147. D'Autreaux, B., Pecqueur, L., de Peredo, A. G., Diederix, R. E. M., Caux-Thang, C., Tabet, L., Bersch, B., Forest, E., and Michaud-Soret, I. (2007) Reversible redox- and zinc-dependent dimerization of the Escherichia coli Fur protein, *Biochemistry 46*, 1329-1342.

148. Tao, X., Zeng, H. Y., and Murphy, J. R. (1995) Transition metal ion activation of DNA binding by the diphtheria tox repressor requires the formation of stable homodimers, *Proc. Natl. Acad. Sci. U. S. A. 92*, 6803-6807.

149. Spiering, M. M., Ringe, D., Murphy, J. R., and Marletta, M. A. (2003) Metal stoichiometry and functional studies of the diphtheria toxin repressor, *Proc. Natl. Acad. Sci. U. S. A. 100*, 3808-3813.

150. Love, J. F., vanderSpek, J. C., Marin, V., Guerrero, L., Logan, T. M., and Murphy, J. R. (2004) Genetic and biophysical studies of diphtheria toxin repressor (DtxR) and the hyperactive mutant DtxR(E175K) support a multistep model of activation, *Proc. Natl. Acad. Sci. U. S. A. 101*, 2506-2511.

151. D'Aquino, J. A., Tetenbaum-Novatt, J., White, A., Berkovitch, F., and Ringe, D. (2005) Mechanism of metal ion activation of the diphtheria toxin repressor DtxR, *Proc. Natl. Acad. Sci. U. S. A. 102*, 18408-18413.

152. Kandegedara, A., Thiyagarajan, S., Kondapalli, K. C., Stemmler, T. L., and Rosen, B. P. (2009) Role of bound Zn(II) in the CadC Cd(II)/Pb(II)/Zn(II)-responsive repressor, *J. Biol. Chem. 284*, 14958-14965.

153. Phillips, C. M., Schreiter, E. R., Stultz, C. M., and Drennan, C. L. (2010) Structural basis of low-affinity nickel binding to the nickel-responsive transcription factor NikR from Escherichia coli, *Biochemistry 49*, 7830-7838.

154. Tanaka, T., Shinkai, A., Bessho, Y., Kumarevel, T., and Yokoyama, S. (2009) Crystal structure of the manganese transport regulatory protein from Escherichia coli, *Proteins: Struct., Funct., Bioinf. 77*, 741-746.

155. Wisedchaisri, G., Chou, C. J., Wu, M. T., Roach, C., Rice, A. E., Holmes, R. K., Beeson, C., and Hol, W. G. J. (2007) Crystal structures, metal activation, and DNA-binding properties of two-domain IdeR from Mycobacterium tuberculosis, *Biochemistry 46*, 436-447.

156. Canneva, F., Branzoni, M., Riccardi, G., Provvedi, R., and Milano, A. (2005) Rv2358 and FurB: Two transcriptional regulators from Mycobacterium tuberculosis which respond to zinc, *J. Bacteriol. 187*, 5837-5840.

157. Cavet, J. S., Graham, A. I., Meng, W. M., and Robinson, N. J. (2003) A cadmium-lead-sensing ArsR-SmtB repressor with novel sensory sites - Complementary metal discrimination by NMTR and CMTR in a common cytosol, *J. Biol. Chem. 278*, 44560-44566.

158. Cole, S. T., Brosch, R., Parkhill, J., Garnier, T., Churcher, C., Harris, D., Gordon, S. V., Eiglmeier, K., Gas, S., Barry, C. E., III, Tekaia, F., Badcock, K., Basham, D., Brown, D., Chillingworth, T., Connor, R., Davies, R., Devlin, K., Feltwell,

T., Gentles, S., Hamlin, N., Holroyd, S., Hornsby, T., Jagels, K., Krogh, A., McLean, J., Moule, S., Murphy, L., Oliver, K., Osborne, J., Quail, M. A., Rajandream, M. A., Rogers, J., Rutter, S., Seeger, K., Skelton, J., Squares, R., Squares, S., Sulston, J. E., Taylor, K., Whitehead, S., and Barrell, B. G. (1998) Deciphering the biology of Mycobacterium tuberculosis from the complete genome sequence, *Nature 393*, 537-544.

159. Agranoff, D., and Krishna, S. (2004) Metal ion transport and regulation in mycobacterium tuberculosis, *Front. Biosci. 9*, 2996-3006.

160. Brosch, R., Gordon, S. V., Eiglmeier, K., Garnier, T., Tekaia, F., Yeramian, E., and Cole, S. T. (2000) Genomics, biology, and evolution of the Mycobacterium tuberculosis complex, in *Molecular Genetics of Mycobacteria* (Hatfull, G. F., and Jacobs Jr, W. R., Eds.), pp 19-36, ASM Press, Washingron, D.C.

161. Weinberg, E. D. (2009) Iron availability and infection, *Biochimica Et Biophysica Acta-General Subjects 1790*, 600-605.

162. Kehl-Fie, T. E., and Skaar, E. P. Nutritional immunity beyond iron: a role for manganese and zinc, *Curr. Opin. Chem. Biol. 14*, 218-224.

163. Mulrooney, S. B., and Hausinger, R. P. (2003) Nickel uptake and utilization by microorganisms, *FEMS Microbiol. Rev. 27*, 239-261.

164. Ragsdale, S. W. (2009) Nickel-based enzyme systems, *J. Biol. Chem. 284*, 18571-18575.

165. Sukdeo, N., Daub, E., and Honek, J. F. (2007) Biochemistry of the nickel-dependent Glyoxalase I enzymes, in *Nickel and its Surprising Impact in Nature* Volume 2 (Sigel, A., Sigel, H., Sigel R.K.O., Eds), pp 445-471, John Wiley & Sons, Ltd, Chichester, UK.

166. Smith, N. H., Gordon, S. V., de la Rua-Domenech, R., Clifton-Hadley, R. S., and Hewinson, R. G. (2006) Bottlenecks and broomsticks: the molecular evolution of Mycobacterium bovis, *Nat. Rev. Microbiol. 4*, 670-681.

167. Clemens, D. L., Lee, B. Y., and Horwitz, M. A. (1995) Purification, characterization, and genetic analysis of Mycobacterium tuberculosis urease, a potentially critical determinant of host- pathogen interaction, *J. Bacteriol. 177*, 5644-5652.

168. Sendide, K., Deghmane, A.-E., Reyrat, J.-M., Talal, A., and Hmama, Z. (2004) Mycobacterium bovis BCG urease attenuates major histocompatibility complex class II trafficking to the macrophage cell surface, *Infect. Immun. 72*, 4200-4209.

169. Baena, A., and Porcelli, S. A. (2009) Evasion and subversion of antigen presentation by Mycobacterium tuberculosis, *Tissue Antigens 74*, 189-204.

170. Yokoi, K., Uthus, E. O., and Nielsen, F. H. (2003) Nickel deficiency diminishes sperm quantity and movement in rats, *Biol. Trace Elem. Res. 93*, 141-154.

171. Nielsen, F. H. (1991) Nutritional requirements for boron, silicon, vanadium, nickel, and arsenic: current knowledge and speculation, *FASEB J. 5*, 2661-2667.

172. Nielsen, F. H. (1993) Ultratrace elements of possible importance for human health: an update, *Prog. Clin. Biol. Res. 380*, 355-376.

173. Agranoff, D. D., and Krishna, S. (1998) Metal ion homeostasis and intracellular parasitism, *Mol. Microbiol. 28*, 403-412.

174. Rodriguez, G. M., and Smith, I. (2003) Mechanisms of iron regulation in mycobacteria: role in physiology and virulence, *Mol. Microbiol. 47*, 1485-1494.

175. Wagner, D., Maser, J., Moric, I., Boechat, N., Vogt, S., Gicquel, B., Lai, B., Reyrat, J.-M., and Bermudez, L. (2005) Changes of the phagosomal elemental concentrations by Mycobacterium tuberculosis Mramp, *Microbiology 151*, 323-332.

176. Wagner, D., Maser, J., Lai, B., Cai, Z., Barry, C. E., III, Honer zu Bentrup, K., Russell, D. G., and Bermudez, L. E. (2005) Elemental analysis of Mycobacterium avium-, Mycobacterium tuberculosis-, and Mycobacterium smegmatis-containing phagosomes indicates pathogen-induced

microenvironments within the host cell's endosomal system, *J. Immunol. 174*, 1491-1500.

177. Pennella, M. A., and Giedroc, D. P. (2005) Structural determinants of metal selectivity in prokaryotic metal-responsive transcriptional regulators, *Biometals 18*, 413-428.

178. Delany, I., Ieva, R., Soragni, A., Hilleringmann, M., Rappuoli, R., and Scarlato, V. (2005) In vitro analysis of protein-operator interactions of the NikR and Fur metal-responsive regulators of coregulated genes in Helicobacter pylori, *J. Bacteriol. 187*, 7703-7715.

179. Contreras, M., Thiberge, J. M., Mandrand-Berthelot, M. A., and Labigne, A. (2003) Characterization of the roles of NikR, a nickel-responsive pleiotropic autoregulator of Helicobacter pylori, *Mol. Microbiol. 49*, 947-963.

180. Moore, C. M., and Helmann, J. D. (2005) Metal ion homeostasis in Bacillus subtilis, *Curr. Opin. Microbiol. 8*, 188-195.

181. Chivers, P. T., and Sauer, R. T. (2000) Regulation of high affinity nickel uptake in bacteria. Ni2+-dependent interaction of NikR with wild-type and mutant operator sites, *J. Biol. Chem. 275*, 19735-19741.

182. Rodriguez, G. M., and Smith, I. (2006) Identification of an ABC transporter required for iron acquisition and virulence in Mycobacterium tuberculosis, *J. Bacteriol. 188*, 424-430.

183. Ryndak, M. B., Wang, S., Smith, I., and Rodriguez, G. M. (2010) The Mycobacterium tuberculosis high-affinity iron importer, IrtA, contains an FAD-binding domain, *J. Bacteriol. 192*, 861-869.

184. Rodriguez, G. M., Voskuil, M. I., Gold, B., Schoolnik, G. K., and Smith, I. (2002) ideR, an essential gene in Mycobacterium tuberculosis: Role of IdeR in iron-dependent gene expression, iron metabolism, and oxidative stress response, *Infect. Immun. 70*, 3371-3381.

185. Chen, P. R., and He, C. (2008) Selective recognition of metal ions by metalloregulatory proteins, *Curr. Opin. Chem. Biol. 12*, 214-221.

186. Chivers, P. T. (2010) Coordinating intracellular nickel-metal-site structure-function relationships and the NikR and RcnR repressors, *Nat. Prod. Rep. 27*, 658-667.

187. Kuzmic, P. (1996) Program DYNAFIT for the analysis of enzyme kinetic data: application to HIV proteinase, *Anal. Biochem. 237*, 260-273.

188. Fahrni, C. J., and O'Halloran, T. V. (1999) Aqueous coordination chemistry of quinoline-based fluorescence probes for the biological chemistry of zinc, *J. Am. Chem. Soc. 121*, 11448-11458.

189. Perrin, D. D., and Dempsey, B. (1979) *Buffers for pH and Metal Ion Control*, 2nd ed., Chapman and Hall, New York, USA.

190. Martell, A. E., and Smith, R. M., (Eds.) (2003) *NIST Standard Reference Database 46. Version 8.0*, National institute of standards and technology, Gaithersburg, MD.

191. Xiao, Z., and Wedd, A. G. (2010) The challenges of determining metal-protein affinities, *Nat. Prod. Rep. 27*, 768-789.

192. Ye, J., Kandegedara, A., Martin, P., and Rosen, B. P. (2005) Crystal structure of the Staphylococcus aureus pI258 CadC Cd(II)/Pb(II)/Zn(II)-responsive repressor, *J. Bacteriol. 187*, 4214-4221.

193. Sovago, I., and Osz, K. (2006) Metal ion selectivity of oligopeptides, *Dalton Trans.*, 3841-3854.

194. Farkas, E., Sovago, I., and Gergely, A. (1983) Studies on transition-metal peptide complexes. 8. Parent and mixed-ligands complexes of histidine-containing dipeptides., *Journal of the Chemical Society-Dalton Transactions*, 1545-1551.

195. Barondeau, D. P., Kassmann, C. J., Bruns, C. K., Tainer, J. A., and Getzoff, E. D. (2004) Nickel superoxide dismutase structure and mechanism, *Biochemistry 43*, 8038-8047.

196. Herbst, R. W., Guce, A., Bryngelson, P. A., Higgins, K. A., Ryan, K. C., Cabelli, D. E., Garman, S. C., and Maroney, M. J. (2009) Role of conserved tyrosine residues in NiSOD catalysis: A case of convergent evolution *Biochemistry 48*, 3354-3369.

197. Ryan, K., Johnson, O., Cabelli, D., Brunold, T., and Maroney, M. (2010) Nickel superoxide dismutase: structural and functional roles of Cys2 and Cys6, *Journal of Biological Inorganic Chemistry 15*, 795-807.

198. Festa, R. A., Jones, M. B., Butler-Wu, S., Sinsimer, D., Gerads, R., Bishai, W. R., Peterson, S. N., and Darwin, K. H. (2011) A novel copper-responsive regulon in Mycobacterium tuberculosis, *Mol. Microbiol. 79*, 133-148.

199. Salgado, E. N., Ambroggio, X. I., Brodin, J. D., Lewis, R. A., Kuhlman, B., and Tezcan, F. A. (2009) Metal templated design of protein interfaces, *Proceedings of the National Academy of Sciences 107*, 1827-1832.

200. Brodin, J. D., Medina-Morales, A., Ni, T., Salgado, E. N., Ambroggio, X. I., and Tezcan, F. A. (2010) Evolution of metal selectivity in templated protein interfaces, *J. Am. Chem. Soc. 132*, 8610-8617.

201. Benanti, E. L., and Chivers, P. T. (2007) The N-terminal arm of the Helicobacter pylori Ni2+-dependent transcription factor NikR is required for specific DNA binding, *J. Biol. Chem. 282*, 20365-20375.

202. Benanti, E. L., and Chivers, P. T. (2010) Geobacter uraniireducens NikR displays a DNA binding mode distinct from other members of the NikR Family, *J. Bacteriol. 192*, 4327-4336.

203. van der Poll, T., and Opal, S. M. (2009) Pathogenesis, treatment, and prevention of pneumococcal pneumonia, *Lancet 374*, 1543-1556.

204. Denny, F. W., and Loda, F. A. (1986) Acute respiratory infections are the leading cause of death in children in developing countries, *Am J Trop Med Hyg 35*, 1-2.

205. Rudan, I., Boschi-Pinto, C., Biloglav, Z., Mulholland, K., and Campbell, H. (2008) Epidemiology and etiology of childhood pneumonia, *Bull World Health Organ 86*, 408-416.

206. Frist, B., and Sezibera, R. (2009) Time for renewed global action against childhood pneumonia, *Lancet 374*, 1485-1486.

207. Henriques-Normark, B., Blomberg, C., Dagerhamn, J., Battig, P., and Normark, S. (2008) The rise and fall of bacterial clones: Streptococcus pneumoniae, *Nat Rev Microbiol 6*, 827-837.

208. Ding, F., Tang, P., Hsu, M. H., Cui, P., Hu, S., Yu, J., and Chiu, C. H. (2009) Genome evolution driven by host adaptations results in a more virulent and antimicrobial-resistant Streptococcus pneumoniae serotype 14, *BMC Genomics 10*, 158.

209. Hava, D. L., LeMieux, J., and Camilli, A. (2003) From nose to lung: the regulation behind Streptococcus pneumoniae virulence factors, *Mol Microbiol 50*, 1103-1110.

210. Dintilhac, A., Alloing, G., Granadel, C., and Claverys, J. P. (1997) Competence and virulence of Streptococcus pneumoniae: Adc and PsaA mutants exhibit a requirement for Zn and Mn resulting from inactivation of putative ABC metal permeases, *Mol Microbiol 25*, 727-739.

211. Claverys, J. P., Dintilhac, A., Mortier-Barriere, I., Martin, B., and Alloing, G. (1997) Regulation of competence for genetic transformation in Streptococcus pneumoniae, *Soc Appl Bacteriol Symp Ser 26*, 32S-41S.

212. Dintilhac, A., and Claverys, J. P. (1997) The adc locus, which affects competence for genetic transformation in Streptococcus pneumoniae, encodes an ABC transporter with a putative lipoprotein homologous to a family of streptococcal adhesins, *Res Microbiol 148*, 119-131.

213. Ellison, D. W., and Miller, V. L. (2006) Regulation of virulence by members of the MarR/SlyA family, *Curr. Opin. Microbiol. 9*, 153-159.

214. Alekshun, M. N., Levy, S. B., Mealy, T. R., Seaton, B. A., and Head, J. F. (2001) The crystal structure of MarR, a regulator of multiple antibiotic resistance, at 2.3 A resolution, *Nat. Struct. Biol. 8*, 710-714.

215. Lim, D., Poole, K., and Strynadka, N. C. (2002) Crystal structure of the MexR repressor of the mexRAB-oprM multidrug efflux operon of Pseudomonas aeruginosa, *Journal of Biological Chemistry 277*, 29253-29259.

216. Wu, R. Y., Zhang, R. G., Zagnitko, O., Dementieva, I., Maltzev, N., Watson, J. D., Laskowski, R., Gornicki, P., and Joachimiak, A. (2003) Crystal structure of Enterococcus faecalis SlyA-like transcriptional factor, *Journal of Biological Chemistry 278*, 20240-20244.

217. Hong, M., Fuangthong, M., Helmann, J. D., and Brennan, R. G. (2005) Structure of an OhrR-ohrA operator complex reveals the DNA binding mechanism of the MarR family, *Mol. Cell 20*, 131-141.

218. Chen, P. R., Bae, T., Williams, W. A., Duguid, E. M., Rice, P. A., Schneewind, O., and He, C. (2006) An oxidation-sensing mechanism is used by the global regulator MgrA in Staphylococcus aureus, *Nat. Chem. Biol. 2*, 591-595.

219. Bordelon, T., Wilkinson, S. P., Grove, A., and Newcomer, M. E. (2006) The crystal structure of the transcriptional regulator HucR from Deinococcus radiodurans reveals a repressor preconfigured for DNA binding, *J Mol Biol 360*, 168-177.

220. Mahdi, L. K., Ogunniyi, A. D., LeMessurier, K. S., and Paton, J. C. (2008) Pneumococcal virulence gene expression and host cytokine profiles during pathogenesis of invasive disease, *Infect. Immun. 76*, 646-657.

221. Aranda, J., Garrido, M. E., Cortes, P., Llagostera, M., and Barbe, J. (2008) Analysis of the protective capacity of three Streptococcus suis proteins induced under divalent-cation-limited conditions, *Infect Immun 76*, 1590-1598.

222. Aranda, J., Garrido, M. E., Fittipaldi, N., Cortes, P., Llagostera, M., Gottschalk, M., and Barbe, J. (2009) Protective capacities of cell surface-associated proteins of Streptococcus suis mutants deficient in divalent cation-uptake regulators, *Microbiology 155*, 1580-1587.

223. Garmory, H. S., and Titball, R. W. (2004) ATP-binding cassette transporters are targets for the development of antibacterial vaccines and therapies, *Infect. Immun. 72*, 6757-6763.

224. Tanabe, M., Atkins, H. S., Harland, D. N., Elvin, S. J., Stagg, A. J., Mirza, O., Titball, R. W., Byrne, B., and Brown, K. A. (2006) The ABC transporter protein OppA provides protection against experimental Yersinia pestis infection, *Infect. Immun. 74*, 3687-3691.

225. Song, X. M., Connor, W., Jalal, S., Hokamp, K., and Potter, A. A. (2008) Microarray analysis of Streptococcus pneumoniae gene expression changes to human lung epithelial cells, *Can J Microbiol 54*, 189-200.

226. Hava, D. L., and Camilli, A. (2002) Large-scale identification of serotype 4 Streptococcus pneumoniae virulence factors, *Mol Microbiol 45*, 1389-1406.

227. Loo, C. Y., Mitrakul, K., Voss, I. B., Hughes, C. V., and Ganeshkumar, N. (2003) Involvement of the adc operon and manganese homeostasis in Streptococcus gordonii biofilm formation, *Journal of Bacteriology 185*, 2887-2900.

228. Mitrakul, K., Loo, C. Y., Gyurko, C., Hughes, C. V., and Ganeshkumar, N. (2005) Mutational analysis of the adcCBA genes in Streptococcus gordonii biofilm formation, *Oral Microbiol Immunol 20*, 122-127.

229. Owen, G. A., Pascoe, B., Kallifidas, D., and Paget, M. S. B. (2007) Zinc-responsive regulation of alternative ribosomal protein genes in Streptomyces coelicolor involves Zur and sigma(R), *J. Bacteriol. 189*, 4078-4086.

230. Adamou, J. E., Heinrichs, J. H., Erwin, A. L., Walsh, W., Gayle, T., Dormitzer, M., Dagan, R., Brewah, Y. A., Barren, P., Lathigra, R., Langermann, S., Koenig, S., and Johnson, S. (2001) Identification and characterization of a novel family of

pneumococcal proteins that are protective against sepsis, *Infect. Immun. 69*, 949-958.

231. Riboldi-Tunnicliffe, A., Isaacs, N. W., and Mitchell, T. J. (2005) 1.2 A crystal structure of the S. pneumoniae PhtA histidine triad domain a novel zinc binding fold, *FEBS Lett. 579*, 5353-5360.

232. Ogunniyi, A. D., Grabowicz, M., Mahdi, L. K., Cook, J., Gordon, D. L., Sadlon, T. A., and Paton, J. C. (2008) Pneumococcal histidine triad proteins are regulated by the Zn2+-dependent repressor AdcR and inhibit complement deposition through the recruitment of complement factor H, *FASEB. J. 23,* 731-738.

233. Loisel, E., Jacquamet, L., Serre, L., Bauvois, C., Ferrer, J. L., Vernet, T., Di Guilmi, A. M., and Durmort, C. (2008) AdcAII, a new pneumococcal Zn-binding protein homologous with ABC transporters: Biochemical and structural analysis, *J. Mol. Biol. 381*, 594-606.

234. Linke, C., Caradoc-Davies, T. T., Young, P. G., Proft, T., and Baker, E. N. (2009) The laminin-binding protein Lbp from Streptococcus pyogenes is a zinc receptor, *J. Bacteriol. 191*, 5814-5823.

235. Weston, B. F., Brenot, A., and Caparon, M. G. (2009) The metal homeostasis protein, Lsp, of Streptococcus pyogenes is necessary for acquisition of zinc and virulence, *Infect. Immun. 77*, 2840-2848.

236. Patzer, S. I., and Hantke, K. (2000) The zinc-responsive regulator Zur and its control of the znu gene cluster encoding the ZnuABC zinc uptake system in Escherichia coli, *J Biol Chem 275*, 24321-24332.

237. Maciag, A., Dainese, E., Rodriguez, G. M., Milano, A., Provvedi, R., Pasca, M. R., Smith, I., Palu, G., Riccardi, G., and Manganelli, R. (2007) Global analysis of the Mycobacterium tuberculosis Zur (FurB) regulon, *Journal of Bacteriology 189,* 730-740.

238. Feng, Y., Li, M., Zhang, H., Zheng, B., Han, H., Wang, C., Yan, J., Tang, J., and Gao, G. F. (2008) Functional definition and global regulation of Zur, a zinc uptake regulator in a Streptococcus suis serotype 2 strain causing streptococcal toxic shock syndrome, *J Bacteriol 190*, 7567-7578.

239. Ogunniyi, A. D., Grabowicz, M., Mahdi, L. K., Briles, D.E., Cook, J., and Paton, J. C. (2007) Development of a vaccine against invasive pneumococcal disease based on combinations of virulence proteins of Streptococcus pneumoniae, *Infect. Immun. 75*, 350-357.

240. Llull, D., and Poquet, I. (2004) New expression system tightly controlled by zinc availability in Lactococcus lactis, *Appl Environ Microbiol 70*, 5398-5406.

241. Bijlsma, J. J., Burghout, P., Kloosterman, T. G., Bootsma, H. J., de Jong, A., Hermans, P. W., and Kuipers, O. P. (2007) Development of genomic array footprinting for identification of conditionally essential genes in Streptococcus pneumoniae, *Appl Environ Microbiol 73*, 1514-1524.

242. Grass, G., Fan, B., Rosen, B. P., Franke, S., Nies, D. H., and Rensing, C. (2001) ZitB (YbgR), a member of the cation diffusion facilitator family, is an additional zinc transporter in *Escherichia coli*, *Journal of Bacteriology 183*, 4664-4667.

243. Lu, M., and Fu, D. (2007) Structure of the zinc transporter YiiP, *Science 317*, 1746-1748.

244. Versieck, J. (1985) Trace elements in human body fluids and tissues, *Crit Rev Clin Lab Sci 22*, 97-184.

245. Thurnham, D. I., Mburu, A. S., Mwaniki, D. L., and De Wagt, A. (2005) Micronutrients in childhood and the influence of subclinical inflammation, *Proc Nutr Soc 64*, 502-509.

246. Barendt, S. M., Land, A. D., Sham, L.-T., Ng, W.-L., Tsui, H.-C. T., Arnold, R. J., and Winkler, M. E. (2009) Influences of capsule on cell shape and chain formation of wild-type and pcsB mutants of serotype 2 Streptococcus pneumoniae, *The Journal of Bacteriology 191*, 3024-3040.

247. Busenlehner, L. S., and Giedroc, D. P. (2006) Kinetics of metal binding by the toxic metal-sensing transcriptional repressor *Staphylococcus aureus* pI258 CadC, *J. Inorg. Biochem. 100*, 1024-1034.

248. VanZile, M. L., Chen, X., and Giedroc, D. P. (2002) Allosteric negative regulation of smt O/P binding of the zinc sensor, SmtB, by metal ions: a coupled equilibrium analysis, *Biochemistry 41*, 9776-9786.

249. Walkup, G. K., and Imperiali, B. (1997) Fluorescent chemosensors for divalent zinc based on zinc finger domains. Enhanced oxidative stability, metal binding affinity, and structural and functional characterization., *J Am Chem Soc 119*, 3443-3450.

250. Jefferson, J. R., Hunt, J. B., and Ginsburg, A. (1990) Characterization of indo-1 and quin-2 as spectroscopic probes for Zn2(+)-protein interactions, *Anal Biochem 187*, 328-336.

251. Hansen, R. E., and Winther, J. R. (2009) An introduction to methods for analyzing thiols and disulfides: Reactions, reagents, and practical considerations, *Anal. Biochem. 394*, 147-158.

252. Delaglio, F., Grzesiek, S., Vuister, G. W., Zhu, G., Pfeifer, J., and Bax, A. (1995) NMRPipe: a multidimensional spectral processing system based on UNIX pipes, *J Biomol NMR 6*, 277-293.

253. Wishart, D. S., Bigam, C. G., Yao, J., Abildgaard, F., Dyson, H. J., Oldfield, E., Markley, J. L., and Sykes, B. D. (1995) 1H, 13C and 15N chemical shift referencing in biomolecular NMR, *J Biomol NMR 6*, 135-140.

254. Kay, L. E., Keifer, P., and Saarinen, T. (1992) Pure absorption gradient-enhanced heteronuclear single quantum correlation spectroscopy with improved sensitivity, *J Am Chem Soc 114*, 10663-10665.

255. Yamazaki, T., Lee, W., Arrowsmith, C. H., Muhandiram, D. R., and Kay, L. E. (1994) A suite of triple resonance NMR experiments for the backbone assignment of 15N, 13C, 2H labeled proteins with high sensitivity, *J. Am. Chem. Soc. 116*, 11655-11666.

256. Yamazaki, T., Lee, W., Revington, M., Mattiello, D. L., Dahlquist, F. W., Arrowsmith, C. H., and Kay, L. E. (1994) An HNCA pulse scheme for the backbone assignment of 15N,13C,2H-labeled proteins: Application to a 37-kDa Trp repressor-DNA complex, *J. Am. Chem. Soc. 116*, 6464-6465.

257. Scott, R. A. (2000) X-ray Absorption Spectroscopy, in *Physical Methods in Bioinorganic Chemistry: Spectroscopy and Magnetism* (Que, L., Ed.), pp 465-503, University Science Books, Sausalito, CA.

258. Ankudinov, A. L., Ravel, B., Rehr, J. J., and Conradson, S. D. (1998) Real-space multiple-scattering calculation and interpretation of X-ray-absorption near-edge structure., *Phys. Rev. B 58*, 7565–7576.

259. Poiarkova, A. V., and Rehr, J. J. (1999) Multiple-scattering X-ray absorption fine-structure Debye–Waller factor calculations., *Phys. Rev. B 59*, 948–957.

260. Brenot, A., Weston, B. F., and Caparon, M. G. (2007) A PerR-regulated metal transporter (PmtA) is an interface between oxidative stress and metal homeostasis in Streptococcus pyogenes, *Mol. Microbiol. 63*, 1185-1196.

261. Demeler, B., and Brookes, E. (2008) Monte Carlo analysis of sedimentation experiments, *Colloid Polym. Sci. 286*, 129-137.

262. Grimsley, G. R., Scholtz, J. M., and Pace, C. N. (2009) A summary of the measured pK values of the ionizable groups in folded proteins, *Protein Sci. 18*, 247-251.

263. Thurlkill, R. L., Grimsley, G. R., Scholtz, J. M., and Pace, C. N. (2006) pK values of the ionizable groups of proteins, *Protein Sci. 15*, 1214-1218.

264. Simons, T. J. B. (1993) Measurement of free Zn2+ ion concentration with the fluorescent probe mag-fura-2 (furaptra), *J. Biochem. Biophys. Methods 27*, 25-37.

265. Zimmermann, M., Xiao, Z., Cobbett, C. S., and Wedd, A. G. (2009) Metal specificities of Arabidopsis zinc and copper transport proteins match the relative, but not the absolute, affinities of their N-terminal domains, *Chem Commun (Camb) 42*, 6364-6366.

266. Frausto da Silva, J., and Williams, R. (2001) *The biological chemistry of elements: The inorganic chemistry of life*, Second ed., Oxford University Press, Oxford, UK.

267. Outten, C. E., Tobin, D. A., Penner-Hahn, J. E., and O'Halloran, T. V. (2001) Characterization of the metal receptor sites in Escherichia coli Zur, an ultrasensitive zinc(II) metalloregulatory protein, *Biochemistry 40*, 10417-10423.

268. Guo, J., Wang, S., Dong, J., Qiu, H., Scott, R. A., and Giedroc, D. P. (1995) X-ray and visible absorption spectroscopy of wild-type and mutant T4 gene 32 proteins: His64, not His81, is the non-thiolate zinc ligand, *J Am Chem Soc 117*, 9437-9440.

269. Cornilescu, G., Delaglio, F., and Bax, A. (1999) Protein backbone angle restraints from searching a database for chemical shift and sequence homology, *J. Biomol. NMR 13*, 289-302.

270. Sieminska, E. A., Xu, X., Savchenko, A., and Sanders, D. A. (2007) The X-ray crystal structure of PA1607 from Pseudomonas aureginosa at 1.9 A resolution--a putative transcription factor, *Protein Sci. 16*, 543-549.

271. Edgcomb, S. P., and Murphy, K. P. (2002) Variability in the pKa of histidine side-chains correlates with burial within proteins, *Proteins: Struct., Funct., Genet. 49*, 1-6.

272. Gunner, M. R., Nicholls, A., and Honig, B. (1996) Electrostatic potentials in Rhodopseudomonas viridis reaction centers: Implications for the driving force and directionality of electron transfer, *The Journal of Physical Chemistry 100*, 4277-4291.

273. Becher, D., Hempel, K., Sievers, S., Zuhlke, D., Pane-Farre, J., Otto, A., Fuchs, S., Albrecht, D., Bernhardt, J., Engelmann, S., Volker, U., van Dijl, J. M., and Hecker, M. (2009) A proteomic view of an important human pathogen--towards the quantification of the entire Staphylococcus aureus proteome, *PLoS One 4*, e8176.

274. Lee, J. W., Soonsanga, S., and Helmann, J. D. (2007) A complex thiolate switch regulates the Bacillus subtilis organic peroxide sensor OhrR, *Proceedings of the National Academy of Sciences of the United States of America 104*, 8743-8748.

275. Chen, H., Hu, J., Chen, P. R., Lan, L., Li, Z., Hicks, L. M., Dinner, A. R., and He, C. (2008) The Pseudomonas aeruginosa multidrug efflux regulator MexR

uses an oxidation-sensing mechanism, *Proc Natl Acad Sci U S A 105*, 13586-13591.

276. Cotton, F. A., and Hanson, H. P. (1958) Soft X-Ray absorption edges of metal ions in complexes .3. Zinc(II) complexes, *J. Chem. Phys. 28*, 83-87.

277. Llull, D., Son, O., Blanie, S., Briffotaux, J., Morello, E., Rogniaux, H., Danot, O., and Poquet, I. (2011) Lactococcus lactis ZitR is a zinc responsive repressor active in low, non-toxic zinc concentrations in vivo, *J. Bacteriol. 193*, 1919-1929.

278. Banci, L., Bertini, I., McGreevy, K. S., and Rosato, A. (2010) Molecular recognition in copper trafficking, *Nat. Prod. Rep. 27*, 695-710.

279. Banci, L., Bertini, I., Ciofi-Baffoni, S., Kozyreva, T., Zovo, K., and Palumaa, P. (2010) Affinity gradients drive copper to cellular destinations, *Nature 465*, 645-648.

280. Hantke, K. (1981) Regulation of ferric iron transport in Escherichia coli K12: Isolation of a constitutive mutant, *Molecular and General Genetics MGG 182*, 288-292.

281. Hantke, K. (1982) Negative control of iron uptake systems in Escherichia coli, *FEMS Microbiol. Lett. 15*, 83-86.

282. Hantke, K. (1984) Cloning of the repressor protein gene of iron-regulated systems in Escherichia coli K12, *Molecular and General Genetics MGG 197*, 337-341.

283. Hantke, K. (1987) Selection procedure for deregulated iron transport mutants in Escherichia coli K 12: not only affects iron metabolism, *Molecular and General Genetics MGG 210*, 135-139.

284. Zawadzki, K. M., Hamuro, Y., Kim, J. S., Garrod, S., Stranz, D. D., Taylor, S. S., and Woods, V. L., Jr. (2003) Dissecting interdomain communication within cAPK regulatory subunit type II{beta} using enhanced amide

hydrogen/deuterium exchange mass spectrometry (DXMS), *Protein Science 12*, 1980-1990.

285. Tzeng, S. R., and Kalodimos, C. G. (2011) Protein dynamics and allostery: an NMR view, *Curr. Opin. Struct. Biol. 21*, 62-67.

286. Hsin, K., Sheng, Y., Harding, M. M., Taylor, P., and Walkinshaw, M. D. (2008) MESPEUS: a database of the geometry of metal sites in proteins, *J. Appl. Crystallogr. 41*, 963-968.

287. Harding, M. M., Nowicki, M. W., and Walkinshaw, M. D. (2010) Metals in protein structures: a review of their principal features, *Crystallography Reviews 16*, 247 - 302.

APPENDIX A

Microarray analysis of relative transcript amounts in strains IU2594 (Δ*adcR*) and IU1781 (*adcR*$^{+}$) grown exponentially in BHI. A representative log-scale scatter plot of relative transcript amounts is shown.

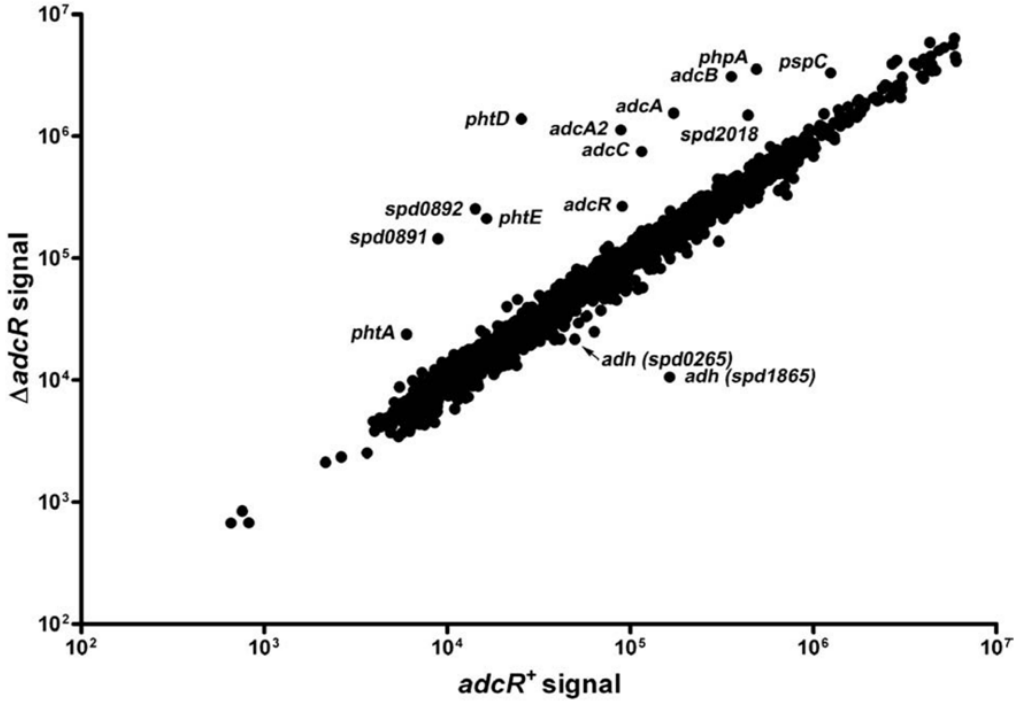

This data was acquired, processed and analyzed by Dr. Faith Jacobsen and published in: Reyes-Caballero, H., Guerra, A. J., Jacobsen, F. E., Kazmierczak, K. M., Cowart, D., Koppolu, U. M. K., Scott, R. A., Winkler, M. E., and Giedroc, D. P. (2010) The Metalloregulatory Zinc Site in *Streptococcus pneumoniae* AdcR, a Zinc-activated MarR Family Repressor, *J. Mol. Biol. 403*, 197-216.

APPENDIX B

Growth and cellular zinc content of adcR mutants. (a) Growth curves of *adcR* parent, Δ*adcR*, *adcR* C30A, *adcR* H108Q, *adcR* H111Q, and *adcR* H112Q strains of *S. pneumoniae* in the presence of 200 μM ZnSO4. (b) Cellular zinc concentration in bacteria growing exponentially (A620 0.1-0.3). The average of biological triplicates are shown with SEMs ($P<0.05$).

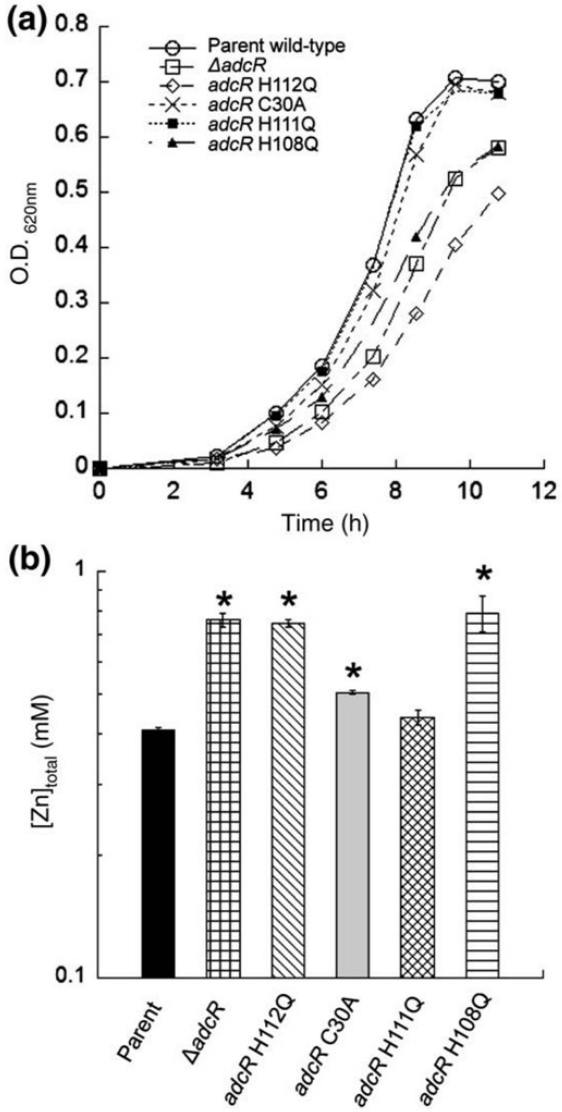

This data was acquired processed and analyzed by Dr. Faith Jacobsen and published in: Reyes-Caballero, H., Guerra, A. J., Jacobsen, F. E., Kazmierczak, K. M., Cowart, D., Koppolu, U. M. K., Scott, R. A., Winkler, M. E., and Giedroc, D. P. (2010) The Metalloregulatory Zinc Site in *Streptococcus pneumoniae* AdcR, a Zinc-activated MarR Family Repressor, *J. Mol. Biol. 403*, 197-216.

APPENDIX C

^{1}H-^{15}N TROSY spectra of WT AdcR in the absence (a) and in the presence (b) of Zn(II). Sequence specific resonances assignments are shown for each conformer, with the single-contour red crosspeaks in panel (b) corresponding to those of apo-AdcR. (c) Secondary structural analysis of apo- and Zn(II)-bound AdcR as determined by analysis of the backbone chemical shifts in TALOS (*269*)

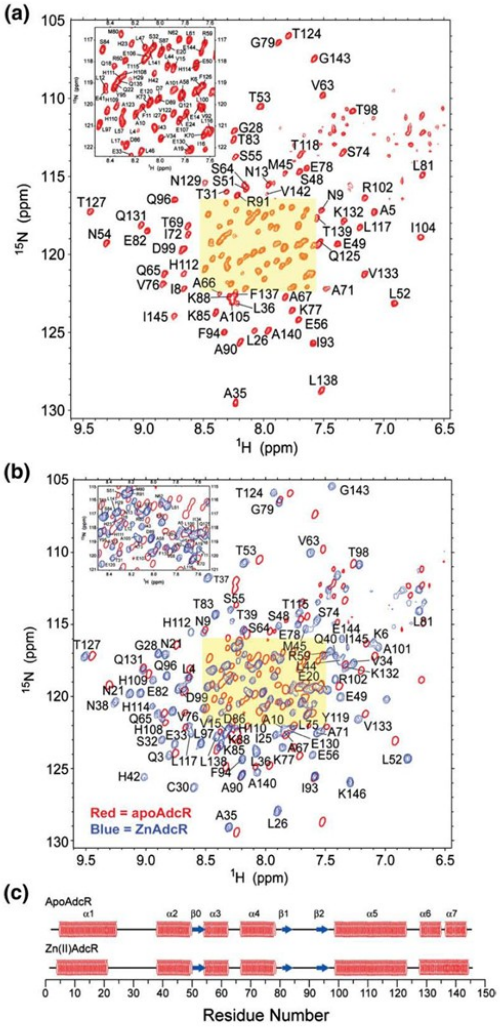

This data was acquired, processed and analyzed by Alfredo J. Guerra and published in: Reyes-Caballero, H., Guerra, A. J., Jacobsen, F. E., Kazmierczak, K. M., Cowart, D., Koppolu, U. M. K., Scott, R. A., Winkler, M. E., and Giedroc, D. P. (2010) The Metalloregulatory Zinc Site in *Streptococcus pneumoniae* AdcR, a Zinc-activated MarR Family Repressor, *J. Mol. Biol. 403*, 197-216.

APPENDIX D

Chemical shift (^{1}H,^{15}N) perturbation maps | apo – Zn| of AdcR variants (35^{o}C, pH 6.0)

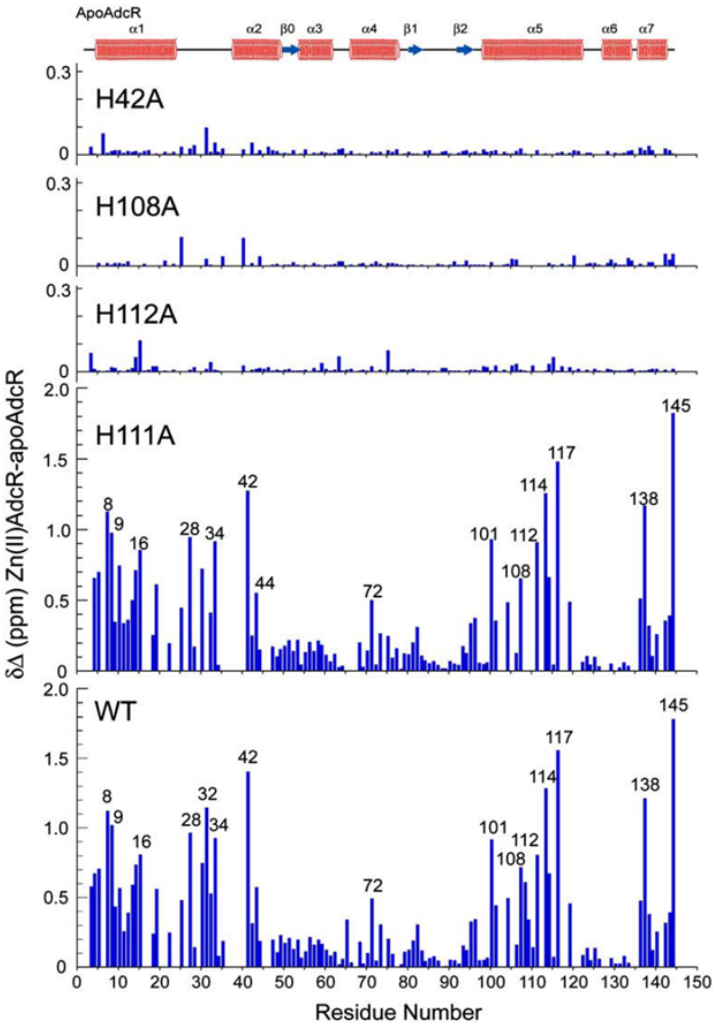

This data was acquired, processed and analyzed by Alfredo J. Guerra and published in: Reyes-Caballero, H., Guerra, A. J., Jacobsen, F. E., Kazmierczak, K. M., Cowart, D., Koppolu, U. M. K., Scott, R. A., Winkler, M. E., and Giedroc, D. P. (2010) The Metalloregulatory Zinc Site in *Streptococcus pneumoniae* AdcR, a Zinc-activated MarR Family Repressor, *J. Mol. Biol. 403*, 197-216.

APPENDIX E

Chemical shift (1H, 15N) perturbation map of mutant AdcR apoproteins relative to wild-type AdcR (35°C, pH 6.0). Δppm= sqrt[(Δppm $^{1}H)^{2}$ + ((Δppm $^{15}N)/7)^{2}$]. The red arrows indicate the residue number of the mutation in each case.

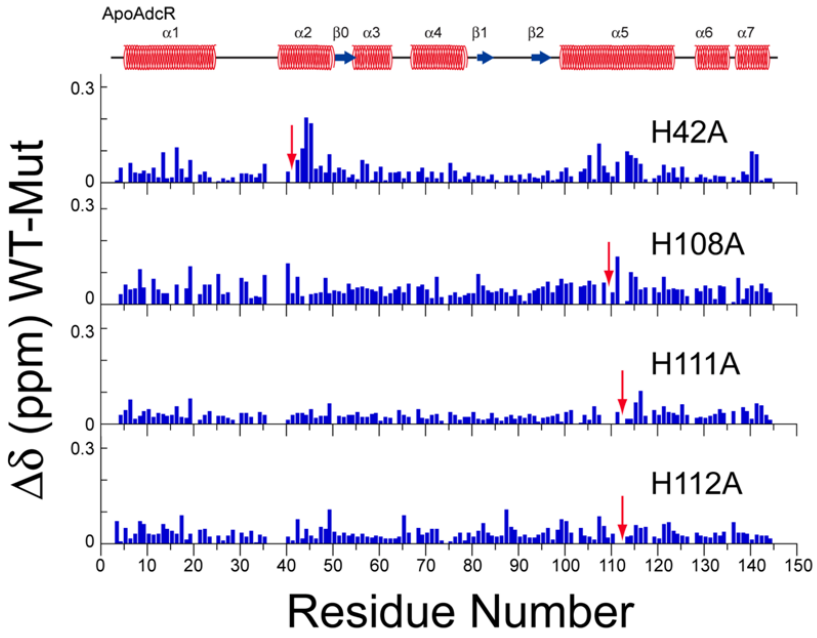

This data was acquired, processed and analyzed by Alfredo J. Guerra and published in: Reyes-Caballero, H., Guerra, A. J., Jacobsen, F. E., Kazmierczak, K. M., Cowart, D., Koppolu, U. M. K., Scott, R. A., Winkler, M. E., and Giedroc, D. P. (2010) The Metalloregulatory Zinc Site in *Streptococcus pneumoniae* AdcR, a Zinc-activated MarR Family Repressor, *J. Mol. Biol. 403*, 197-216.

APPENDIX F

Electrospray ionization-mass spectrometry (LC-ESI-MS) of apo wild-type and variants NmtR.[a]

NmtR variant	Expected MW (Da)	MW observed	Δ(amu)	Identified NmtR (res num.)[b]
WT	12835.6	12703.1	132.5	WT (2-120)
H3Q	12826.5	12694.7	131.8	H3Q (2-120)
D91Q	12848.6	12717.4	131.2	D91Q (2-120)
H93Q	12826.5	12695.7	130.8	H93Q (2-120)
H107Q	12826.5	12695.7	130.8	H107Q (2-120)
H109Q	12826.5	12695.7	130.8	H109Q (2-120)
D114Q	12848.6	12717.8	130.8	D114Q (2-120)
H116Q	12826.5	12695.6	130.0	H116Q (2-120)
Δ111NmtR	11914.6	11784.6	130.0	Δ111NmtR (2-120)

[a]Conditrions: Protein concentration 30-80μM, C4 column filtered.
[b]In agreement with a Δ of 130-132 amu, Met1 is processed in NmtR, thus the protein is only 119 residues long

APPENDIX G

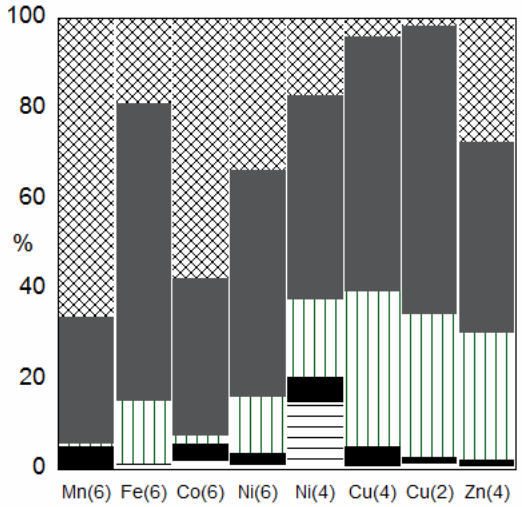

Ligand preferences of transition metals found in structural database. The structural information was obtained from a search in MESPEUS database (*286*) from data deposited in the Protein Data Bank (PDF) up to 2007. The number of events in which each kind of ligand is found as a donor to a metal in structures with the preferred coordination number for each atom (show in parenthesis) is show as a percentage of all the structures accessed for each metal . Asp/GLu; closed mesh, Hys; solid grey, Cys; vertical lines, O from main chain carbonyl; solid black, N from main chain; horizontal lines. The polarizabilty define the ionic or covalent character of the bond. As we move from left to right in the Period of the transition metals (Mn to Zn), the ligand-metal interaction tends to be less ionic and more covalent-like, which reflect in the preference from less polirizable "hard" ligands (carboxy ligands form Glu and Asp) to more polarizible "soft" ligands (sulfur ligands from cysteine). The covalent like bonds have higher energy of formation than the ionic like bonds and are more dependable on the bond length, which are aspects to consider in the structural analysis of metal centers. The ion radii is important to define the coordination number because repulsion between the bonds increases with smaller radii. The tendency is to reduce the number of ligands as the ionic radii decreases. In contrast to Cys and Asp/Glu ligand donors, the neutral ligand N from imidazole ring of His ligand donor are found with the same high frequency in all the metal centers. Note that zinc has almost equal preference for Asp/Glu, His and Cys donor ligands and that N of amide main chain is a rare ligand but is find often as donor ligand to nickel. The preference for ligands show here are in agreement with previously published data (*287*). The coordination number (in parenthesis) is based on the preferred coordination geometry of each metal that is reported on recent studies of structural databases (*103*).

VITA

Name: Hermes Reyes Caballero

Address: 800 E. Kirkwood
Chemistry Department
Indiana University
Bloomington, IN 47405

Email Address: hreyesca@indiana.edu

Education: B.S. Biochemistry Engineer in Marine Resources Management, ITESM at Mexico, 1997
M.S. Genetics and Molecular Biology, CINVESTAV at Mexico, 2003
Ph.D. Biochemistry, Texas A&M University, 2011

Publications:

Reyes-Caballero, H., Guerra, A. J., Jacobsen, F. E., Kazmierczak, K. M., Cowart, D., Koppolu, U. M. K., Scott, R. A., Winkler, M. E., and Giedroc, D. P. (2010) The metalloregulatory zinc site in Streptococcus pneumoniae AdcR, a zinc-activated MarR family repressor, *J. Mol. Biol. 403*, 197-216.

Reyes-Caballero, H., Campanello, G.C., Giedroc, D.P. (2011) Metalloregulatory proteins: metal selectivity and allosteric switching, *Biophysical Chemistry* in press. doi:10.1016/j.bpc.2011.03.010

Reyes-Caballero, H., Lee C.W., Giedroc, D.P. (2011) Mycobacterium tuberculosis NmtR harbors a nickel sensing site with strong parallels to Escherichia coli RcnR and Streptomyces coelicolor Ni(II)-superoxide dismutase, *Manuscript in preparation*.

Lui, T, Reyes-Caballero, H., Li C., Scott, R.A., Giedroc, D.P. (2007) Multiple metal binding domains enhance the Zn(II) selectivity of the divalent metal ion transporter AztA, *Biochemistry 46*, 11057-68